1-1-1998

Characterization of the regulatory domain of the mammalian multifunctional De Novo pyrimidne biosynthetic enzyme CAD

Nisha Sahay

CHARACTERIZATION OF THE REGULATORY DOMAIN OF THE MAMMALIAN MULTIFUNCTIONAL *DE NOVO* PYRIMIDNE BIOSYNTHETIC ENZYME CAD

by

NISHA SAHAY

DISSERTATION

Submitted to the Graduate School

of Wayne State University,

Detroit, Michigan

in partial fulfillment of the requirements

for the degree of

DOCTOR OF PHILOSOPHY

1998

MAJOR: BIOCHEMISTRY and
MOLECULAR BIOLOGY

Approved by:

3/30/98
Advisor Date

Bharati Mitra 3/30/98

3/30/98

3/30/98

ACKNOWLEDGEMENTS

I came to the United States with the sole purpose of attaining a doctorate in Biochemistry and I feel very proud to have finally achieved this goal. This work would not have been complete without the support, guidance and friendship of several individuals. I wish to extend my appreciation and gratitude to my dissertation advisor, my 'guru' and friend Dr. David R. Evans, for giving me the opportunity to pursue my goal under his direction. Dr. Evans nurtured my interest in research and helped me develop as an independent researcher. More importantly, he helped me acquire and maintain confidence in my capabilities. My sincerest thanks to my doctoral committee, Dr. Daniel Walz, Dr. Sharon Ackerman, and Dr. Bharati Mitra for their support, critiques and suggestions. My warm regards to Dr. Hedeel I. Evans, who not only provided invaluable direction in the implementation of this project, but also supported and enhanced both my academic and personal development.

I wish to thank some special colleagues I have had the pleasure of working with, especially Avigail Posner and Dr. Jose Molina for helping me settle down in Detroit, and for their constant encouragement and sincere friendship! To my closest friend and colleague Dr. Andrea Rotgeri – you will always be very special! Thanks to all my colleagues within the lab, especially to Anne Bouvier and Anupama Ahuja for making all of this an enjoyable experience!

My deep gratitude to a very special friend, Suresh Valsangkar, for his encouragement and unfailing confidence, and for making Michigan a home! To Teresa Fannin, Diane Wren, Amatul Mateen, Dr. Robert Lipsitz, Sujata Madan, Dr. Vrinda Dutt, Pratiti Das and Dr. Badrinarayan Bandaru – your constant

support, encouragement and friendship helped sustain my focus. To my professors at Presidency College, Calcutta – I shall always be grateful for the confidence you all instilled in me!

I dedicate this thesis to my family, to my Mom and strongest advocate, Indu Sahay, to my Dad Capt. N.K. Sahay, for showing me the world and making me adventurous, to my brother Deepak, for his support in every possible way, and to my sis-in-law Galina for all her encouragement. Without their constant love and support, the completion of this undertaking would not have been possible!

TABLE OF CONTENTS

LIST OF TABLES

LIST OF FIGURES

CHAPTER 1 INTRODUCTION

1.1 The *de novo* Pyrimidine Biosynthetic Pathway and the Mammalian Multifunctional Protein CAD

Pyrimidine nucleotides play a central role in cellular regulation by contributing not only to the synthesis of nucleic acids, but also to nitrogen, carbohydrate, lipid, and membrane metabolism. Most cells have two pathways to fulfill their pyrimidine nucleotide requirements. The *de novo* pathway begins with glutamine, ATP, and bicarbonate and through six enzymatic reactions catalyzes the formation of uridine monophosphate (Figure 1.1) (1). The salvage pathway is a two step process involving transport of uridine through the cell membrane followed by phosphorylation of uridine to yield UMP.

The six reactions in the *de novo* pyrimidine pathway are catalyzed by glutamine-dependent carbamoyl phosphate synthetase (CPSase II, EC 6.3.5.5), aspartate transcarbamoylase (ATCase, EC 2.1.3.2), dihydoorotase (DHOase EC 3.5.2.3), dihydroorotate dehydrogenase, orotidylate phosphoribosyl-transferase and orotidylate decarboxylase. The metabolic intemediates in the pathway are identical in eukaryotic and prokaryotic cells. However, compared to the monofunctional bacterial proteins, the eukaryotic enzymes have a more complex structural organization and a more sophisticated mode of control.

In mammals, the first three enzymatic activities in the *de novo* pyrimidine pathway are carried on a single 240 kDa polypeptide chain called CAD (2-4). This multifunctional protein has the glutamine-dependent carbamoyl phosphate synthetase (CPSase), aspartate transcarbamoylase (ATCase) and the dihydroorotase (DHOase) activities. George Stark and colleagues first demonstrated the multifunctional nature of CAD in 1978 (4). A series of mutant resistant strains were isolated by treating cultured

Figure 1.1 The *de novo* Pyrimidine Biosynthetic Pathway of Higher Eukaryotic Organisms

In mammals, the initial three reactions are catalyzed by the multifunctional protein CAD. The three enzymatic activities of CAD are glutamine-dependent carbamoyl phosphate synthetase (CPSase), aspartate transcarbamoylase (ATCase), and dihydroorotase (DHOase). Among the three enzymes, only the CPSase is allosterically regulated. The CPSase is inhibited by the end product uridine triphosphate (UTP), activated by phosphoribosyl-5-pyrophosphate (PRPP), and undergoes cAMP-dependent phosphorylation. In mammals, the last two steps of the pathway are catalyzed by a bifunctional protein UMP synthetase, which has the orotidylate phosphoribosyltransferase and orotidylate decarboxylase activities.

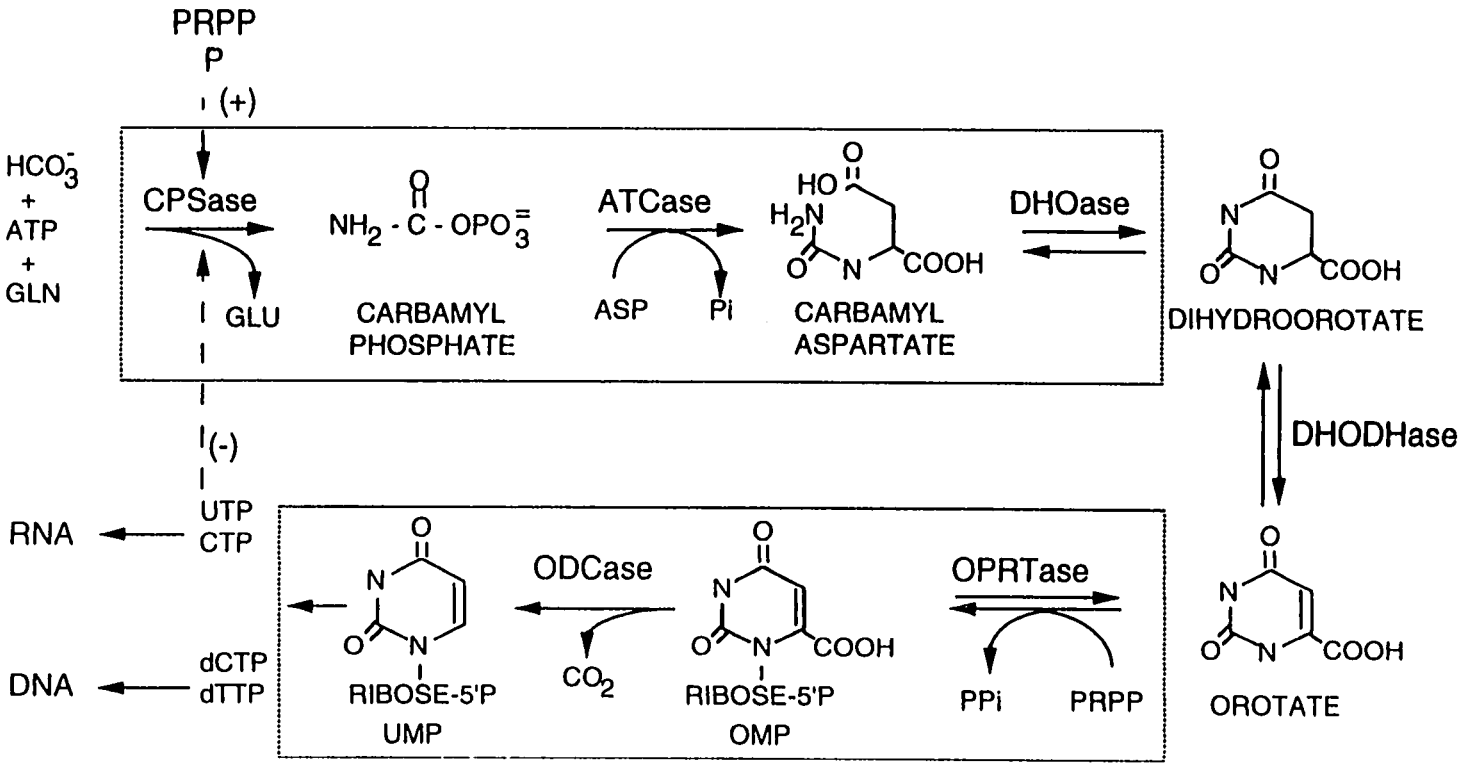
PRPP
P
(+)
HCO3-
+
ATP
+
GLN
CPSase
GLU
NH2 - C - OPO3=
CARBAMYL
PHOSPHATE
ATCase
ASP
Pi
CARBAMYL
ASPARTATE
DHOase
DIHYDROOROTATE
DHODHase
(-)
UTP
CTP
RNA
dCTP
dTTP
DNA
RIBOSE-5'P
UMP
ODCase
CO2
RIBOSE-5'P
OMP
OPRTase
PPi
PRPP
OROTATE

Syrian hamster cells with increasing concentrations of PALA, a potent bisubstrate inhibitor of aspartate transcarbamoylase (5). It was shown that PALA resistance resulted from a 150-fold overproduction of the intracellular concentration of CAD. The native protein was a mixture of higher oligomeric forms, primarily of trimers and hexamers (6). Padgett et al subsequently showed that the overproduction of the protein resulted from a proportional increase in the intracellular concentration of a specific 7.8 kb mRNA that could direct the synthesis of CAD both in vivo and in vitro (7). From this mRNA, a partial cDNA clone was made which complemented an *E. coli pyr*B mutant lacking the ATCase activity (8).

1.2 Controlled Proteolysis of CAD

The controlled cleavage of CAD by proteases has provided evidence for the domain structure of CAD. In vitro, controlled proteolysis of CAD resulted in enzymatically active fragments, suggesting that regions of the polypeptide were folded into separate structural domains that carry the different functions of the molecule (9-17).

The molecule was susceptible to digestion by elastase and trypsin (9,11). When purified hamster CAD was digested with low concentrations of elastase, the molecule was cleaved into a small number of well-defined fragments. Digestion kinetics obtained by a time-dependent concentration of each species showed that the parent molecule was subsequently cleaved into 200, 150, 140, 80, 60, 44 and 40 kDa species. Partial fractionation of the digest by sucrose gradient centrifugation and subsequent isolation of some of these fragments showed that the 40 and 44 kDa proteolytic fragments corresponded to the fully active ATCase (12) and DHOase domains respectively. The CPSase activity was rapidly lost since the larger fragment underwent a series of subsequent cleavages. Similar results were obtained when CAD was treated with trypsin. Based on early controlled proteolysis studies, CAD was postulated to have a complex domain structure. Mally, Grayson and Evans proposed that CAD consisted of

Figure 1.2 Domain Structure of CAD and its Proteolytic Fragments

The domains of CAD, starting from the amino end to the carboxyl end are organized in the following order: GLNase, GLN-CPSase linker, CPS-A, CPS-B, DHO, DHO-ATC linker, and ATC Controlled proteolysis showed that CAD is sequentially cleaved into a number of distinct fragments, the arrowheads representing the start and end of each proteolytic fragment. The 36 kDa ATCase domain is the first fragment to be released by cleavage of the linker connecting the ATCase and DHOase domains. The next species to be cleaved is the 44 kDa DHOase domain leaving behind the 150 kDa fragment that has the GLN dependent CPSase activity. The active 150 kDa fragment is very labile and undergoes a rapid cleavage at its carboxyl end resulting in a 140 kDa inactive protein. The 140 kDa is then cleaved at the end of CPS-A into a 60 and 80 kDa species. The 60 kDA is further cleaved into 40 and then into 28 kDa proteins. The 80 kDa is further cleaved into a 30 kDa and 50 kDa protein. The 50 kDa was subsequently cleaved into a 30 kDa protein.

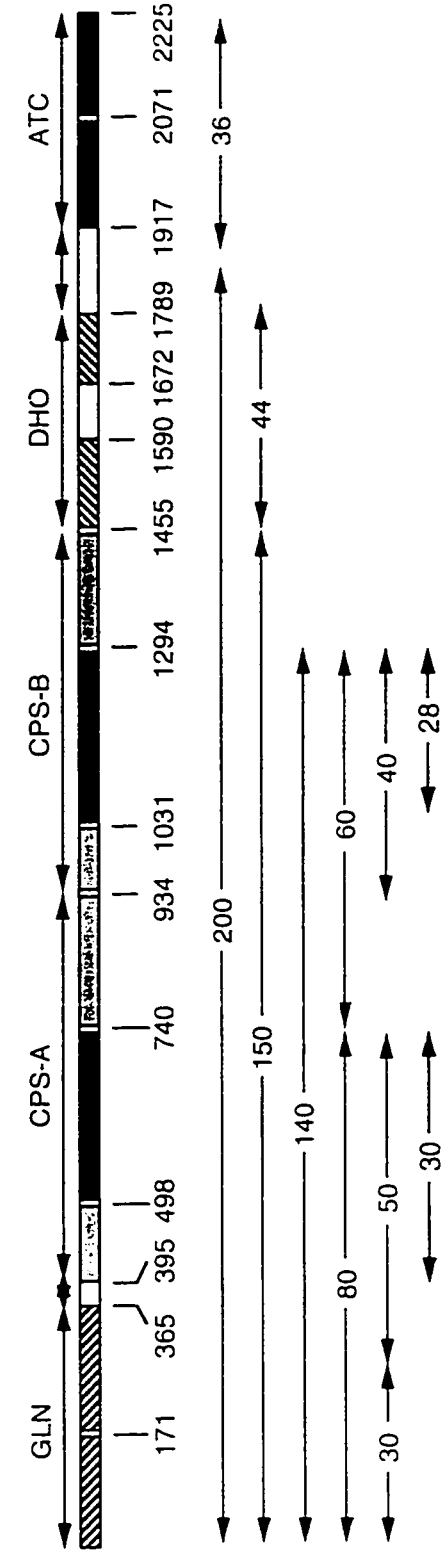
GLN
CPS-A
CPS-B
DHO
ATC
171
365
395
498
740
934
1031
1294
1455
1590
1672
1789
1917
2071
2225
30
50
80
140
150
200
60
40
28
30
44
36

six functional domains (Figure 1.2):

1) The glutamine amidotransferase or glutaminase (GLNase) domain that catalyzes the hydrolysis of glutamine to ammonia for the synthesis of carbamoyl phosphate

2) The carbamoyl phosphate synthetase (CPSase) domain that accepts the amino group from glutamine, binds bicarbonate and two moles of Mg-ATP catalyzing the formation of carbamoyl phosphate.

3) The aspartate transcarbamoylase (ATCase) domain that catalyzes the formation of carbamoyl aspartate form carbamoyl phosphate and aspartate.

4) The dihydroorotase (DHOase) domain that catalyzes the reversible condensation of carbamoyl aspartate to dihydroorotate.

5) A uridine 5'-triphosphate (UTP) domain that binds the inhibitor UTP, and relays the allosteric signal to the CPSase active site

6) A phosphoribosyl-5'-pyrophosphate (PRPP) domain that binds the allosteric activator PRPP.

All the proteolytic fragments have been isolated and partially sequenced in our laboratory.

1.3 The CAD gene, mRNA and cDNA

The 25 kb hamster CAD gene was cloned and found to contain 37 intervening sequences (5,18). The recombinant plasmid pCAD142, a gift from George Stark, containing 6.5 kb CAD cDNA insert encoding most of CAD, but lacking the 5' end of the molecule was sequenced by Simmer et al in our laboratory (16). Sequence homology to other known CPSases, DHOases and ATCases provided the strongest evidence for the definition of the individual domains and allowed the identification of the four major domains in the CAD sequence. Starting from the amino end of the protein, these are the GLNase, CPSase, DHOase, and ATCase. It was also shown that these three regions

Figure 1.3 The CAD Gene, mRNA and Domain Structure

The genomic CAD DNA is 28 Kb and has GC boxes in the control region upstream of the coding sequence. The CAD mRNA is 7.5 Kb with the black region representing coding sequences and the clear areas representing untranslated regions. pCAD142, has the CAD coding sequence but lacks the amino half of the molecule (about 519 bp). PKB11 contains the entire first half of the gene including the start codon. The bottom shows the structural organization of the CAD protein. The glutaminase domain is divided into two subdomains, the amino and carboxyl terminal domains. A linker connects the GLN and CPS domains. The CPS domain consists of two highly homologous subdomains, the CPS-A and CPS-B that contain the two ATP binding sites. There is a phosphorylation site at the extreme carboxyl end of CPS-B. The DHO-ATC linker contains the second phosphorylation site of the molecule. The ATC domain is further divided into carbamoyl phosphate and aspartate subdomains.

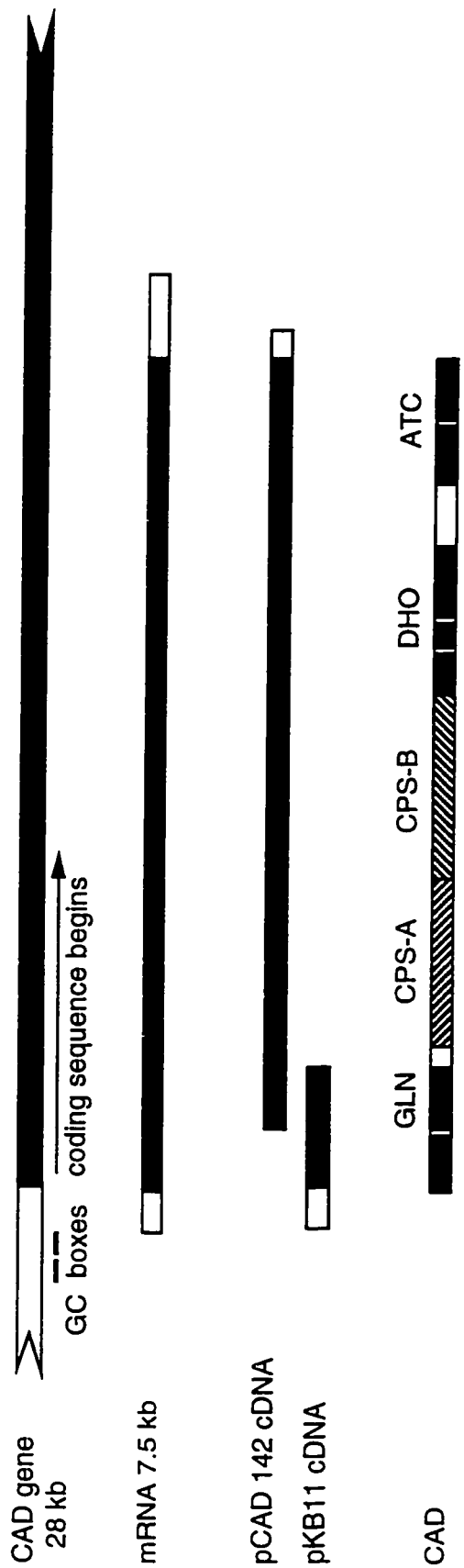
CAD gene
28 kb
GC boxes
coding sequence begins
mRNA 7.5 kb
pCAD 142 cDNA
pKB11 cDNA
CAD
GLN
CPS-A
CPS-B
DHO
ATC

were connected by stretches of non-homologous regions termed linkers.

As mentioned earlier, the cDNA clone pCAD142 lacked the region corresponding to the 5' end of the CAD mRNA. In our laboratory, Dr Kiflai Bein used primer extension and RNaseH mapping techniques, to clone the cDNA encoding the amino end of the molecule, resulting in the partial clone, pKB11. A full length CAD cDNA clone was then constructed that expressed functional CAD when transfected into hamster cells (19). Recently, another full-length clone, CAD cDNA clone, pCKCAD10, has been constructed by Dr. Hedeel Guy in our laboratory for expression in *E. coli* (20).

1.4 The Carbamoyl Phosphate Synthetase Domain

Carbamoyl phosphate synthetase (CPSase), the first enzyme in the *de novo* pyrimidine pathway catalyzes the formation of carbamoyl phosphate using two molecules of ATP, bicarbonate, and glutamine (21-28). Glutamine is the nitrogen donor but ammonia added exogenously in the form of ammonium ion, can also be used as a substrate. Monovalent and divalent cations are required for the enzymatic activity of CPSase.

The chemical mechanism for the synthesis of carbamoyl phosphate has been postulated to occur in four partial reactions via the formation of two reactive intermediates, a highly unstable carboxy phosphate and an acid stable carbamate.

$$\text{Glutamine} + H_2O \rightarrow \text{glutamate} + NH_3$$

$$HCO_3 + \text{ATP} \rightarrow \text{carboxy phosphate} + \text{ADP}$$

$$\text{Carboxy phosphate} + NH_3 \rightarrow \text{carbamate} + \text{Pi}$$

$$\text{Carbamate} + \text{ATP} \rightarrow \text{carbamoyl phosphate}$$

Carbamoyl phosphate is an essential precursor in the metabolic pathways of arginine, urea and pyrimidine nucleotide biosynthesis. The carbamoyl phosphate produced in the *de novo* pathway is subsequently utilized in two separate biosynthetic pathways. The molecule may react either with aspartate in a reaction catalyzed by

aspartate transcarbamoylase for the eventual synthesis of pyrimidine nucleotides or, alternatively, the carbamoyl phosphate reacts with ornithine for the subsequent synthesis of arginine and/or urea. In lower organisms, a single CPSase catalyzes the synthesis of carbamoyl phosphate for both pathways, whereas in higher organisms there is a separate enzyme for each pathway, one CPSase belonging to the arginine pathway, and the other to the pyrimidine pathway. In both lower and higher organisms, ammonia is used but in most cases glutamine is the physiological donor. The glutaminase activity may be on a separate subunit or combined with the ammonia-dependent synthetase activity on a single polypeptide chain.

E. coli CPSase catalyzes the synthesis of carbamoyl phosphate for both the pyrimidine and the arginine pathway and undergoes regulation by intermediates of both pathways (29,30). In mammals, the mitochondrial CPSase (CPSase I, E.C. 6.3.4.16) is specific for the arginine pathway (31-36) while CAD CPSase II is a pyrimidine specific domain. This allows the arginine and pyrimidine pathway to be separately regulated. (Figure 1.4). CPSase III is present in a number of elasmobranchs where it functions in the synthesis of urea for osmoregulation, and in fresh water teleostats (37-40).

E. coli CPSase

E. coli carbamoyl phosphate synthetase initiates both *de novo* pyrimidine and arginine biosynthesis (41,42) and is regulated by metabolites from both pathways. The enzyme consists of a small 40 kDa GLNase subunit that hydrolyzes glutamine, encoded by *carA*, and a large 120 kDa subunit (CPS subunit) (43,44) encoded by *carB*, which catalyzes the synthesis of carbamoyl phosphate from ammonia derived from the hydrolysis of glutamine or added exogenously in the form of ammonium ion, two molecules of ATP and bicarbonate (Figure 1.5). The *carA* and *carB* genes have been cloned, and the amino acid sequences of the small and the large subunits were deduced from the corresponding nucleotide sequences (45,46).

Figure 1.4 Comparison of the *De novo* Pyrimidine Biosynthesis in *E. coli* and Mammalian Cells

In *E. coli*, only one CPSase provides carbamoyl phosphate for both arginine and pyrimidine pathways (A). In addition to being inhibited by the pyrimidine product UMP, the *E. coli* CPSase undergoes activation by ornithine, an intermediate of the arginine pathway and by IMP, an intermediate of the purine pathway. The *E. coli* ATCase is also an allosteric enzyme that responds specifically to ATP, UTP, and CTP in the pyrimidine pathway.

In mammalian cells, there are two CPSases, CPSase I and CPSase II (B). The mitochondrial CPSase I provides carbamoyl phosphate for the arginine pathway. CPSase II of CAD is specific for the pyrimidine pathway and is feedback inhibited by UTP and activated by PRPP, an important intermediate for both the pyrimidine and the purine pathway. The ATCase of CAD unlike in *E. coli* is not under allosteric control.

A

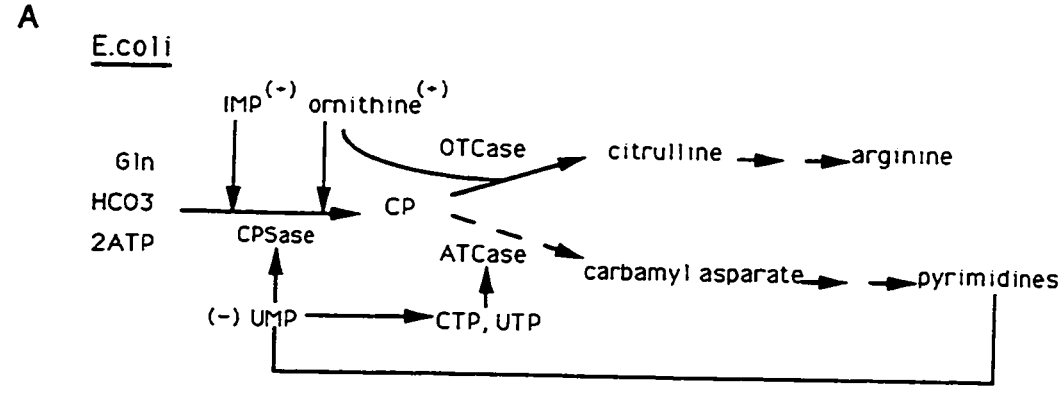
E.coli
IMP(-)
ornithine(-)
OTCase
citrulline
arginine
Gln
HCO3
2ATP
CP
CPSase
ATCase
carbamyl asparate
pyrimidines
(-) UMP
CTP, UTP

B

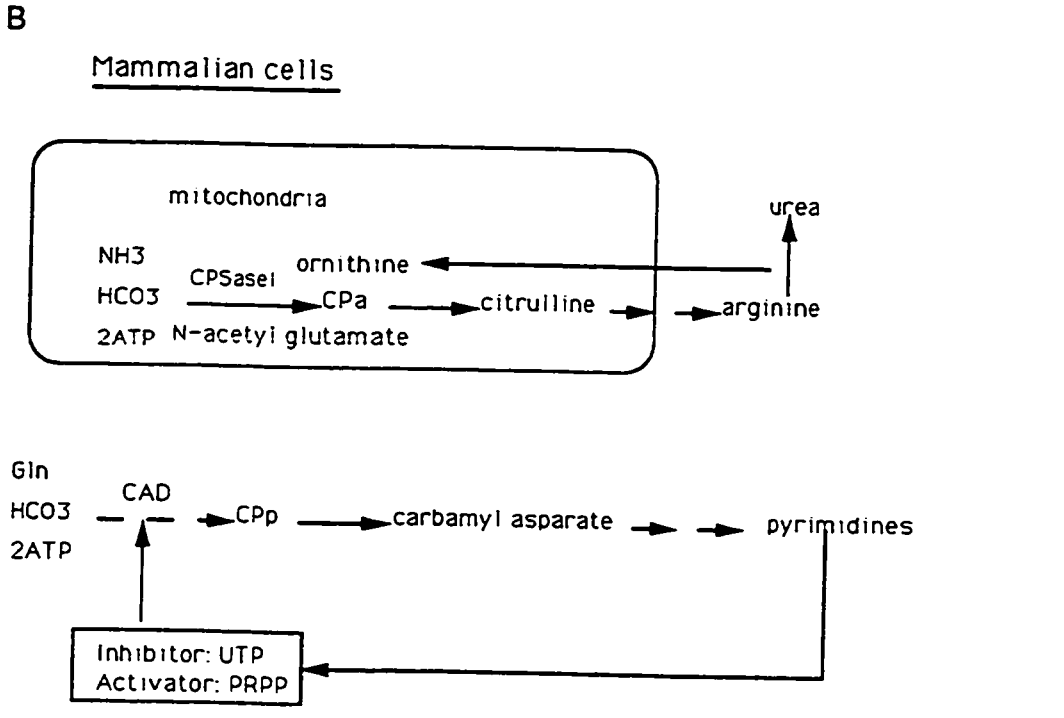
Mammalian cells
mitochondria
urea
NH3
HCO3
2ATP
CPSasel
ornithine
CPa
citrulline
arginine
N-acetyl glutamate
Gln
HCO3
2ATP
CAD
CPp
carbamyl asparate
pyrimidines
Inhibitor: UTP
Activator: PRPP

Sequence homology demonstrated an evolutionary relationship between the *carA* gene that codes for the glutaminase and other amidotransferase genes. This subunit has been shown to consist of two subdomains: the amino and carboxyl subdomains (45,47). The amino terminal of *carA* is unique to the carbamoyl phosphate synthetases and is not found in other amidotransferases. The recently solved crystal structure of the *E. coli* CPSase (48) shows that the amino terminal domain delineated by Leu1-Leu153, is composed primarily of four major α-helices and two layers of β-sheet, one of which contains four antiparallel and the other four parallel β-strands. These layers of β-sheet are oriented nearly perpendicular to each other. The carboxy terminal domain of *carA* contains the active site for the small subunit and is termed the catalytic domain (49). The COOH terminal is dominated by a ten strand mixed β-sheet, flanked on either side by two and three alpha helices respectively. Cys 269 and His 353 were identified as essential amino acid residues in the active site (42,50,51). Cys269Ser and His 353Asn mutant proteins cannot hydrolyze glutamine but can bind the substrate enhancing the rate of ATP hydrolysis within the carboxyphosphate domain significantly (51,52). It is suggested that there are conformational changes associated with the binding of glutamine that serve to prevent the release of the substrate, ammonia, into the solvent, preventing protonation to NH_4^+, and thereby maintaining catalytic efficiency.

Nyunoya and Lusty (45) sequenced the *E. coli carB* gene and found significant sequence similarity between the amino and carboxyl-terminal halves of the large subunit, suggesting that the *carB* gene may have arisen by internal duplication of a smaller ancestral gene, possibly, a carbamate kinase (53), an enzyme which produces ATP and carbamate from carbamoyl phosphate and ADP in the arginine deiminase pathway (Aabdelal 1997). Recently, a novel type of ammonia-dependent CPSase, consisting of a single 34 kDa chain, has been found in the thermophilic marine archaea *P. furiosus* (Durbecqb 1997) and *P. abyssi* (54) that could constitute an evolutionary

Figure 1.5 Partial Reactions in Carbamoyl Phosphate Synthesis

The GLNase domain hydrolyses glutamine to ammonia which is used for carbamoyl phosphate synthesis. CPS-A is known to be involved in bicarbonate activation by using one mole of ATP to produce carboxy phosphate. Ammonia is then channeled into the carboxy phosphate domain where it reacts with the carboxy phosphate to form carbamate. The CPS-B or carbamoyl phosphate synthetic domain uses a second mole of ATP to catalyze the formation of carbamoyl phosphate from carbamate.

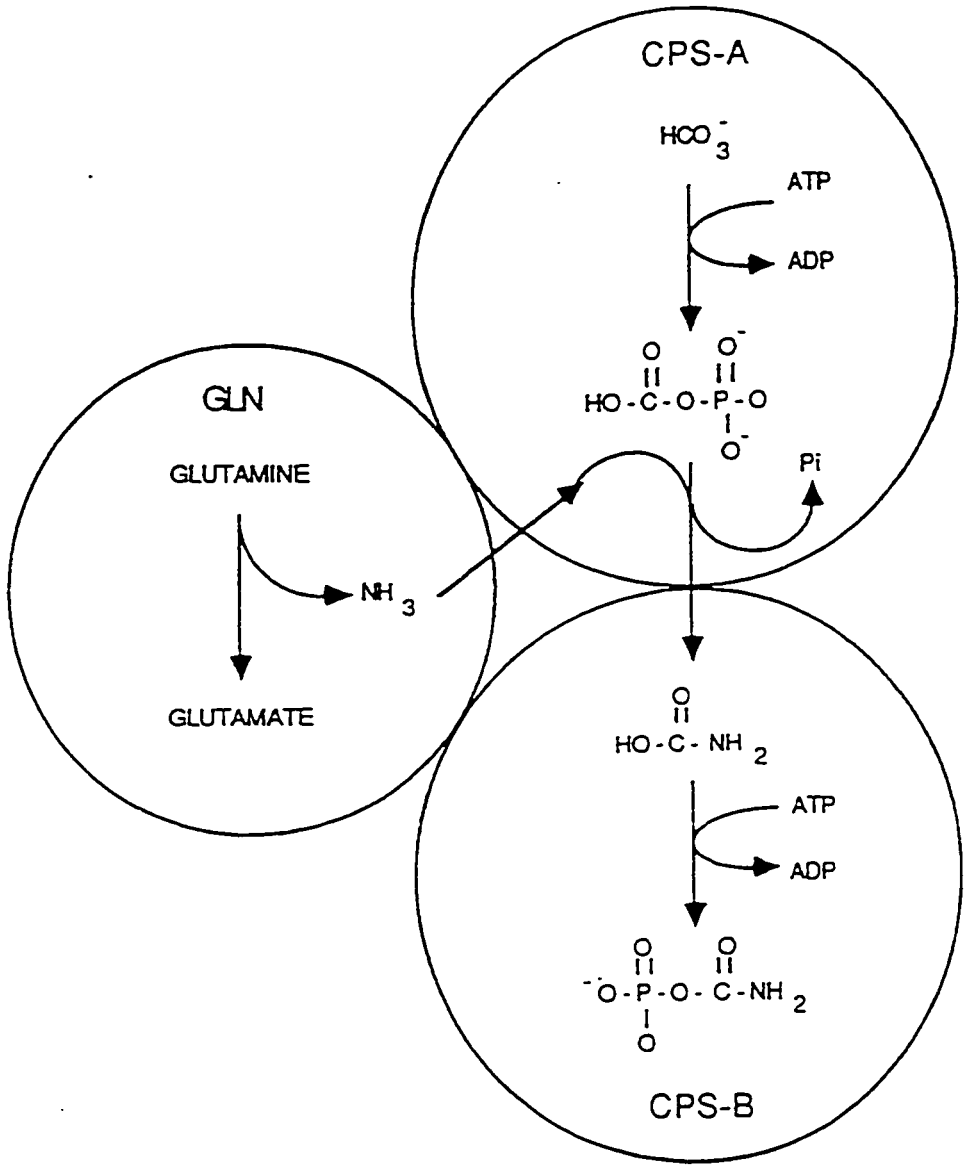
CPS-A
HCO 3 -
ATP
ADP
HO-C-O-P-O
O-
Pi
GLN
GLUTAMINE
NH 3
GLUTAMATE
HO-C- NH 2
ATP
ADP
-O-P-O- C-NH 2
CPS-B

intermediate between carbamate kinase and other known CPSases.

The crystal structure of *E. coli* CPSase (48) revealed that the large subunit, as expected from the amino acid sequence analysis, is folded into two similar halves related by a nearly exact two-fold rotational axis and is defined by Met1-Ala553 and Asn554-Lys1073. These halves referred to as the carboxy phosphate and the carbamoyl phosphate synthetic components, share forty-percent sequence identity. Both the components have been envisioned as consisting of four well-defined subdomains labeled A-D according to Raushel et al. The first three subdomains labeled A, B, and C, in the carboxy phosphate synthetic component (defined by Met1-Gly 140, Leu 141-Leu 210 and 211- Glu 403 respectively) are topologically identical to the first three subdomains (Asn 554-Lys 686, Leu 687-Leu 756, and Asp 757-Asn 936) of the carbamoyl phosphate synthetic component. Interestingly, the first three subdomains A-C in each half of the large subunit are homologous to those (residues 1-327) in biotin carboxylase, an enzyme that utilizes both ATP and bicarbonate and whose catalytic mechanism is thought to proceed via a carboxyphosphate intermediate. Amino acid sequence analysis demonstrates a forty seven percent similarity and a twenty four percent identity between biotin carboxylase and the first half of the CPSase large subunit. The D-domain in both halves is significantly different. From biochemical studies, it is known that the D-domain in the carbamoyl phosphate synthetic component is responsible for binding UMP and ornithine (55-57), the allosteric effectors of *E. coli* CPSase.

Several studies have shown that there are two physically distinct sites on the carbamoyl phosphate synthetase domain that bind the two moles of ATP utilized in the overall reaction (25,26,42,58-63). It was postulated that one of the nucleotide binding sites is responsible for the phosphorylation of bicarbonate in the synthesis of carboxy phosphate, while the other site is responsible for the phosphorylation of carboxy

phosphate to form carbamoyl phosphate (64). Site-directed mutagenesis of conserved glycine residues in the CPSase domain, demonstrated that mutants in the N-terminal half were impaired in the bicarbonate dependent ATPase reaction while the ATP synthesis reaction was not disrupted. Conversely, mutations on the C-terminal half were defective in the ATP synthetase reaction while the ATPase activity occurred at wild type rates (64). These results were interpreted to suggest that the N-terminal domain is primarily responsible for the phosphorylation of bicarbonate to carboxy phosphate while the C-terminal domain is primarily responsible for the phosphorylation of carbamate to form carbamoyl phosphate.

CAD CPSase

In mammals, the glutamine-dependent carbamoyl phosphate synthetase activity is catalyzed by two distinct functional domains of CAD. The 40 KDa GLNase and the 120 KDa CPSase domains are connected by a 29 amino acid residue GC-linker which is resistant to proteolysis, but is cleaved if digestion is allowed to proceed long enough (17).

The GLNase domain in CAD is homologous to the small subunit of *E. coli* CPSase and catalyzes the hydrolysis of the substrate glutamine resulting in the transfer of the ammonia thus produced, directly to the carbamoyl phosphate synthetase active site. The CAD GLNase domain has been cloned and expressed in *E. coli* (65). The purified GLNase domain can form a stable hybrid complex with the *E. coli* CPSase subunit. It was shown to consist of two subdomains, a catalytic subdomain that hydrolyzes glutamine to ammonia, and an interaction subdomain that is necessary for the interaction of the GLNase domain with the CPSase domain, and in suppressing the intrinsically high activity of the catalytic subdomain (49).

The GLNase and CPSase subunits are joined by a linker temed GC. The linker appears to serve as a spacer, that allows the GLN-CPS complex to cycle between two

conformations: an open low activity form in which the ammonia site on the CPS domain is accessible, and an activated conformation, in which, the ammonia generated *in situ* from glutamine hydrolysis is directly channeled to the CPSase active site, and access to exogenous ammonia is blocked. (66)

Sequencing studies have revealed that the CPSase domain of CAD has three major levels of significance (16). First, by alignment with seven other analogous sequences it was evident that the CAD CPSase was homologous to CPSases from different organisms. Based on this homology, the borders of the CPSase domain in CAD were identified. Second, as in the *E. coli* CPSase, the deduced amino acid sequence showed that there existed a significant homology between the amino (CPS.A) and carboxyl (CPS.B) halves of the CPSase domain of CAD, suggesting that CPS.A and CPS.B evolved from gene duplication of an ancestral kinase gene (53). Third, each half was found to have an ATP binding region, identified by strong homology to other ATP binding proteins.

The presence of two ATP binding sites in carbamoyl phosphate synthetases has been documented in the *E. coli* CPSase (23,59-60,67) and the mitochondrial CPSase (106). Evidence for the existence of the two ATP binding sites that exists in CAD, came from the FSBA modification experiments (Figure 1.6). FSBA, 5'-p-fluorosulfonyl benzoyl adenosine, is an ATP analog that covalently modifies the amino acid residues involved in ATP binding. In order to study the ATP binding sites, CAD was labeled with ^{14}C labeled FSBA. Sequencing studies of the isolated ^{14C} FSBA labeled peptides generated from the controlled proteolysis of FSBA modified CAD, mapped to the proposed ATP binding sites in CPS.A and CPS.B (68). The fact that the CPSase domain consists of two homologous halves, and that each half contains an ATP binding site, led to the proposal that each of the CPS.A and CPS.B subdomains can independently catalyze one of the two ATP dependent partial reactions involved in the synthesis of carbamoyl

Figure 1.6 Mapping of the ATP Binding Sites in CAD

The two solid bars indicate the proposed ATP binding region based on sequence homology. The vertical arrows represent the position of the FSBA labeled tryptic peptides. The numbering corresponds to the amino acid numbering in CAD.

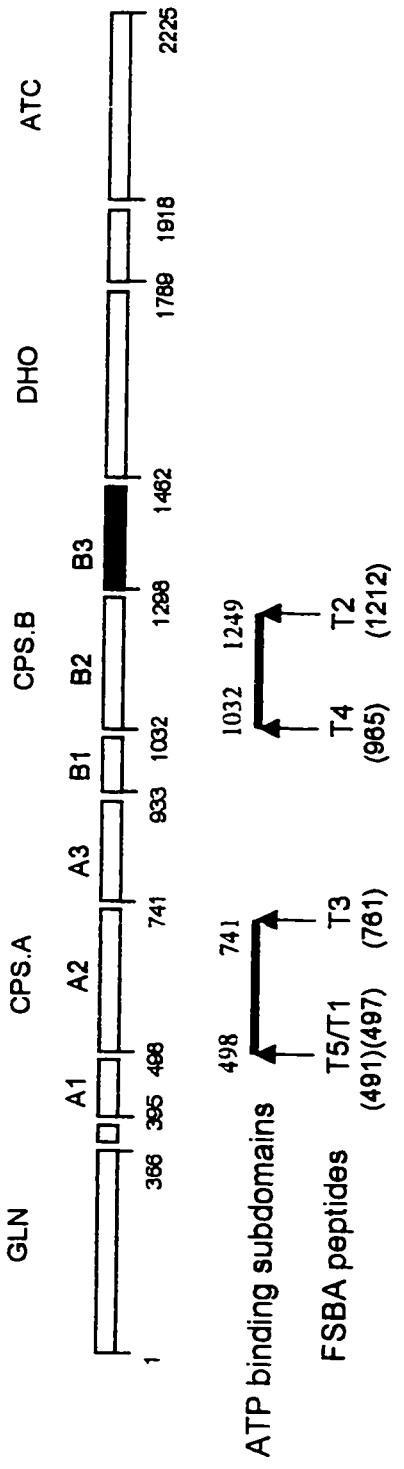
GLN
CPS.A
CPS.B
DHO
ATC
A1
A2
A3
B1
B2
B3
1
366
395
498
741
833
1032
1298
1462
1789
1918
2225
ATP binding subdomains
498
741
1032
1249
FSBA peptides
T5/T1
(491)(497)
T3
(781)
T4
(985)
T2
(1212)

phosphate. In the case of *E.coli* CPSase, mutational studies have demonstrated that the N-terminal half uses ATP for the phosphorylation of bicarbonate while the C-terminal half uses ATP to phosphorylate carbamate (69).

Although these results showing that the CPS.A and CPS.B had distinct functions were convincing, the separately expressed mammalian and *E. coli* CPS.A and CPS.B subdomains showed a surprising result. Each subdomain catalyzed the overall reaction leading to the synthesis of carbamoyl phosphate (70). The recombinant molecules were dimers but reversibly dissociate into monomers when subjected to a pressure of 1500 bars. The monomers could catalyze both partial reactions, but only the homodimer could catalyze the overall synthesis of carbamoyl phosphate. This introduced a novel finding that not only are the CPS.A and CPS.B half domains functional, but that they are functionally equivalent (Figure 1.7). The overall CPSase reactions were catalyzed by both mammalian and bacterial CPS.A and CPS.B subdomains, suggesting that this finding may be a general characteristic of all CPSase molecules.

1.5 Allosteric Regulation

CAD is the major locus of control in the *de novo* pyrimidine biosynthetic pathway (1). The CPSase domain catalyzes the first committed rate-limiting step and is subject to feedback inhibition by UTP and activation by PRPP, a purine precursor that coordinates purine and pyrimidne biosynthesis (107,108). Allosteric effects do not occur in either the ATCase or DHOase.

In addition to allosteric regulation, Carrey *et al* showed that CAD is phosphorylated by cAMP-dependent protein kinase (71). The effect of phosphorylation is to activate the CPSase and in particular, to relieve the feedback inhibition by UTP. Two sites of phosphorylation have been documented (72). Site 1, a serine 1406 residue in the carboxyl region of CPS.B, and site 2, a serine 1859 residue in the interdomain linker between the DHOase and ATCase. Limited proteolysis of CAD cleaves

Figure 1.7 Functional Model of Whole CPSase and CPS.A/CPS.B homodimers

The scheme represents a tentative model for the function of the wild type carbamoyl phosphate synthetase (GLN-CPS.A-CPS.B) and the recombinant half molecules (GLN-CPS.A and GLN-CPS.B). Only GLN-CPS.A is shown, but GLN-CPS.B is presumed to function in a similar fashion. In the wild type protein, CPS.A activates bicarbonate, while CPS.B phosphorylates carbamate and forms carbamoyl phosphate. For the recombinants, the model assumes that 1) the noncovalently associated dimer is essential for activity, 2) both subunits in the dimer A and A', in this schematic, are functionally equivalent, and 3) in some catalytic cycles glutamine binds to the GLN domain associated with the A subunit, which then catalyzes the ATP-dependent bicarbonate activation, and carbamoyl phosphate formation is catalyzed by the A' subunit, by default. In other cycles, glutamine first binds to the GLNase domain associated with A', and the roles of A and A' are reversed.

GLN-CPS.A-CPS.B

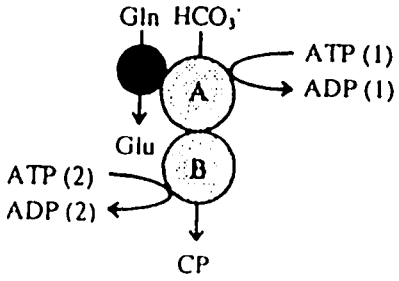

GLN-CPS.A

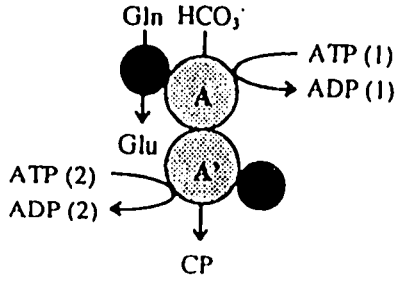

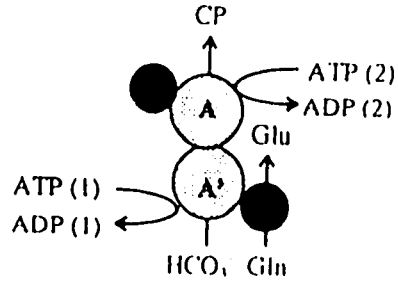

predominantly at interdomain regions releasing catalytically active fragments corresponding to the ATCase and DHOase domains (17). Phosphorylation of CAD markedly activates the rate of proteolysis. This suggested that phosphorylation causes a conformational change, probably involving interdomain movements to an 'open" form of the CAD complex in which the CPSase has higher activity with a high affinity for Mg and ATP, but one that is susceptible to proteolytic attack. UTP favors the conversion to a 'closed' conformation that is a less active form of the CPSase and less susceptible to proteolytic attack as UTP protects the hinge region between the CPSase and DHOase from proteolysis. In the phosphorylated enzyme, the open conformation is stabilized to an extent that abolishes both the effects of UTP (73). These observations suggest that the regulatory signals generated from the binding of effectors are transmitted to other domains of CAD, so that a global conformational change may be induced in the CAD molecule.

Localization of the Regulatory Domain

Carbamoyl phosphate synthetases from different organisms show a high degree of sequence homology but are controlled by different effectors. Although the overall sequence identity of these CPSases is 37- 67%, the extreme carboxyl end of the CPS.B domain, i.e. the B3 region is poorly conserved with a sequence homology of only 24-58%. The significantly lower homology found in the B3 region may be a reflection of the different types of allosteric effectors that regulate these enzymes.

Several lines of evidence confirmed that the allosteric effectors bind to the carboxyl end of CPS.B. Photoaffinity labeling studies by Rubio and associates (57,74,75), have clearly established the UMP binding site in *E. coli* CPSase. They have shown that UMP, an allosteric inhibitor of *E. coli* CPSase, and IMP, an allosteric activator, bind specifically and label the protein within 15 kDa (about 140 amino acids) of the carboxyl terminus of the large subunit (74). This observation, along with earlier

studies by Rodriguez-Aparacio et al (76) demonstrating that the activator acetylglutamate bound to the same region of ureotelic CPSase, strengthened the proposal that the carboxyl terminal domain of carbamoyl phosphate synthetases was the region involved in allosteric control and effector binding. Scanning calorimetry studies of a truncated mutant lacking 171 residues of the carboxyl end of the *E. coli* synthetase subunit suggested that ornithine also bound near the end of CPS.B (55). Another study involving the deletion of the last 119 residues, produced mutants that lacked UMP inhibition but retained sensitivity to ornithine (77). These results suggested that the UMP and ornithine binding sites are distinct. To further narrow down the UMP binding site in the *E.coli* CPSase subunit, Rubio and associates demonstrated that photolabelling of the enzyme by [^{14}C] UMP was due to the formation of a covalent adduct between UMP and lysine 992 (57). Analysis of the sequence around this lysine residue in the *E. coli* enzyme, and in other CPSases, supports the existence of a nucleotide-binding fold located entirely within the COOH-terminal domain of the protein. In CAD, further evidence implicating the carboxyl terminal domain in allosteric regulation comes from the finding of Carrey et al that phosphorylation of the pyrimidine-specific hamster enzyme at Ser 1406 located within the COOH-terminal domain decreases inhibition by UTP. Another set of experiments in which a series of CAD deletion mutants involving truncation of the carboxyl end of CPS.B were created. These mutants lost UTP inhibition while sensitivity to PRPP increased (78). These results suggested that the binding sites for both effectors in mammalian CPSase are near the carboxyl end of CPS.B, that the UTP and PRPP sites are distinct, and that the UTP site is downstream of the PRPP binding site. One of the most convincing experiments involved domain swapping between the *E. coli* and the pyrimidine–specific hamster carbamoyl phosphate synthetase (56). The *E. coli* region of *car*B gene encoding the 20-kDa putative regulatory domain was replaced by the corresponding sequence of the CAD cDNA. The

resulting chimeric protein consisted of *E. coli* catalytic domains and the putative hamster CAD regulatory region. The protein was fully active but was no longer regulated by the *E. coli* effector UMP. Instead, the protein was under the control of mammalian effectors UTP and PRPP.

Although the evidence for the location of the putative regulatory domain converges on the carboxyl end of the CPS.B, the carboxyl domain has yet to be shown to exist as an independent functional domain. My dissertation research focuses on further characterization of the regulatory domain of CAD, specifically to determine the following:

1. Can a replacement of A3 by B3 in the CPS.A domain place the CPS.A under allosteric control?
2. Can the regulatory domain function independently as an autonomously folded functional stable subdomain that binds the allosteric ligands, UTP and PRPP?
3. Can the regulatory domain form a stoichiometric complex with the isolated CPS.A domain and transmit the allosteric signals to the catalytic subdomain A2 of CPS.A?

1.6 *De novo* Pyrimidine Metabolism and Aspartate Transcarbamoylase of *P. aeruginosa*

Aspartate Transcarbamoylase catalyzes the formation of carbamoyl aspartate from carbamoyl phosphate and aspartate in the *de novo* pyrimidine biosynthetic pathway. Previously, Bethel and Jones (79) identified three classes of bacterial ATCases that differ in size and regulatory properties. Class A ATCases are the largest, sensitive to allosteric effectors and are dimeric. *Pseudomonas fluorescens* ATCase, a class A protein originally characterized by Adair and Jones (80) was found to be dimeric and composed of two 180-kDa subunits. Class B ATCases are trimeric. A typical class B protein is the *E. coli* ATCase consisting of two catalytic trimers and three regulatory dimers. Class C ATCases are smaller, insensitive to allosteric effectors and exemplified

by *Bacillus. B. subtilis* ATCase which has been shown (81) to be a trimer composed of 33.5 kDa subunits with a tertiary structure that is very similar to the *E. coli* catalytic subunit.

The class A ATCase are large molecular mass enzymes (470-600kDa) and were thought to be dimeric until the studies of the *Pseudomonas fluorescens* ATCase by Bergh and Evans (82). They demonstrated that the *P. fluorscens* ATCase exists as a trimer, with a 34-kDa catalytic chain in a dodecameric association with a 45-kDa chain of unknown origin and function. Sequencing studies of the *P. putida* (83) and the *P. aeruginosa* (Dr. J.F. Vickrey) ATCase genes further confirmed that the genes consisted of two distinct open reading frames encoding two polypeptides with a molecular weight of 34 kDa and 45 kDa. Gel filtration and non-denaturing polyacrylamide gel electrophoresis revealed that the molecular mass of the complex was about 474 kDa. Based on the mass of the constituent subunits and the stoichiometry of the complex, the *Pseudomonas putida* and *aeruginosa* proteins are dodecameric complexes composed of six copies of the 34 kDa catalytic chain and six copies of the 45 kDa polypeptide, with a calculated molecular weight of approximately 474 kDa. Given the stoichiometry of the complex, the class A ATCases are actually dodecamers, a structural organization analogous to that found in class B.

Based on the above evidence, the ATCases may be reclassified into two groups according to stoichiometry: trimers and dodecamers. However, in both classes, a common theme is that the catalytic activity is associated with the 34-kDa domain that associates to form trimers.

1.6.1 *E. coli* Aspartate Transcarbamoylase

In *E. coli*, ATCase catalyzes the first committed step in pyrimidine biosynthesis, the synthesis of carbamoyl aspartate from carbamoyl phosphate and aspartate, and is the major locus of control. *E. coli* ATCase is an allosteric enzyme which binds both

aspartate and carbamoyl phosphate cooperatively and is inhibited by CTP and activated by ATP. It consists of two distinct functional units: 33 kDa catalytic subunits which are enzymatically active, but which exhibit no allosteric transitions, and 17 kDa regulatory subunits which bind allosteric effectors, but are inactive. X-ray studies (84-86) showed that two catalytic trimers are stacked above each other in nearly an eclipsed configuration and are held together by three regulatory dimers, which remain clustered around the periphery of the molecule.

1.6.2 *Pseudomonas* Aspartate Transcarbamoylase

The *pseudomonads* are ubiquitous, gram negative obligate pathogens. The genus *Pseudomonas* is known at this time to consist of at least ten species including *Pseudomonas aeruginosa, P. acidovorans, P. fluorescens, P. maltophilia* and *P. putida*. Initially, the *pseudomonads* were divided into five distinct groups based on rRNA/DNA hybridizations. Many former species have now been reassigned to new genera based on physiological tests.

Although the pyrimidine metabolism pathway remains conserved in *Pseudomonas*, it differs significantly from that found in well-characterized species. The aspartate transcarbamoylase (ATCase) of *Pseudomonas* is unique, requiring the recruitment of a duplicated inactive dihydoorotase-like chain (DHOase-like or pseudo DHOase) possibly for catalytic activity. A comparison of the sequence of the first three pyrimidine enzymes in *Pseudomonas* with other organisms led to the identification of a new class of ATCases having unique properties and important evolutionary implications. This class and four other major classes of ATCase are shown in Figure 1.7. The *Pseudomonas* ATCase genes are arranged in an operon with two open reading frames: a 5' ORF corresponding to the *pyr*B gene, with a 40 percent (87) sequence homology to the ATCase gene from *E. coli*, and a downstream ORF with a significant sequence homology to *pyr*C gene encoding DHOase. In *P. aeruginosa*, the *pyr*B gene encodes a

Figure 1.8: Structural Organization of GATase CPSase, ATCase, and DHOase genes in the pyrimidine pathway

The arrangements are shown for genes encoding the first three enzymes from pyrimidine biosynthesis from *E. coli, S. marcescens, S. typhimurium, P. vulgaris, P.subtilis, B. caldolyticus, D. melanogaster, M. auratus, S. cerevisiae, D. discoideum, P aeruginosa and P. putida*

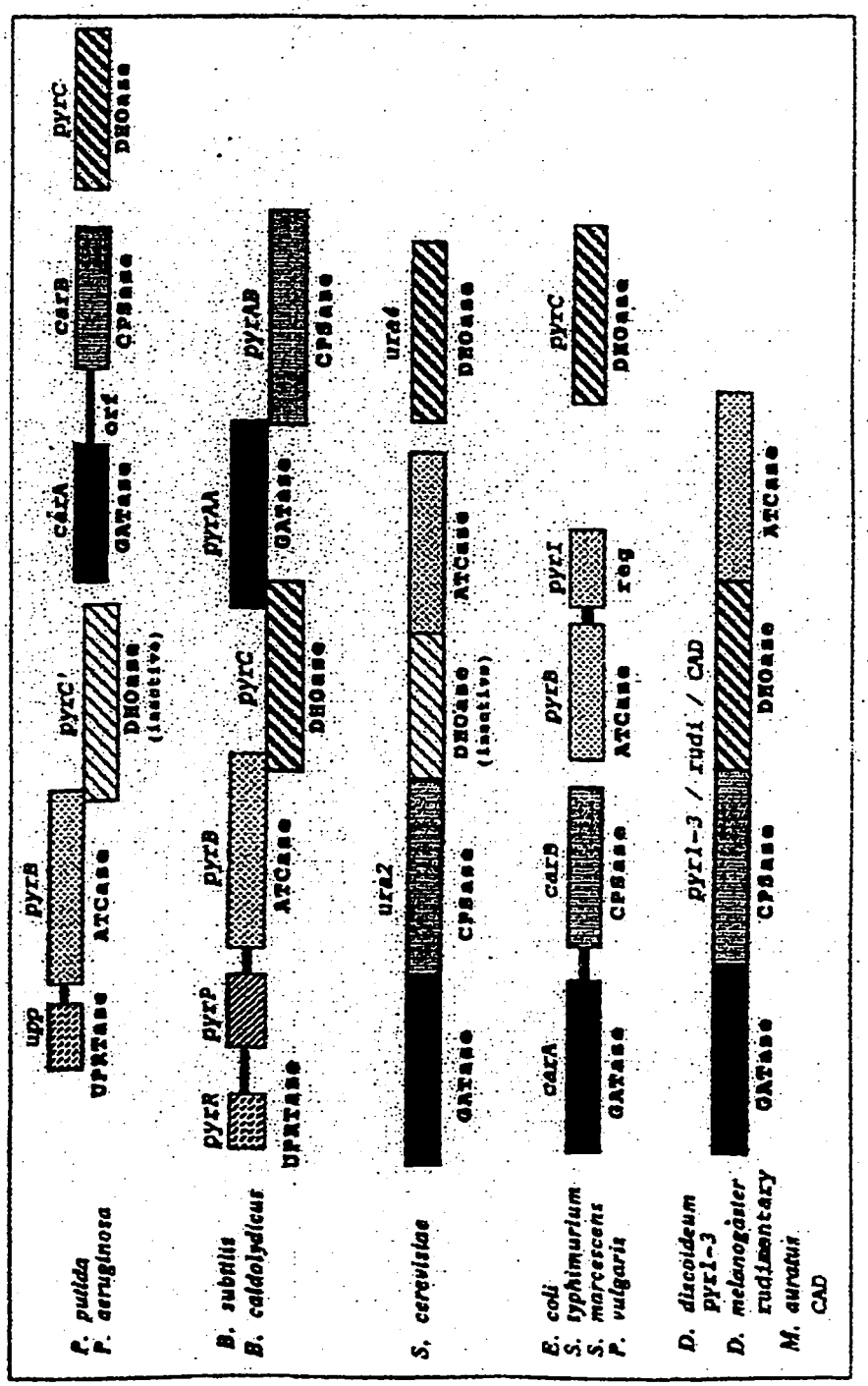
P. putida
P. aeruginosa
upp
pyrB
pyrC'
UPRTase
ATCase
DHOase (inactive)
cadA
carB
orf
GATase
CPSase
pyrC
DHOase
B. subtilis
B. caldolyticus
pyrR
pyrP
pyrB
pyrC
pyrAA
pyrAB
UPRTase
ATCase
DHOase
GATase
CPSase
S. cerevisiae
ura2
ura4
GATase
CPSase
DHOase (inactive)
ATCase
DHOase
E. coli
S. typhimurium
S. marcescens
P. vulgaris
carA
carB
pyrB
pyrI
pyrC
GATase
CPSase
ATCase
reg
DHOase
D. discoideum pyr1-3
D. melanogaster rudimentary
M. auratus CAD
pyr1-3 / rudi / CAD
GATase
CPSase
DHOase
ATCase

polypeptide of 34 kDa and the downstream ORF, with 30% homology to the *E.coli* DHOase, codes for a 44.1-kDa protein. The coding region for the downstream ORF overlaps the 3' end of the *pyr*B gene by 4 base pairs such that translational coupling can occur. Such an overlapping reading frame assures a stoichiometric expression of both the polypeptides.

Although the downstream ORF has significant sequence homology to the *pyr*C gene encoding for the dihydroorotase, the product of this downstream *pyrC'* is devoid of dihydroorotase activity. Purified ATCase holoenzymes associated with the DHOase-like chain, from several *Pseudomonas* species, including *P. aeruginosa* and *P. putida* have no DHOase activity. Moreover, in addition to the *pyr*BC' operon, there exists a separate *pyr*C gene that encodes for a catalytically active DHOase. This *pyr*C gene encoding for an active DHOase maps to a locus neighboring, yet distinct from the *pyrC'*.

The *P. putida* ATCase has an amino terminal carbamoyl phosphate domain and a carboxy terminal aspartate binding domain, as found in the *E. coli* ATCase. In *E. coli*, the ATCase domain is active only after assembly into a trimer since the active site is formed from two discrete polypeptides (88). In *Pseudomonas,* the *pyr*B and *pyr*C' ORF have been separately cloned into expression vectors. The *pyr*B clone by itself does not complement ATCase deficient *pyr*B mutant strains of *E. coli* nor produces measurable ATCase activity. However, when cotransformation of *E. coli pyr*B mutant strains with two different plasmids, one carrying a functional *pyr*B and another carrying *pyr*C', enabled the cells to grow in the absence of uracil. These complementation studies suggested that the expression of a functional ATCase requires the presence of both *pyr*B and *pyr*C' gene products. A functional dodecameric large molecular weight enzyme was assembled by both *pyrB* and *pyrC'* polypeptides suggesting that the DHOase-like subunit is essential for catalytic activity of the ATCase (Dr. John Vickrey, personal communication). This role has been proposed as the *Pseudomonas* ATCase trimer

preserves many of the same C1-C3 contacts known to exist in *E. coli* and is known to be involved in bringing the catalytic half sites together to form the active sites (89). Despite the homology, however, the *Pseudomonas* ATCase trimer, encoded by *pyr*B, has not been shown to be catalytically active, the activity is presumed to be restored by the pseudo DHOase polypeptide.

The *Pseudomonas* ATCase has a functional nucleotide effector-binding region proposed to be at the amino terminus of the ATCase catalytic chain (Gerry O'Donovan). This theory is based on three lines of evidence: 1) Bergh and Evans demonstrated that labeled ATP bound to the 34 kDa catalytic polypeptide of the ATCase holoenzyme from *Pseudomonas fluoroscens* (82). 2) A deletion of 34 amino acids from the amino terminus end of the *P. putida pyr*B polypeptide resulted in a mutant that still had ATCase activity but lost sensitivity to ATP. 3) A weak consensus ATP/GTP nucleotide binding motif was located on the amino terminus end (83).

In prokaryotes, DHOases are monofunctional proteins but in higher eukaryotes, DHOase is part of the first three enzymes of the pyrimidine pathway that exist as a multifunctional enzyme encoded by the CAD gene. However, there is a low degree of similarity between the multienzyme eukaryotic CAD DHOase sequences and the DHOase sequences in *E. coli, S. typhimurium, and the URA4 gene in S. cervisiae.* Simmer et al (15) have speculated on whether the genes encoding the two families have diverged from a common ancestor, or have arisen by convergent evolution. With respect to divergence, they proposed that after the fusion of the genes encoding the CPSase and ATCase in the CAD precursor, a linker region was left between them. The next event was the insertion of a DHOase sequence into this region, produced by the duplication of a monofunctional *E. coli*-like DHOase gene. In case of CAD, this gene, following several changes, became fully functional, while the other copy of the gene would become redundant and eventually extinct. Failure of the inserted gene to become

fully functional could explain the situation in the yeast *URA2* gene, where the linker region between the CPSase and ATCase encodes an inactive DHOase, while the functional DHOase is encoded by the monofunctional *URA4* gene.

In the case of *Pseuodmonas*, a careful examination of the *pyr*C' amino acid sequence shows that the sequence homology to other DHOases is not conserved at critical residues. In all known active DHOases, five histidine residues are found at the active sites and thought to be involved in substrate binding (15). In the *P. aeruginosa* and *P. putida* DHOase, only one of the five critical histidines is present. Detailed kinetics studies of the *Pseudomonas aeruginosa* ATCase are being carried on by Dr. John Vickrey in our laboratory. Velocity-substrate plots give Michaelis-Menten kinetics for both the substrates carbamoyl phosphate and aspartate. The results obtained have shown that micromolar concentrations of ATP, UTP and CTP strongly inhibit the enzyme, despite the fact that the intracellular concentrations are in the millimolar range. This prompted the search for metabolites that may reverse the nucleotide inhibition.

2.1 Plasmids and Strains

See Table 2.1 for *E. coli* strains and Table 2.2 for plasmids used.

2.2 Buffers and Reagents

Preparation of Neutralized Phenol

BRL ultrapure phenol (ca # 5509 UA/UB, 100 g bottle) stored at -20°C was thawed to room temperature. The cap was loosened and the bottle placed in a 68°C water-bath until it became completely liquid. Filter sterilized 1M Tris-HCl, pH 8.0 was added up to the neck of the bottle, to about 80 ml, while the solution was warm. An antioxidant, 8-hydroxyquinoline (0.1% w/w, typically 0.1g) was added and the solution mixed by inverting the bottle. The mixture was stored overnight at 4°C to saturate the phenol with buffer. The phenol was warmed to room temperature and then poured into a separatory funnel and the lower yellow layer was extracted three times with 100 mM Tris-HCl in the hood in the dark. The phenol was stored in an amber bottle with about an equal volume of 100 mM Tris-HCl, pH 8.0 at 4°C. The neutralized phenol was used within a month.

Preparation of [^{14}C]-Carbamoyl Phosphate

Radioactive carbamoyl phosphate was purchased from American Radiolabeled Chemical Inc. Non-radioactive dilithium carbamoyl phosphate (200 mg), purchased from Sigma, was dissolved in ice-cold sterile water to 218 mM. The [^{14}C] carbamoyl phosphate (1.5 mg, 50 μCi) was dissolved in a known volume (about 1 ml) of the 218 mM stock solution added directly to the vial. A small aliquot of the dissolved stock solution, about 5 μl, was counted at this point. Since the contaminants were insignificant, the specific radioactivity could be calculated and used to determine the final concentration of the carbamoyl phosphate. The final concentration was then adjusted to

50 mM. Aliquots of 0.5 ml were then transferred to capped vials and stored at -20°C. Under these conditions, the carbamoyl phosphate is indefinitely stable. The specific activity of the [^{14}C]-CP prepared by this procedure, typically 75,000 cpm/μmole, was measured by adding 0.01 ml to 10 ml of ACS (Amersham) scintillation fluid and counting in a Tri CARB 460 scintillation counter (^{14}C program).

Column Buffer A

This is the CAD storage buffer. It consists of 0.02 M Tris-HCl pH 7.4, 0.05 M KCl, 4 mM aspartate, 4 mM glutamine, 0.1 mM EDTA, 5% glycerol, and 30% DMSO.

SDS PAGE Buffer

Stacking gel buffer

1.0 M Tris-HCl, pH 6.9

Running gel buffer

1.5 M Tris-HCl, pH 8.8

Sample Buffer

This is a 5X buffer consisting of 0.78 ml 1M Tris-HCl, pH 6.9, 0.625 ml of β-mercaptoethanol, 0.5 ml of glycerol, 0.25 ml of 1% bromophenol blue, 0.125 ml of 0.1 M EDTA and 10% SDS.

TAE Buffer for Agarose Gel Electrophoresis

This buffer contains 40 mM Tris-HCl, pH 8.0, 1 mM EDTA. Normally it is prepared as a 50X buffer and diluted with water just prior to electrophoresis.

2.3 Media

LB Medium

This media contains 10 g tryptone, 5 g yeast extract and 10 g sodium chloride per liter of media prepared. The solution is sterilized by autoclaving for 45 min at 121°C. The media can be stored at 4°C with or without any antibiotic.

Table 2.1. *E. coli* Strains

Strain	Genotype	Phenotype	Growth Requirements
L673 (90)	HfrH, carA50, thi-1 relA1, lon-10, lac122 I^-, spoT1	lacks both CPSase subunits, Lon protease deficient	arg (100 μg/ml) uracil (100 μg/ml) thiamine (2 μg/ml)
EK1104 (91)	F^-, ara, thi, Δ-lac, ΔpyrB, $pyrF^+$, rpsL	lacks ATCase catalytic and regulatory chains	uracil (50 μg/ml)
RC50 (91)	carA 50, thi-1, malA1, xyl-7, rspL135, λ^r, λ tsx-273	lacks *E. coli car* A and *car* B genes	0.1% glucose
BL21(DE3)	F^- omp T hsd $S_B(r_B^- m_B^-)$ gal dcm (DE3)	expression host, λ DE3 lysogen	

Table 2.2 Recombinant Plasmids

Plasmid	Vector	(kb)	Insert	Protein Encoded
pEK81(91)	pUC119	(6.0))	2800 (1-2800)	*E.coli* ATCase
pCK-CAD10(20)	pEK81	(10.8)	6863 (-2-6863)	CAD
pHN-12(50)	pUC19	(6.8)	3219 (1-3219)	*E.coli* CPSase
pHL-2(56)	pHN-12	(6.1)	2679 (1-2679)^{e} 603 (3780-4383)^{m}	A123B12^{e}B3^{m} hybrid
pHE-A12^{e}B3^{m}	pHL2	(4.3)	1077 (1-1077)^{e} 491 (3892-4383)^{m}	A12^{e}B3^{m}
pNS-A12^{e}B3$^{m}\Delta$	pHL2	(4.2)	1077 (1-1077)^{e} 313 (3892-4205)^{m}	A12^{e}B3$^{m}\Delta$
pJB-B3	pEK81	(4.0)	570 (3795-4365)	CAD-B3
pRSET	pUC19	(2.9)	———	His-tag vector
pNS-R27	pRSETA	(3.5)	570 (3795-4365)	CAD B3
pHL-1	pEK81	(7.8)	4362 (-2-4362)	GLN-CPS^{m}
pHN-AB	pRSETC	(6.1)	2267 (1095-4362)	CPS-AB
pNS-A72	pHN-AB	(4.7)	1790 (1095-2885)	CPSA

e= *E. coli*. m=mammalian

2XYT Medium

This medium consisted of 8 g tryptone, 5 g of yeast extract, and 5 g of NaCl in 500 ml of Milli-Q water. The solution is sterilized by autoclaving at 121°C for 45 min.

Minimal medium for induction of plasmids in L673/EK1104 *E. coli* strains

For 1 liter, a solution consisting of 6 g Na_2HPO_4, 3 g KH_2PO_4, 1 g NH_4Cl, 0.5 g NaCl, 5 g Casamino acids (DIFCO 0230), 965 ml H_2O was autoclaved and allowed to cool below 50°C. The following filter sterilized stocks were added to the cooled broth: 20 ml of 20% glucose, I ml of 50 mg/100 ml $ZnSO_4.7H_2O$, 1 ml of 0.5% vitamin B1, 1 ml of 1.0% of tryptophan. This medium which contained all the supplements necessary for growth except for uracil and ampicillin, was stored at 4°C. Appropriate amounts of uracil (12 μg/m) and ampicillin (100 μg/ml) were then added to the desired amount of medium for induction.

2.4 Plasmid Isolation

Isolation of Plasmid DNA by the mini-prep method

The RPM Kit from BIO 101 was used for the isolation of DNA on a small scale. A 10 ml overnight culture in 2XYT/LB containing 100μg/ml ampicillin was grown from a single colony at 37°C. The cell culture was pipeted into epitubes, 1.5-2 ml per epitube, and the tubes centrifuged for 1 min at 3000 rpm in a micro-centrifuge. The supernatant was decanted and any remaining media carefully pipeted out. Each pellet was resuspended in 50 μl of a kit supplied Pre-Lysis buffer. The cells were treated with 100 μl of the Lysis Buffer for 5 minutes. The increasing viscosity followed by a clearing of the solution was an indication of complete lysis. Following lysis, 75 μl of the Neutralizing buffer was added and the solution mixed by gently inverting the epitube. This allowed precipitation of the genomic DNA. In order to pellet the precipitated genomic DNA, the tube was centrifuged at 14,000 rpm, at room temperature for 2 minutes. The clear supernatant containing the plasmid DNA was then carefully

pipetted out on to a fresh, sterile spin filter provided with the kit and 250 µl of glassmilk was added. The contents were mixed by gently resuspending and then centrifuged for 1 minute. After the flowthrough was discarded, 350 µl of the Wash Buffer was added to the spin filter and incubation continued for 5 minutes. The epitube holding the spin filter was centrifuged for 2 minutes at 14,000 rpm and the flowthrough discarded. The spin filter was then transferred to a fresh, sterile epitube. The DNA was eluted by the addition of 50 µl of sterile water or TE to the center of the spin filter and the tube centrifuged at 14,000 rpm for 30 seconds. A more concentrated DNA could be obtained by using only 30 µl water or TE. The DNA was stored at 4°C. The quality of the plasmid prep was assessed by running about 0.5-1 µg on a 0.8% agarose gel as described below.

Large scale Plasmid Isolation

The QIAGEN plasmid purification kit was used for preparations of up to 500 µg of plasmid. QIAGEN plasmid purification protocols are optimized for use with cultures grown in standard Luria-Bertani (LB) medium at a cell density of approximately 1 X 10^9 cells per ml (approximately 1-1.5 A_{600} units/ml). A single colony of cells harboring the desired plasmid was inoculated in 5 ml LB containing 100 µg/ml ampicillin and grown overnight at 37°C. The overnight culture was used to inoculate 100 ml of media in a 1 liter flask. When the cells reached an absorbance of 0.8-1.0 at 600 nm, they were chilled on ice for about 5 min and harvested by centrifugation in a refrigerated benchtop centrifuge at 4000 rpm, 4°C, for 30 minutes. The pellet was resuspended in 4 ml of buffer P1. Buffer P2 (4 ml) was added, mixed by resuspending, and incubation continued for 5 minutes at room temperature to ensure complete lysis of the cells. The genomic DNA was precipitated with 4 ml of chilled buffer P3. Following a 15 minute incubation on ice, the precipitate was pelleted by centrifugation at 14,000 rpm for 30 minutes at 4°C. The supernatant containing the plasmid DNA was applied to a QIAGEN-tip 500, previously equilibrated with 4 ml of buffer QBT. The QIAGEN-tip 500

was washed with 2 X 10 ml of buffer QC. The DNA was eluted with 5 ml of buffer QF and precipitated with 0.7 volumes of isopropanol. The precipitate was pelleted by centrifuging at 15,000 xg at 4°C for 30 minutes. The DNA pellet was washed with 5 ml of cold 70% ethanol, air dried for 5 minutes and redissolved in a suitable volume of water or TE buffer. Typically, 200-300 μg DNA could be obtained from a 100 ml culture.

2.5 Polymerase Chain Reaction

The PCR reaction was carried out in a Perkin Elmar *Cetus* DNA Thermal Cycler (*Cetus* Corporation) according to the procedure included in the Bohringher Mannheim PCR Kit.

A typical reaction mixture (50 μl) contained 100-250 μM of each dNTP, 0.5-1 μM of each primer, 10 ng of template DNA, 1.5-2.5 units/50 μl *Pfu* DNA Polymerase (Stratagene), and 10X reaction buffer (Stratagene). The 5' and the 3' primers, typically 15-30 bases, with mismatches at the 5' end resulting from engineered sequences, were ordered from IDT Technologies or GIBCO BRL. For ease of cloning, restriction sites were engineered at the ends of both primers. To ensure complete restriction digestion at both ends of the PCR product, 4-5 bases were added to the extreme end of both primers. The concentration of the primer was quantitated by absorbance at 260 nm using the conversion value $O.D._{260}$ (1) = 33 ng/μl. The primers were then diluted to a 10 mM stock solution from which 2.5 μl was used for each PCR reaction. Standard PCR amplification reactions typically required 25-30 cycles to obtain a high yield of the PCR product. Because high fidelity was a concern in case of expression cloning, a minimum number of cycles for *Pfu* DNA polymerase-based PCR were used. The PCR cycle contained the following segments:

Denaturation for 1 min @ 94°C

Annealing for 1 min, @ 40-60°C

Extension for x min @ 72°

Where x depends on the size of the DNA fragment to be amplified.

The annealing temperature was calculated by the following empirical equation

$$T_d = 4X \text{ (number of G, C bases)} + 2X \text{ (number of A, T bases)}$$

$$T_a = Td - 5°C$$

where T_d and T_a, are the temperatures of denaturation and annealing respectively. The reaction was carried out for 25-30 cycles followed by a final elongation for 10 min at 72°C. Once the optimal conditions for the PCR was determined, the reaction volume was scaled up to 100 µl per reaction. Typically, a 5X 100 µl PCR yields enough DNA for subcloning purposes.

The amplified DNA was extracted using the QIAquick PCR purification Kit from QIAGEN. One volume of the PCR reaction was treated with 5 volumes of Buffer PB (QIAGEN). The sample was then applied to a QIAquick spin column placed in a 2 ml collection tube. After centrifuging for 30-60 sec, the flow-through was discarded and the spin column placed back in the same collection tube. To wash, 0.75 ml of Buffer PE (QIAGEN) was added and the column centrifuged at 14.000 rpm for 30-60 seconds. The flow-through was discarded and the spin column spun for an additional 1 min at maximum speed. The QIAquick column was then placed in a sterile 1.5 ml microfuge tube. The DNA was eluted with 50 µl of TE or H_2O added to the center of the filter, let stand for 1 min and centrifuged at 14,000 rpm for 1 minute.

2.6 Electrophoresis

Agarose Gel Electrophoresis

The HOEFER mini DNA electrophoresis apparatus was used for electrophoresis of DNA samples. Agarose (0.8 g) was dissolved in 100 ml TAE electrophoresis buffer containing 40 mM Tris-acetate, pH 7.7, 1 mM EDTA and heated in a microwave for 1 5 minutes. The agarose gel concentration ranged from 0.4-3% (w/V) depending on the size of the DNA fragment to be resolved. Fragments in the 1-20 Kb range can be

separated on 0.5% gels, while 2% gels are suitable for 0.1-1 Kb fragments. Typically, 0.8% agarose gels were run. The boiled agarose was cooled down to about 50°C. 1 µl of 0.5 µg/ml ethidium bromide was added. The cooled agarose solution was then poured into the gel casting apparatus. A 1.5 mm thick comb with 5 mm wide teeth was clamped vertically about 2 mm above the plate. The gel was allowed to set for about an hour. The gel surface was dampened with electrophoresis buffer, the comb removed, and the gel plate placed in the gel tank with enough buffer to cover the gel.

Samples were prepared by mixing the DNA with 1/5 the volume of sample buffer prior to loading. Gels were electrophoresed at 10 V/cm for 1-2 hours until the dye front reached about 1 cm from the bottom of the gel. The DNA fragments separated on the gel were then viewed and photographed on a short wave UV- transilluminator using an MP4 camera fitted with suitable ultravoilet filters.

Three forms of the plasmid DNA can be resolved by gel electrophoresis (92). Migrating the fastest through the gel is the supercoiled form while the slowest is the linear form. The nicked form has intermediate mobility.

Preparative Gel Electrophoresis

Samples were run on a 0.8% agarose gel containing ethidium bromide as described previously and visualized using longwave ultravoilet rays. The desired DNA fragments were cut out using a scalpel as close to the edges of the band as possible. The ultravoilet exposure was kept to a minimum in order to avoid any damage to the DNA. The DNA was extracted from the agarose gel using the QIAGEN Gel extraction Kit.

Sterile 1.5 ml epitubes containing the gel pieces were treated with 3 volumes of Buffer PB and incubated at 50°C for about 10 min, inverting every 2 min till the gel completely dissolved. One gel volume of isopropanol was added to the mix and the pH mantained below 5.5 with 10 µl of 3NaAc solution in order to ensure efficient biniding of

the DNA to the QIAquick spin filter. The sample was then added to a QIAquick spin column placed in a 2 ml collection tube. After centrifuging for 30-60 sec, the flowthrough was discarded. As the spin column is equipped to only handle 0.8 ml sample, multiple loading of the column was necessary in case of larger sample volumes. The filter was washed with 0.750 ml of Buffer PE and centrifuged 30-60 sec to discard the flow through. The QIAquick column was spun at maximum speed an additional 1 min to remove any excess wash buffer. The QIAquick column was placed in a clean sterile 1.5 ml microfuge tube. The DNA sample was eluted by the addition of a 50 µl 10 mM Tris-HCl, pH 8.5 or H_2O to the center of the QIAquick column and centrifuging for 1 minute. Alternatively, for increased DNA concentration, the elution volume may be reduced to 30 µl and let stand for 1 min prior to centrifugation. The DNA was stored at 4°C until further use.

SDS-Polyacrylamide Slab Gel Electrophoresis

The Laemmli system, which uses a discontinuous buffer system, is the most common electrophoresis protocol for SDS-denatured proteins (93). The Mighty Small II Gel SE 250 electrophoresis unit from HOEFER consisting of 10 X 8 cm gel slabs were used. The running gel was usually 10% acrylamide, 2.7% crosslinker (bis-acrylamide) which resulted in a medium pore size. The stacking gel was 4% acrylamide with 2.7% crosslinker. The acrylamide stock solution was 30% (w/v) acrylamide (BIO-RAD. electrophoresis grade reagent) and 0.8% (w/v) N, N-methylene-bis-acrylamide (BIS). The gel was polymerized by the addition of 0.03% (v/v) N, N, N', N' tetramethylethylenediamine (TEMED) and 0.03% (w/v) ammonium persulfate (BIO-RAD). The electrode buffer contained 0.192 M glycine, 0.025 M Tris-HCl, pH 8.3 and 0.1% SDS. The electrophoresis was carried out at a constant current of 40 mA. When the dye front reached the bottom of the gel the electrophoresis unit was disassembled. The gel was stained in 0.05% (w/v) Coomasie Brilliant Blue R reagent in 45% (v/v)

methanol and 9% (v/v) acetic acid, and destained in 30% (v/v) methanol and 7.5% (v/v) acetic acid.

2.7 Immunobloting

SDS-polyacrylamide gel electrophoresis was carried out according to Laemmli. The gel was allowed to run until the tracking dye front disappeared. The stacking gel was then carefully cut out and discarded. The running gel, a piece of nitrocellulose cut the same size of the running gel, and the filter paper blotters (HOEFER TE22) to be used in the next step, were soaked in Towbin buffer (25 mM Tris, 192 mM glycine, 0.1% SDS, 20% v/v methanol, pH 8.3) for 15 minutes. A sandwich was then assembled (foam sponge, blotter, gel, nitrocellulose, blotter, foam sponge) taking care to exclude air bubbles. The sandwich was placed in the transfer tank filled to the required mark with chilled Towbin buffer, with the nitrocellulose sheet facing the anode ensuring the transfer of proteins from the gel to the nitrocellulose. Transfer was carried out at constant current of 0.4 A, and the voltage maintained at 100 volts for one hour.

Following transfer, the unit was disassembled and the gel stained with Coomassie stain in order to check the efficiency of the transfer. The immunoblot was incubated in TBST (10 mM Tris-HCl, pH 8.0, 150 mM NaCl, 0.1% Tween 20) containing 3% non-fat dry milk for 30 minutes to block any non-specific binding, then rinsed well in TBST to remove the milk. The membrane was incubated with primary antibody (1:5000 for Anti Xpress antibody from Invitrogen) in TBST for 1 hr at room temperature. Sensitivity was increased by increasing the antibody concentration (1:2500) or by increasing the duration of incubation with the antibody. The membrane was then washed three times for 5 min each by gentle shaking in TBST at room temperature. It was then incubated with a suitable secondary antibody diluted in TBST (1:1000) for 30 minutes at room temperature. Following several washes with TBST, the antibody tagged bands were visualized by a substrate color development with 30 mg 4-chloro-1-

napthol (4CIN) in 10 ml methanol, 50 ml TBS, and 20 µl H_2O_2. With 5-100 ng total protein, strong purple signals appeared within 15 minutes. Development of color continued for at least 4 hours. The reaction was stopped by soaking the membrane in water and stored moist in plastic at 4°C.

2.8 Protein Determination

The Micro BCA Protein Assay Reagent Kit from PIERCE was used for the quantitative colorimetric determination of total protein in dilute aqueous solutions. The reagent system utilizes bicinchoninic acid (BCA) as the detection reagent for Cu^{+1}, which is formed when Cu^{+2} is reduced by protein in an alkaline environment. The purple-colored reaction product is formed by the chelation of two molecules of BCA with one cuprous ion (Cu^{+1}). This water-soluble complex exhibits a strong absorbance at 562 nm, which is linear with increasing protein concentrations. The macromolecular structure of the protein, the number of peptide bonds and the presence of four amino acids (cysteine, cystine, tryptophan and tyrosine) are reported to be responsible for color formation with BCA.

Protein standards were prepared by diluting the 2.0 mg/ml BSA standard stock in the same diluent as the sample. The BCA Working Reagent was prepared by mixing 25 parts of Reagent MA (containing sodium carbonate, sodium bicarbonate, sodium tartarate in 0.2N NaOH) and 24 parts of Reagent MB (containing bicinchoninic acid 4% in H2O) with one part of Reagent MC (containing 4% cupric sulfate, pentahydrate in water). Upon the addition of reagent MC to the solution of the other reagents, turbidity was observed, that quickly disappeared upon mixing to yield a green working reagent.

Each standard or unknown sample (1 ml) was pipetted into appropriately labeled test tubes, while one ml of the diluent was used for the blank. The working reagent (1 ml) was added to each tube and mixed well. All the tubes were incubated at 60°C for 60 minutes. Following incubation, the tubes were cooled to room temperature. The

absorbance at 562 nm of each tube versus a water reference was measured. The average 562 nm readings for the blanks were subtracted from the 562 nm reading of each standard or unknown sample. A standard curve was plotted with the average blank corrected for each BSA standard versus its concentration in μg/ml. Using the standard curve, the protein concentration for each unknown sample was determined.

2.9 Enzyme Assays

Aspartate Transcarbamoylase Assay

The method relies on the enzymatic conversion of radioactively labeled carbamoyl phosphate to acid stable carbamoyl aspartate. The stock assay buffer (common buffer A) consisted of 0.25 M Tris-HCl, pH 8.0, 0.25 M KCl, 0.0625 M $MgCl2.6H_2O$. 18.7% v/v DMSO, 6.25% v/v glycerol. The working assay buffer prepared fresh each time was made by adding 20 ml of common buffer A, 2.5 ml of 20 mM DTT, and 2.5 ml of 240 mM aspartate, pH 8.0. The assay mixture consisted of 0.5 ml of the working assay buffer and 0.490 ml of sample and water. The mixture was pre-equilibrated at 37°C for about 5 minutes. The reaction was initiated by adding 10 ul of the substrate [^{14}C] carbamoyl phosphate (75,000 cpm/μmole, 50 μmole/ml). After 15 min the reaction was terminated with 1 ml of 10-40% trichloroacetic acid (TCA) which converted the unreacted [^{14}C] carbamoyl phosphate to [^{14}C] carbon dioxide. The acid was added under the hood. The samples were then transferred to glass scintillation vials and heated uncovered, at 100°C to dryness. The precipitate was resuspended with 250 μl water. High flash point cocktail safety-solve scintillation fluid (10 ml) was added to each vial. Each vial was mixed thoroughly and counted in a Packard Tri CARB model 460 liquid scintillation counter. Since carbamoyl phosphate is acid labile, the counts represent the acid stable carbamoyl aspartate produced during the 15 min assay.

Carbamoyl Phosphate Synthetase Assay

The assay measures the incorporation of radioactively labeled sodium

bicarbonate into carbamoyl phosphate. The working assay buffer was prepared by adding 10 ml of Common Assay Buffer A (described above for the ATCAse assay), 2.5 ml of 10 mM DTT, 1.25 ml of 70 mM glutamine for the Gln-dependent CPSase assay, or 0.266 ml of 2 M ammonium chloride, pH 8.0, for the ammonia-dependent CPSase assay, and 5.03 ml of water. To trap the carbamoyl phosphate generated during the course of the reaction as an acid stable carbamoyl aspartate, 0.1 ml of 1 mg/ml purified *E. coli* ATCase and 2.10 ml of 240 mM aspartate, were also added to the working assay buffer. The assay consisted of 0.375 ml of the working assay buffer and 0.075 ml of the sample and water. The reaction was initiated by 0.05 ml of an initiation mixture consisting of 480 µl H_2O, 480 µl 250 mM unlabeled reagent grade $NaHCO_3$ and 40 µl [14C]-$NaHCO_3$ [NEN #NEC-086H, 50 mCi/mmole, 1mCi.ml] with a final $NaHCO_3$ concentration of 12 mM. The total assay volume was 0.5 ml. The assays were typically carried out at 37°C for 20 minutes (109), then quenched with 0.5 ml of 10-40% TCA and processed as described for the ATCase assay.

2.10 Immunoprecipitation Using Protein A Sepharose

Immunoprecipitation was carried out as described by Davidson et al. About 0.2 ml of cell extract (4 mg protein), was used for each assay. The cell extracts were dialyzed before incubation to remove any DTT present, in order to prevent cleavage of the disulfide bonds present in the IgG heavy and light chains. To avoid this dialysis step, most of the time reducing agents were not added in the resuspension buffer. The Protein A Sepharose resin which is supplied as a dry powder (Sigma P-3391) was suspended for 15 minutes in 0.1 M phosphate pH 7.0 (2 ml per 250 mg resin). It was then washed with 10 volumes 1X PBS (10 mM phosphate, 130 mM NaCl, pH 7.2) to remove the lactose and dextrans. The resin was recovered after each wash by filtration using a 250 µm filter. After washing, the resin was returned to the original bottle and resuspended (1 ml per 250 mg resin). Sterile solutions were used throughout resin

preparation. The sonicates were incubated overnight with primary antibody on a rotating mixer at 4°C. The resin was then added and the incubation continued for about 1 hour in the cold with gentle mixing. The resin was then washed 3 X with 1X PBS and spun down for 10 min, 6000 rpm each time. At this point, the enzyme attached via the antibody to the resin was assayed for catalytic activity or analyzed by SDS-polyacrylamide gel electrophoresis. For electrophoresis, 5X-sample buffer was added to the resin, and the tubes heated for 15-20 min at 70°C. They were mixed once during the incubation. The resin was removed by centrifugation at 14,000 rpm, 10 min at room temperature, and the supernatant loaded an SDS-gel. The enzyme-antibody complex dissociates from the resin during denaturation in sample buffer. In some instances, the gradient gels resulting in higher resolution were used. Rabbit IgG heavy chains migrating at about 50 KDa, and the light chains at about 23-29 KDa are visible as prominent bands on the gel.

2.11 DNA Sequencing

Sequencing was performed by the Sanger Dideoxy chain termination method, following the Sequenase version 2 method developed by United States Biochemical (USB). Double stranded DNA templates were prepared. The alkaline denaturation method (NKd-97) was used to denature the double stranded DNA. The double stranded DNA was denatured by adding 0.1 volumes of 2 M NaOH, 2 M EDTA and incubating the reaction mix for 30 min at 37°C. The mixture was neutralized by adding 0.1 volume of 3M sodium acetate (pH 4.5-5.5). The DNA was precipitated with 2-4 volumes of ice-cold ethanol for 30 min at -70°C and centrifuged at 14,000 rpm, 4°C for 30 minutes. The pellet was dried, resuspended in 7 µl sterile water, 2µl of Sequenase 5X Reaction buffer, and 1 µl of primer were added. This annealing mix was placed in a 65°C heat block for 2 min, then allowed to cool to room temperature over a 30 min period. The tubes were then transferred to ice. The 5X labeling mix was diluted to a I X concentration. The

Sequenase T7 polymerase enzyme was diluted 1:8 with ice-cold enzyme dilution buffer containing 10 mM Tris-HCl, pH 7.5, 5 mM DTT, 0.5 mg/ml BSA. A mixture of 1 µl of 0.1 M DTT, 2 µl diluted labeling mix (1.5 µM dGTP, 1.5 µM dCTP, 1.5 µM dTTP), 2µl (20 µCi) [^{35}S]-dATP, and 2 µl diluted Sequenase T7 Polymerase were added to the template-primer (10 µl) reaction. The reaction mixture was mixed well and incubated at room temperature for 2-5 minutes. Four sequencing reactions: A, C, G and T, were carried out in 1.5 ml Eppendorf tubes. To each of the tubes labeled A, C, G and T, was added 50 mM NaCl, and 2.5 µl of the respective 80 µM dNTP. The tubes were warmed at 37°C for 1 minute, and 3.5 µl of the labeling mix was then transferred to each of the four sequencing reactions and the reactions mixed well. Incubation at 37°C was continued for 3-5 minutes, and the reactions were stopped by the addition of 4 µl stop solution containing 95% formamide, 20 mM EDTA, 0.05% bromophenol blue, and 0.05% xylene cyanol FF. The tubes were placed on ice and could at this point be stored overnight at -20°C.

The sequencing reactions, 3 µl each, were analyzed by electrophoresis on 6% polyacrylamide urea gels (33 cm X 40 cm) containing 22.5 ml of 40% acrylamide stock solution, 75 g of urea and 15 ml of 10X TBE buffer (121.1 g Tris, pH 8.3, 55 ml boric acid, 7.4 g EDTA to a liter). The gel solution was filtered using a Whatman filter paper #1 and degassed for 10 min using a vaccum pump. Ammonium persulfate (1 ml of a 10% solution) and 10 µl of TEMED were added to initiate polymerization. The gel was polymerized at room temperature overnight. The gel was placed in a BRL DNA sequencing electrophoretic unit. Before loading, each lane was washed with 1X TBE electrode buffer and the gel pre-run at 60W for 30 min at 50°C. The samples were heated at 80°C for 2-3 min prior to loading. For loading, 3 µl of ddATP, ddCTP, ddGTP, and ddTTP reactions, respectively, were used. The gel was run at 60 W till the dye ran off the gel. Multiple loadings were performed to extend the length of the sequence. After

the dye in the first run reached the middle of the gel, the same set of samples were loaded in other adjacent lanes and the electrophoresis continued until the tracking dye of the second load ran off the gel.

The gel unit was disassembled with the sequencing gel resting on the lower plate. The lower plate was placed in the fixing solution (5% acetic acid and 5% methanol) for 30 minutes. The fixing solution was drained and the gel carefully transferred to a Whatman 3mm filter paper by placing the paper on top of the gel and inverting. The sequencing gel was then dried on a Hoefer drying unit, at 80°C for 1-2 hours. The dried gel was then placed on an X-ray cassette with a Polaroid X-ray film. The film was exposed for 16-32 hours. The gel was removed from the cassette and the film placed in a GBX film developer for 5 minutes. It was then placed in warm water for 1 min and in GBX fixer for 15 minutes.

3.1 Overview of the CPSase Domain

E. coli CPSase

E. coli carbamoyl phosphate synthetase is a monofunctional 160 kDa protein consisting of two subunits, a 40 kDa glutaminase subunit and a 120 kDa synthetase subunit. The glutaminase (GLN) subunit hydrolyzes glutamine resulting in the transfer of ammonia to the synthetase subunit. The synthetase subunit consists of two homologous subdomains, CPS.A and CPS.B (33,45) that catalyze carbamoyl phosphate formation from bicarbonate, ATP and ammonia. CPS.A catalyzes the ATP dependent activation of bicarbonate. The intermediate carboxy phosphate reacts with ammonia forming carbamate, which is subsequently converted to carbamoyl phosphate in a second ATP dependent reaction catalyzed by CPS.B. The enzyme provides carbamoyl phosphate for both pyrimidine and arginine biosynthesis, and is allosterically regulated by metabolites from both pathways. UMP is a feedback inhibitor, while ornithine, IMP and NH_3 activate the enzyme.

Mammalian CPSase

Mammalian glutamine-dependent carbamoyl phosphate synthetase catalyzes the first committed step in the *de novo* pyrimidine biosynthetic pathway. The enzyme is a part of the multifunctional protein CAD. The CPSase activity of CAD is the major locus of regulation of pyrimidine biosynthesis. UTP is a feedback inhibitor, while PRPP is an allosteric activator. The CPSase activity and the effect of the allosteric ligands is modulated by cAMP-dependent protein kinase phosphorylation.

CPS.A and CPS.B are functionally equivalent

There is ample evidence indicating that the two homologous halves of the CPSase synthetase subunit are specialized to carry out the two different ATP-dependent

partial reactions. CPS.A catalyzes the initial ATP-dependent activation of bicarbonate, whereas the synthesis of carbamoyl phosphate from carbamate occurs on CPS.B. Although the CPS.A and CPS.B have different specific functions when fused together in the wild-type protein, the isolated domains have been shown to be functionally equivalent (70). When CPS.A and CPS.B were separately cloned, the half molecules, very surprisingly, could each catalyze both partial reactions and the overall synthesis of carbamoyl phosphate from bicarbonate, ATP and ammonia. Moreover, when CPS.A was fused to the glutaminase domain, the isolated domain could catalyze glutamine-dependent carbamoyl phosphate synthesis. Similar results were obtained for the isolated CPS.B domain except in this case, unlike the CPS.A, the activity was inhibited by UTP and activated by PRPP. One requirement for the isolated half domains CPS.A and CPS.B of CAD and *E. coli* CPSase to catalyze the overall synthesis of carbamoyl phosphate was the formation of a homodimer. While the monomeric CPS.A or CPS.B could catalyze both ATP dependent partial reactions, the formation of a homodimer $(CPS.A)_2$ or $(CPS.B)_2$, seemed essential to catalyze the overall synthesis of carbamoyl phosphate. In this model, one monomer assumes the role of bicarbonate activation, and the other catalyzes the phosphorylation of carbamate to form carbamoyl phosphate, presumably mimicking the two fused domains CPS.A and CPS.B in the intact molecule.

Function of the A2 and B2 subdomains

The CPS.A and CPS.B domains are in turn comprised of subdomains. Sequence homology (15,17,45,94) and controlled proteolysis studies (11,13,17,69,110-112) suggest that each of the synthetase domains CPS.A and CPS.B, consist of three subdomains, designated A1, A2, A3 and B1, B2, B3, respectively. The recently solved X-ray crystal structure of *E. coli* CPSase (48) has confirmed the presence of subdomains. The authors identified four subdomains A-D in each half of the synthetase subunit. Subdomain A corresponds to the A1 or B1 in the CAD nomenclature and

subdomain D is equivalent to A3 or B3. The domains A2 and B2 appear to be comprised of two subdomains B and C, each of which participate in catalysis and bind ADP.

The regions A2 and B2 have been implicated in ATP binding. Consensus sequences for the nucleotide binding sites (45,61) and the active site of homologous kinases (16,45,74) are located in the central regions of CPS.A and CPS.B. Chemical modification of CAD (68) and mammalian CPSase1 (60-62,95,96) as well as site-directed mutagenesis of *E. coli* CPSase (64) showed that ATP bound to A2 and B2 subdomains. Recently, Guy and Evans cloned the A2 and B2 subdomains (97) and demonstrated that the catalytic sites are located entirely within the 27-kDa central catalytic subdomains A2 and B2. The intrinsically high catalytic activity of A2 and B2 are suppressed by interactions with an 11-kDa attenuation subdomain A1 or B1 (97). These interactions have been proposed to be a component of a functional linkage that coordinates the two ATP-dependent partial reactions occurring on CPS.A and CPS.B. Subdomains A1 and B1 are necessary for the physical association and functional linkage between the glutaminase and the CPSase domains. The 20-kDa A3 and B3 subdomains are not required for catalytic activity. A3 has been termed the oligomerization domain (48) although its function is quite undefined at this time. B3 is known to bind allosteric effectors and modulates the activity of the catalytic domains (56).

3.2 The Regulatory Subdomain (B3)

Allosteric effectors are now known to bind to the carboxyl end of CPS.B (B3) of all CPSases. Rubio and his associates (57,74,75) clearly established the location of the *E. coli* nucleotide binding site by photoaffinity labeling with UMP. They initially demonstrated that the label was incorporated into a 20 kDa proteolytic fragment derived from the carboxyl end of the synthetase subunit and subsequently narrowed down the modification to smaller regions of the polypeptide. Scanning colorimetry studies (55) of

a truncated mutant lacking 171 residues of the carboxyl end of the synthetase subunit suggested that ornithine also bound near the end of the CPS.B and confirmed the assignment of the nucleotide binding site. Subsequent studies (77) also localized the binding sites for *E. coli* CPSase allosteric ligands to the carboxyl end of the synthetase subunit using a combination of deletion and site-specific mutagenesis (77)] and controlled proteolysis (69). The deletion of the last 119 residues or the replacement of a conserved threonine residue was found to produce mutants that lacked UMP inhibition but retained ornithine sensitivity. This suggested that the UMP and ornithine sites were distinct. The biochemical studies were confirmed by locating the UMP and ornithine binding sites in the X-ray structure (48) of the *E. coli* enzyme. Phosphorylation studies by Carrey et al have demonstrated the existence of two sites in CAD, one of which is located within the carboxyl end (B3) of the CPSase molecule. Alignment of the *E. coli* (57) and mammalian sequences, showed that the target serine residue in CAD, responsible for modulating the CPSase activity, was located 30 residues downstream of the crucial UMP binding residue Lys ^{992} in the *E. coli* enzyme. cAMP-dependent phosphorylation of Ser 1406 in CAD resulted in loss of UTP inhibition (71). This suggested that the UTP and phosphorylation sites overlapped or were in close proximity. Another study involved a series of CAD deletion mutants in which the carboxyl end of CPS.B was truncated, lost sensitivity to UTP, but had increased sensitivity to PRPP. (78). This suggested that the binding site for both ligands was near the carboxyl end of CPS.B, that the UTP and PRPP sites were distinct, and that the UTP site was downstream of the PRPP binding site. Liu, Guy and Evans have shown that allosteric effectors bind to the B3 region of CAD by constructing a chimeric protein in which the putative *E. coli* CPSase regulatory domain was replaced by the B3 of CAD (56). The chimera was inhibited by UTP, but not by the *E. coli* effector UMP and was activated by PRPP, a metabolite that has no effect on the *E. coli* enzyme.

Kinetic studies, which determined the function-linked thermodynamic parameters, suggest that the major target of allosteric regulation is the second partial reaction, namely the ATP-dependent phosphorylation of carbamate. Thus, the allosteric effectors directly modulate the activity of CPS.B, the domain to which they bind. Any changes in the CPS.A are likely to be indirect and result from global conformational changes in the overall molecule. However, there has been no differentiation in the structure or the function of the CPS.B domain that has rendered it subject to allosteric control. Only the tertiary structure of the B3 regulatory subdomain of CPS.B is distinctly different from that of the A3 subdomain of the CPS.A. Binding of allosteric ligands to the regulatory domain B3 triggers an allosteric signal that is transmitted to the active site. In case of the CPS.B homodimer, binding of ligands to B3 leads to the transmission of allosteric signals to the catalytic subdomain B2, leading to a modulation of the catalytic activity. Due to the absence of B3, the CPS.A homodimer is unresponsive to allosteric ligands.

Our proposal is the following: If the CPS.A and CPS.B are functionally equivalent, differing in that CPS.B is normally the regulatory locus due to the presence of the B3 ligand binding subdomain, then CPS.A may be placed under allosteric control or that a chimera A12B3 consisting of the CPS A1 and A2, and a B3 instead of A3, could possibly mimic the allosteric signal transmission in CPS.B.

To test the above hypothesis, a chimera was created that consisted of the *E. coli* CPSA1A2 and mammalian B3 subdomain (Figure 3.1). If the above hypothesis is true, the chimeric $A12^{e}B3^{m}$ should be functional as a CPSase, and respond to allosteric effectors UTP and PRPP.

3.3 Cloning, Expression and Purification of CPSA12^{e}B3^{m}chimera

The 7.3-kb plasmid pHL-2 containing the coding sequences for a hybrid molecule consisting of *E. coli* CPSase catalytic domains and the mammalian regulatory subdomain, was constructed previously by Liu et al (56). The plasmid pHE-$A12^{e}B3^{m}$

Figure 3.1: Subunit and domain structure of CAD, *E. coli* CPSase, and the Chimera CPSA12^{e}B3^{m}

This scheme shows the structural organization of CAD and *E. coli* CPSase. The superscripts indicate the origin of the CPS domain, m signifying mammalian, e *E. coli*. The residue numbers are from the CAD sequence [Simmer 1990] for the CAD domain and from the *E. coli* sequence [Nyunoya 1983] for the *E. coli* domain. The chimera CPSA^{e}B123B3^{m} consists of the entire *E. coli* CPSase with the B3 domain at the carboxyl end repalced with the corresponding segment of CAD. The chimera CPSA12^{e}B3^{m} consists of the regulatory domain of CAD directly fused to the *E. coli* CPSase A1-A2 subdomains.

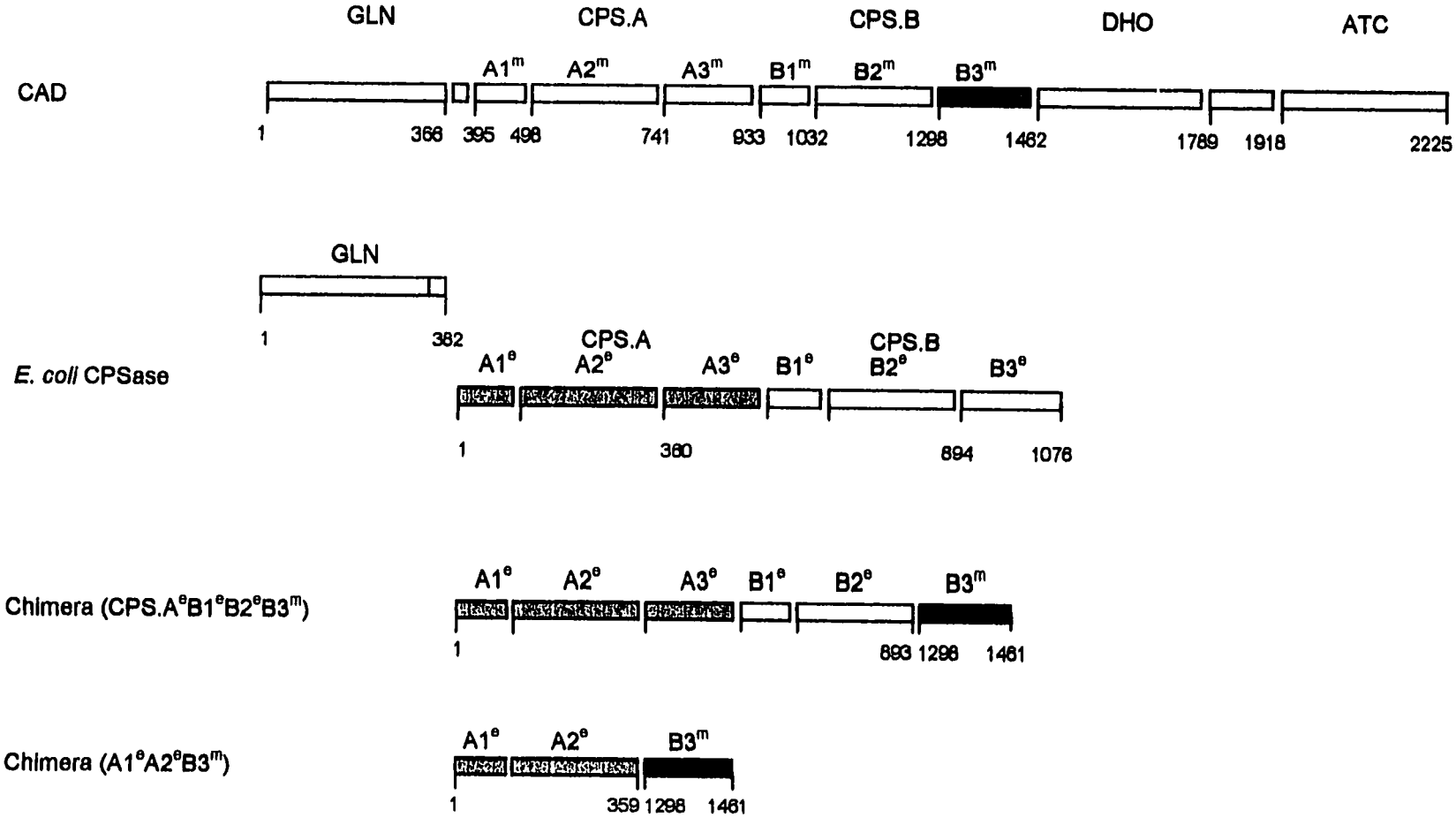
GLN
CPS.A
CPS.B
DHO
ATC
CAD
A1m
A2m
A3m
B1m
B2m
B3m
1
366
395
498
741
933
1032
1298
1462
1789
1918
2225
GLN
1
382
E. coli CPSase
CPS.A
CPS.B
A1e
A2e
A3e
B1e
B2e
B3e
1
360
894
1076
Chimera (CPS.AeB1eB2eB3m)
A1e
A2e
A3e
B1e
B2e
B3m
1
893
1298
1461
Chimera (A1eA2eB3m)
A1e
A2e
B3m
1
359
1298
1461

(Figure 3.1), encoding the *E. coli* CPSA1A2 (residues 1-364) and mammalian B3 subdomain (residue 1297-1464), was constructed (Dr.H.I Evans) by reacting the plasmid pHL-2 with *Nsp* V (site in *the E. coli* sequence, 2730) and *Stu* I (site in the CAD sequence, 3892). The 5' extensions were filled using the klenow fragment of DNA polymerase, and the 4.3-kb fragment was gel purified prior to the blunt end religation with T4 DNA ligase. The resulting construct was called pHE-A12^{e}B3^{m} (Figure 3.2) and was confirmed by restriction analysis and sequencing.

Expression and Purification of the Chimeric A12^{e}B3^{m}

The chimeric plasmid pHE-A12^{e}B3^{m} was transformed into an *E. coli* strain RC50, (kindly provided by Dr. Carol Lusty, The Public Health Research Institute of the City of New York, New York) which lacked the carA and *car*B genes encoding the small and large subunits of *E. coli* CPSase, respectively. The transformants grew on a high ammonia medium lacking uracil, suggesting that a functional CPSase was expressed which complemented the host defect in the *E. coli* synthetase subunit. The chimeric protein is constitutively expressed under the control of the *car* AB promoter. A 20 µl overnight culture was typically inoculated into a 200 ml 2XYT media supplemented with 0.1% glucose and 125 µg/ml ampicillin at 37°C. Cells were grown 18-20 hours, then harvested at stationary phase by centrifugation at 4000 rpm, 4°C, for 30 minutes. SDS-gel electrophoresis revealed a new 58-kDa species not present in extracts of untransformed cells. The recombinant protein constituted approximately 10% of the total soluble protein.

Purification of the chimeric 58-kDa CPS-A12^{e}B3^{m} was carried out by ion-exchange chromatography. A 200-ml cell culture was harvested at stationary phase. The cell pellet was resuspended in 2 ml of a 50 mM Tris, pH 7.5, 1 mM DTT, 1 mM EDTA, 5% glycerol buffer containing 2 mM PMSF. The cells were broken by sonication 5X 15 seconds on ice. The cell sonicate was centrifuged at 14,000 Xg, 4°C for 30 minutes.

Figure 3.2 Construction of the Recombinant CPS-A12^{e}B3^{m}

The plasmid pHE-A12^{e}B3^{m} encoding *E. coli* A1 and A2 subdomains fused to the mammalian B3 subdomain was constructed by reacting the plasmid pHL2, with *Nsp* V (site in the *E. coli* sequence, 2730) and *Stu*I (site in CAD sequence, 3892). The 4.3 kb fragment was religated using T4 DNA Polymerase following treatment with the Klenow fragment of DNA polymerase.

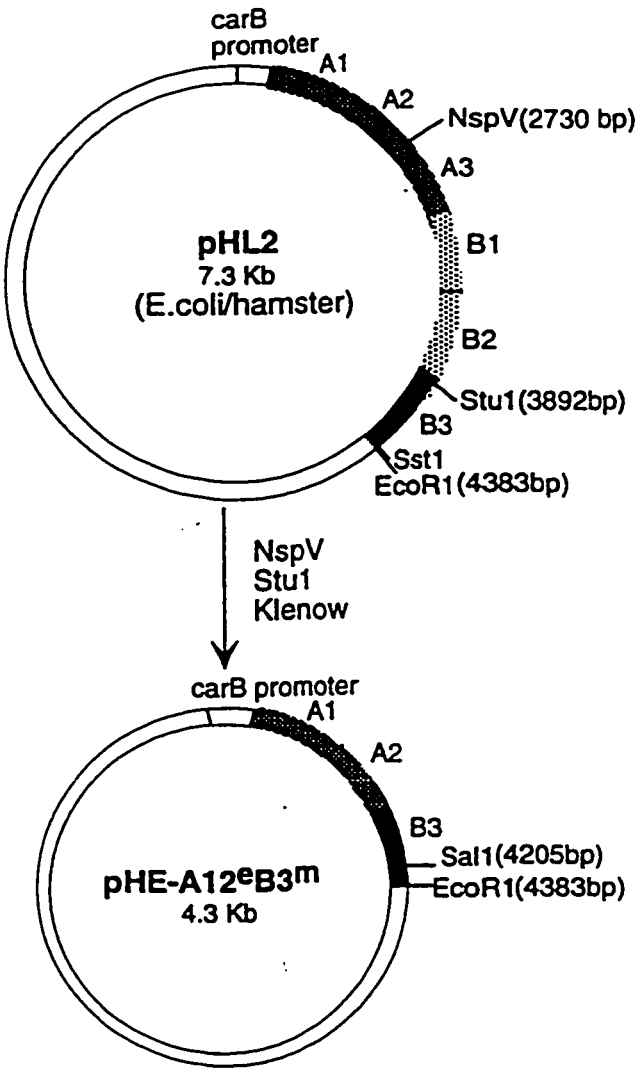
carB
promoter
A1
A2
NspV(2730 bp)
A3
pHL2
7.3 Kb
(E.coli/hamster)
B1
B2
Stu1(3892bp)
B3
Sst1
EcoR1(4383bp)
NspV
Stu1
Klenow
carB promoter
A1
A2
B3
Sal1(4205bp)
pHE-A12eB3m
4.3 Kb
EcoR1(4383bp)

The supernatant containing the 58.6 KDa recombinant was loaded on a fast flow 15 X 3-cm Q-Sepharose column equilibrated with 50 mM Tris, pH 7.5, 1 mM DTT, 1 mM EDTA and 5% glycerol. Purification was carried out at 4°C. The column was washed with two column volumes of buffer at a flow rate of 1 ml/min. The protein was then eluted with a two and a half column volume 0-1 M linear gradient of NaCl at a flow rate of 0.8 ml/min. Fractions containing the CPS-A12^{e}B3^{m} were identified by CPSase activity assays and were analyzed by SDS-PAGE (Figure 3.3).

Protein concentrations were determined using the micro BCA protein assay reagent kit form PIERCE and by scanning Coomassie blue stained polyacrylamide gels using an HP Scan Jet 4C, UN-SCAN-IT gel Automated Digitizing System. The gels were scanned and the concentration of the isolated proteins determined from the scanned gel by measuring the ratio of the peak density to the total density in a given lane and the total amount of protein applied to the gel. The background density was subtracted and all measurements were made within the linear range of the densitometer. The concentration of the partially purified 58-KDa A12^{e}B3^{m} was 0.16 µg/µl.

3.4 Catalytic Activity of the Chimeric CPS-A12^{e}B3^{m} protein

The ammonia-dependent carbamoyl phosphate synthetase activity of the partially purified chimeric CPS-A12^{e}B3^{m} was measured as a function of ATP concentration. The rate of the carbamoyl phosphate synthetase reaction was measured by initiating the reaction with [^{14}C] $NaHCO_3$ and trapping the radiolabeled carbamoyl phosphate as stable carbamoyl aspartate. ATP saturation curves (Figure 3.4) of the chimeric enzyme showed that the steady state kinetic parameters (Table 3.1) were very similar to that of *E. coli* CPSase. The *E. coli* enzyme is much more efficient than the mammalian CPSase. The K_m for ATP is 5 fold lower and the K_{cat} is 10-fold higher than the corresponding values obtained for CAD. While the chimeric protein was insensitive to UMP, the *E. coli* CPSase inhibitor, mammalian effectors modulated its catalytic activity.

Figure 3.3 Expression and Isolation of the Chimera CPS-A12^{e}B3^{m}

The cell pellet from 200 ml of induced culture was resuspended in 2 ml of 50 mM Tris pH 7.5, 1 mM EDTA, 1 mM DTT and 5% glycerol buffer that contained 1 mM PMSF, and sonicated 4 X 15 seconds on ice. The cell extract was centrifuged at 10000 x g for 20 min at 4°C. The clear supernatant was applied on top of a Q-Sepharose column equilibrated in the same buffer. The column was washed with the buffer until the A_{280} was negligible. The protein was eluted at 0.35 M NaCl buffer in a 0-1 M NaCl gradient. The peak fractions were determined by an ammonia-dependent CPSase assay and by SDS-PAGE and were pooled, and stored at -20°C.

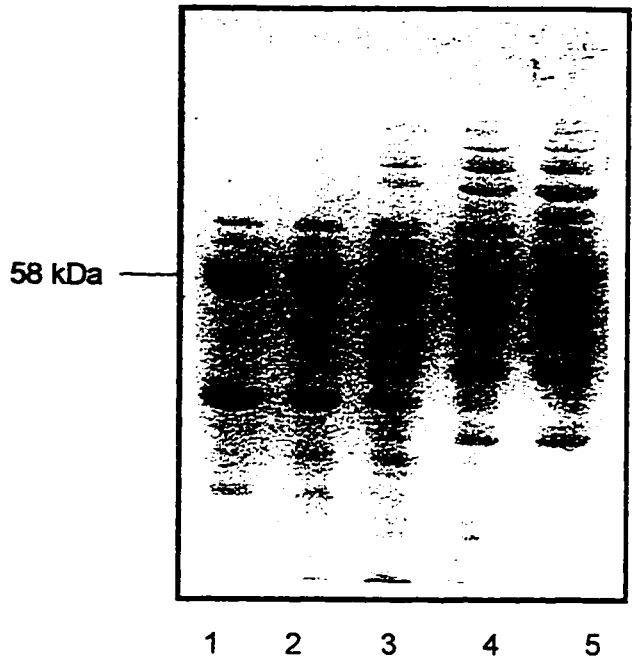
58 kDa
1
2
3
4
5

In the presence of 3 mM UTP, the K_m for ATP remained unaffected, while the k_{cat} was decreased 2-fold. In the presence of the 200 μM activator PRPP, the k_{cat} increased 1.5 fold while the K_m for ATP remained unaffected. However, in the wild type proteins, the effect of allosteric effectors is mainly on the K_m and not on the V_{max}. The assays were conducted as described in the Materials and Methods.

The extent of activation and inhibition of the chimeric protein (Figure 3.6) as a function of the effector concentration was also very similar to that of mammalian CPSase. The apparent dissociation constant K_i obtained for UTP, at a fixed ATP concentration of 0.75 mM was 0.74 mM, compared to a value of 0.64 mM obtained for CAD CPSase. Moreover, saturating concentrations of UTP inhibited the chimera to nearly the same extent as CAD, 72% and 91% respectively. In the case of PRPP, the apparent dissociation constant K_a for the chimera at a fixed ATP concentration of 0.75 mM was 78 μM versus 13.5 μM for CAD. The maximum activation was approximately the same, 251% for the chimera and 238% for CAD (Table 3.2).

3.5 Phosphorylation of the Chimera

cAMP-dependent protein kinase A phosphorylation was performed as described in Materials and Methods. Phosphorylation has no effect on the *E.coli* CPSase, but the kinetics of the chimeric protein CPS-A12^{e}B3^m was significantly affected by the phosphorylation (Figure 3.5). In CAD, protein kinase A mediated phosphorylation alters the activation of bicarbonate and the effectiveness of allosteric effectors (71). The phosphoenzyme is activated slightly, but the most striking effect is a complete loss of UTP inhibition (Table 3.1).

In the phosphorylated chimera, the K_m and K_{cat} remained the same as the unphosphorylated protein in the absence of any allosteric ligands, while the extent of inhibition by UTP decreased significantly on phosphorylation. The effect of phosphorylation on the allosteric regulation of the chimeric CPS-A12^{e}B3^m is very similar

Figure 3.4: ATP saturation curves of the Chimeric protein

The ammonia-dependent carbamoyl phosphate synthetase activity was measured as a function of ATP concentration as described in Materials and Methods. 3.2 μgs of the chimera CPS-A12^{e}B3^{m} were used. The activity is measured in the absence of ligands (-●-), in the presence of 200 μM PRPP (-○-), and 3 mM UTP (-□-)

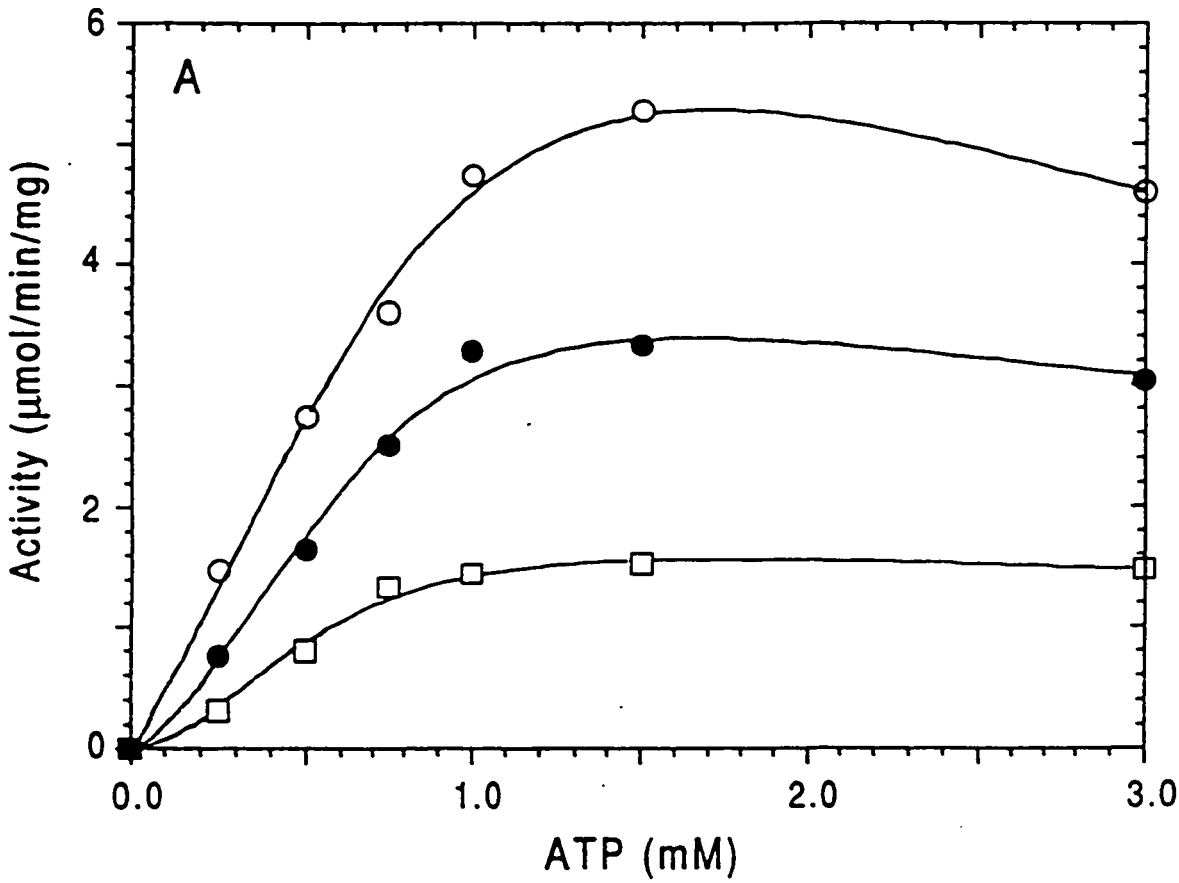
A
Activity (µmol/min/mg)
ATP (mM)
0
2
4
6
0.0
1.0
2.0
3.0

Figure 3.5: Effect of Phosphorylation on the ATP saturation curves of the Chimera

Phosphorylation was performed as described by Liu et al (56). The ammonia-dependent carbamoyl phosphate synthetase activity of the phosphorylated chimera was measured as a function of ATP concentration as described in Materials and Methods. 3.0 μgs of the phosphorylated chimeric protein CPS-A12^{e}B3^{m} were used. The activity was measured in the absence of ligands (-●-), in the presence of 200 μM PRPP (-○-), and 3 mM UTP (-□-).

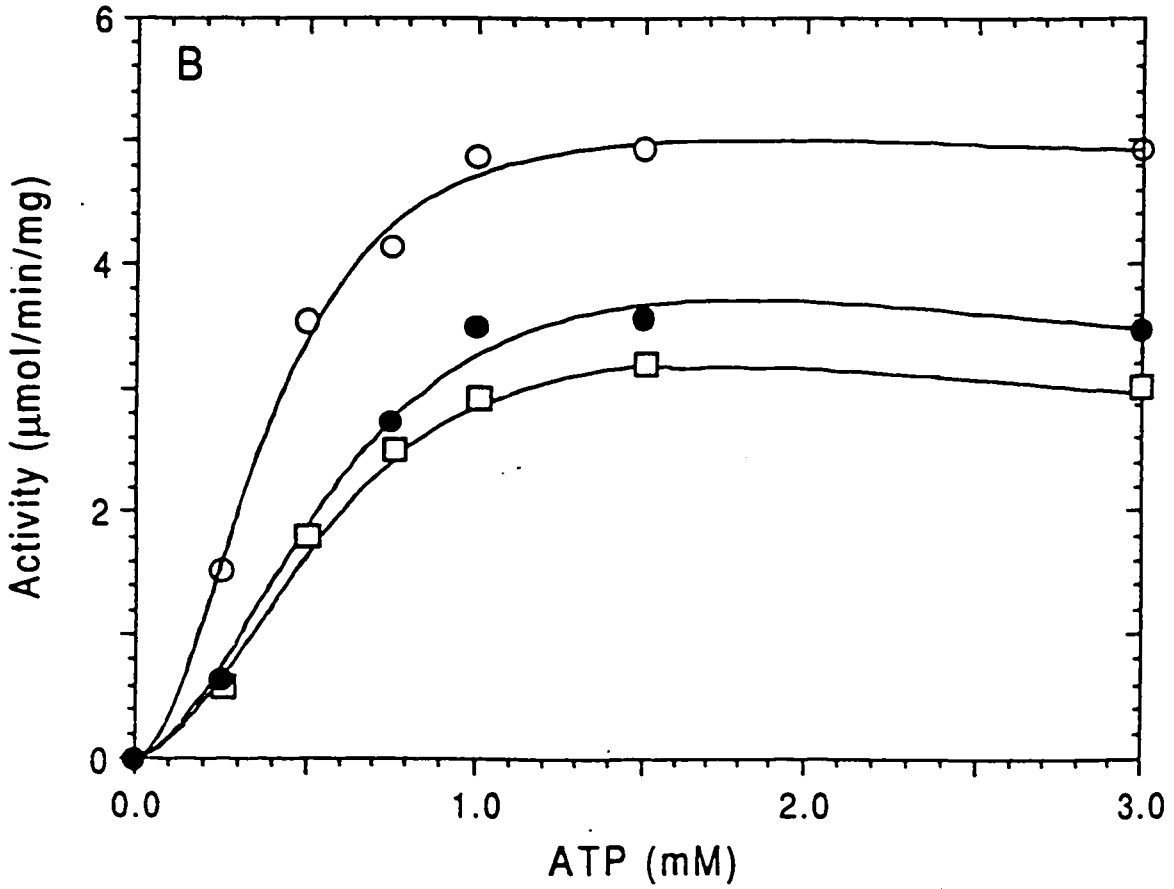
B
Activity (µmol/min/mg)
ATP (mM)
0
2
4
6
0.0
1.0
2.0
3.0

Table 3.1 Summary of Kinetic Parameters for Chimeric CPS-A12^{e}B3^{m}

Protein	Ligand	Km	Vmax	Kcat	Kcat/Km
		mM	μmol/min/mg	s^{-1}	$M^{-1}s^{-1}$
E.coli CPSase[a]	none	0.43±0.02	3.0±0.10	8.0±0.3	18,600
CAD CPSase[b]					
unphosphorylated	none	2.14±0.16	0.194±0.006	0.78±0.02	363
Chimeric CPSase					
unphosphorylated	none	0.46±0.14	3.46±0.22	3.35±0.21	7270
	200μM PRPP	0.43±0.12	5.18±0.30	5.01±0.29	11,600
	3 mM UTP	0.45±0.11	1.64±0.08	1.59±0.08	3520
phosphorylated	none	0.50±0.11	3.87±0.20	3.74+0.19	7480
	200μM PRPP	0.36±0.08	5.19±0.13	5.02±0.13	13,900
	3 mM UTP	0.48±0.11	3.22±0.17	3.11±0.16	6490

[a]Data from ref 66
[b]Data from ref 65

Figure 3.6 Effector Response curves of the chimeric protein

The effect of increasing concentrations of PRPP (-●-) and UTP (-■-) on the ammonia-dependent carbamoyl phosphate synthetase activity of 3.2 μg of the unphosphorylated chimeric protein was determined. The ATP concentration was maintained at 0.75 mM and all other substrates were at saturating concentrations. Again, the effect of increasing PRPP (-○-) and increasing UTP (-□-) on 3 μg of the phosphorylated chimera was compared to that in the unphosphorylated protein.

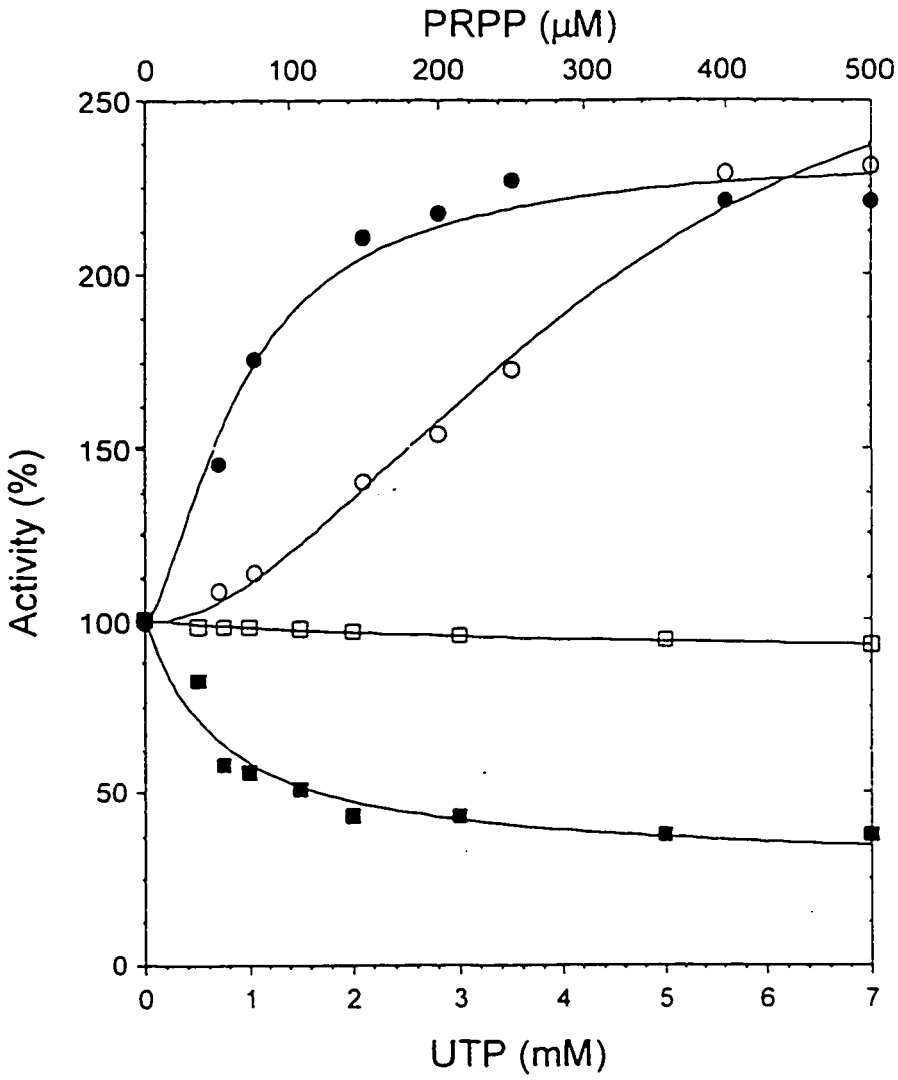
PRPP (μM)
0
100
200
300
400
500
250
200
150
100
50
0
Activity (%)
0
1
2
3
4
5
6
7
UTP (mM)

Table 3.2 Allosteric Regulation of CAD and the Chimeric protein

	Chimeric CPS $A12^{e}B3^{m}$		CAD [a]	
	UTP inhibition	PRPP activation	UTP inhibition	PRPP activation
Unphosphorylated protein				
K_d [b] (μM)	739 ± 193	78.0 ± 22.5	640 ± 80	1 3.5 ± 0.9
Maximum effect (%)	72.0 ± 13.6	251 ± 12.2	91.0 ± 0.9	2 38 ± 1.20
Phosphorylated protein				
K_d [b] (μM)	4028 ± 707	384.4 ± 06.2 [c]	3660 ± 580	66.5 ± 3.6
Maximum Effect (%)	11.3 ± 0.13	293.1 ± 43.9 [c]	62.3 ± 5.2	271 ± 0.06

[a] data from ref 56

[b] the apparent dissociation constants were calculated from the equation $[X]_{½} = \alpha K_d([S]+K_s)/(K_d+[S])$, where $[X]_{½}$ is the concentration of the allosteric effector which produced half maximum activation or inhibition, [S] is the substrate concentration, K_d and K_s is the apparent dissociation constant of the allosteric ligand and the substrate respectively and α is the ratio of Km (no ligand)/Km (saturating ligand)

[c] the curve was fit to an isotherm that incorporates cooperativity with a hill coefficient of 1.90± 0.41

to that of CAD. UTP inhibition is effectively abolished. The maximum activation with saturating PRPP was not altered appreciably, but the apparent affinity of the chimera for PRPP was significantly decreased. Phosphorylation resulted in a four-fold increase in the concentration of PRPP required for half maximal activation.

Thus, the catalytic activity of the chimera closely resembled that of *E. coli* CPSase, while the regulation and the effect of phosphorylation was essentially characteristic of the mammalian protein.

3.6 Binding of Allosteric Ligands to the Chimeric CPS-A12^{e}B3^{m} protein

Synthesis of [^{32}P] PRPP

^{32}PRPP was synthesized enzymatically based on the following reaction:

ATP + ribose 5'-phosphate $\rightarrow$ AMP + PRPP

A procedure of Khorana et al (98) was used for the enzymatic synthesis of radiolabeled PRPP. The 1-ml reaction mix consisted of 22 mM potassium phosphate, pH 7.4, 11 mM ATP (500 μCi [γ-32P] ATP, Amersham), 2.8 mM ribose-5'-phosphate, 2.2 mM $MgCl_2$, 0.4 mM EDTA, 0.11 mM DTT. The reaction was initiated by the addition of 0.15 mg PRPP synthetase, kindly provided by Dr. Robert Switzer. This enzyme was purified to homogeneity from *B.subtilus* and studied extensively by Switzer and co-workers (99). The enzyme was stored in a 6 mg/ml potassium phosphate solution, pH 7.5. The specific activity of the enzyme was 52 μmol/min/mg at pH 7.4 in potassium phosphate buffer.

The reaction was incubated for 30 min at 37°C and then stopped by the addition of 0.130 ml of 30% Norit A charcoal solution. Norit A was cleared by centrifugation at 14,000 X g for 2 minutes. The supernatant was passed through a 1-ml syringe-filter to ensure removal of the charcoal. ^{32}PRPP synthesized was quantitated as below.

Determination of the ^{32}PRPP concentration

A PRPP assay was performed using an orotidylate phosphoribosyl transferase (OPRTase)-orotidylate decarboxylase (ODCase) coupling system. In this assay, orotic

acid is converted to UMP in two steps:

$$\text{Orotic acid (carboxyl } ^{14}\text{C)} + \textbf{PRPP} \rightarrow \text{OMP} + \text{PPi}$$

$$\text{OMP} \rightarrow {}^{14}\text{CO}_2 + \text{UMP}$$

The final concentrations in the 1-ml assay mixture were 0.1 M Tris-HCl, pH 7.5, 2 mM $MgCl_2$, 100 μM [^{14}C] orotate. The reaction was initiated with 1-10 units of PRPP transferase-OMP decarboxylase mixed enzyme. The reaction was carried out in a modified 10 ml Erlenmeyer flask containing a glass center well, an air-tight rubber stopper, and a side arm reservoir (Figure 3.7). Prior to the initiation of the reaction, 0.2 ml of CO_2 trapping solution containing a mixture of ethylene glycol and ethanolamine (2:1, v/v) was added to the center of the well. In addition, 0.2 ml of 4-M perchloric acid was added to the side arm. Following incubation for 1 hr at room temperature, the reaction was quenched by tilting the flask to allow the mixing of the acid solution in the side arm of the flask with the reaction mixture. The [^{14}C] carbon dioxide generated in the reaction was trapped in 200 μl of an ethylene glycol/ethanolamine solution placed within the center-well of the flask for another hour. Previous study by Shoaf and Jones showed that the absorption of CO_2 was complete in 60 min at room temperature. The CO_2 trapping solution was transferred to a scintillation vial. High flash point cocktail safety-solve scintillation fluid (10ml) was added to each vial. After mixing thoroughly, the vials were counted in a Packard Tri-Carb model 460 liquid scintillation counter. The concentration of the synthesized ^{32}PRPP was determined by the amount of [^{14}C] carbon dioxide produced in the assay. Up to 25 nmoles of PRPP can be accurately assayed by this method.

The result of a PRPP assay is shown in Figure 3.7, where it can be seen that there is a very good linear relationship between the amount of PRPP and the amount of [^{14}C] CO_2 generated. The linear range of this standard curve is 1-25 nmoles of PRPP.

Figure 3.7 PRPP Assay Flask and a PRPP standard curve

The PRPP assay was carried out in a modified 10 ml Erlenmeyer flask. As indicated in the figure, the flask contained an air-tight rubber stopper, a glass center well for holding the CO_2 trapping solution, and a side arm for adding the acid quench solution. The assay was done as described in the text. After the incubation, the 200 µl CO_2 trapping solution was transferred to a scintillation vial and counted. A standard curve was obtained by plotting the radioactivity ^{14}C counts versus the PRPP concentrations.

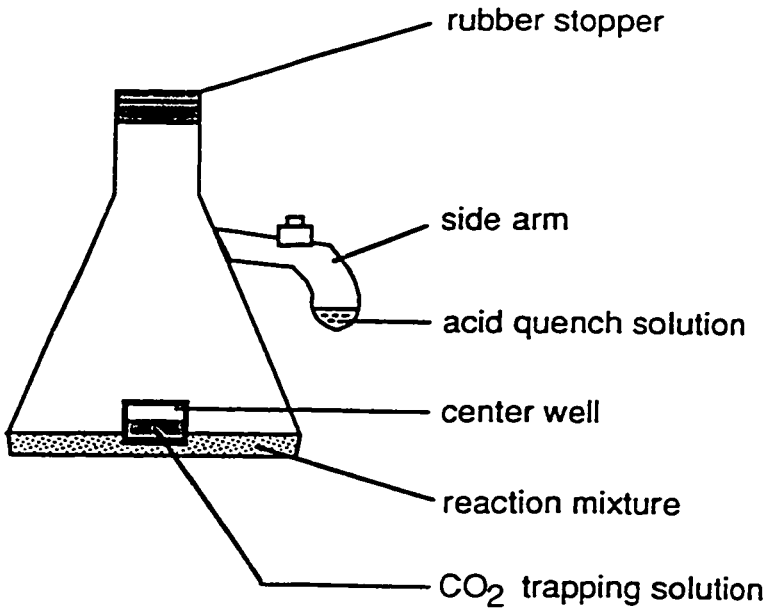
rubber stopper
side arm
acid quench solution
center well
reaction mixture
CO_2 trapping solution

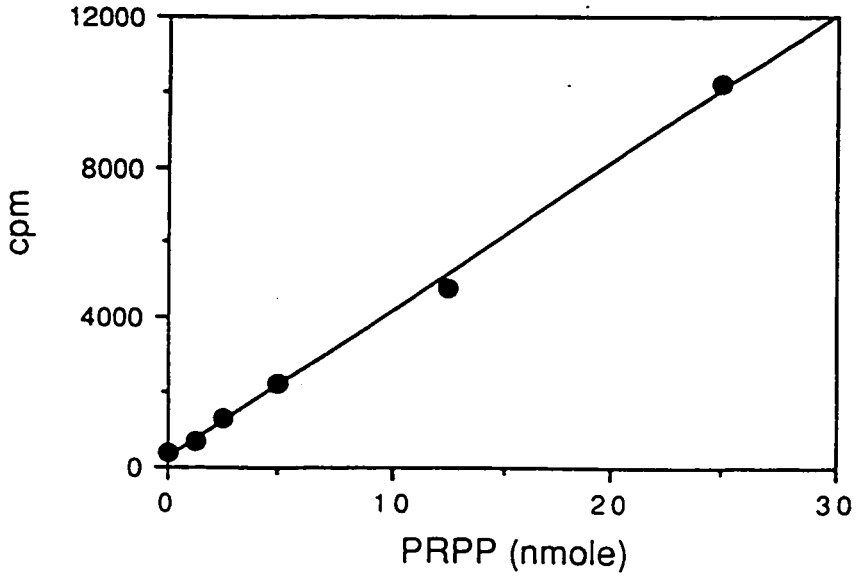
12000
8000
4000
0
cpm
0
10
20
30
PRPP (nmole)

PRPP Binding by the Microcolumn Procedure

The binding of PRPP to the chimeric protein was determined using the microcolumn procedure (100) which separates free ligand and protein bound ligand. The protein sample was incubated with increasing concentrations of ^{32}PRPP in a 150 µl reaction mix at 37°C for 15 minutes. The reaction was then transferred to the top of a 0.7 X 2.8 cm bed G-50 Sephadex NICK spin column (Pharmacia). The columns were pre-treated by washing with 50 mM Tris, pH 7.5, 1mM DTT, 5% glycerol. The bed was prepared by centrifuging the column at 1000 X g, 4 min, 4°C. After adding the reaction mix carefully to the center of the bed, the column was centrifuged at 1000 X g, 4 min at 4°C. This separates the free ligand from protein-bound ligand. Under these conditions, the volume of the effluent collected varied from 145-155 µl and the recovery of the protein was 98-100%. The effluent containing ^{32}PRPP-bound chimera was transferred to a scintillation via, 5 ml of scintillation fluid was added to the vial and the amount of bound PRPP was determined by liquid scintillation counting.

Binding of Allosteric Ligands to the Chimeric Protein

The binding of PRPP to the chimeric protein was determined by the microcolumn procedure as described above. The data obtained by plotting PRPP bound per mole of protein as a function of the PRPP concentration was fitted to a Michaelis Menten equation. (Figure 3.8). PRPP bound to the chimeric protein with a dissociation constant, K_d, of 46 uM as compared to a value of 10 µM for the CAD complex. A Scatchard plot was generated (Figure 3.8) using the following equation:

$$\upsilon / [L] = n / K - \upsilon / K$$

where υ is the mole of ligand bound per mole of protein, [L] is the concentration of free ligand (µM), n is the total number of binding sites, K is the dissociation constant (µM). The Scatchard plot of the binding data was linear and gave a dissociation constant (Table 3.3) that was 5-fold higher than the value determined for CAD. The Scatchard

Figure 3.8 PRPP Binding to the chimeric protein

The binding of [^{32}P] PRPP (18,000 cpm/nmol) to 12 μg of the chimeric protein (-●-) was measured by the microcolumn method. A plot of PRPP bound per mole of protein as a function of PRPP gave a Kd of 46 μM. In the Scatchard plot, V represents the ratio of PRPP-protein complex/protein and PRPP represents free PRPP. The effect of 5 mM UTP on the binding of PRPP (-○-) was also measured. Kinetic parameters obtained by a least square fit of this Scatchard plot is shown in Table 3.3

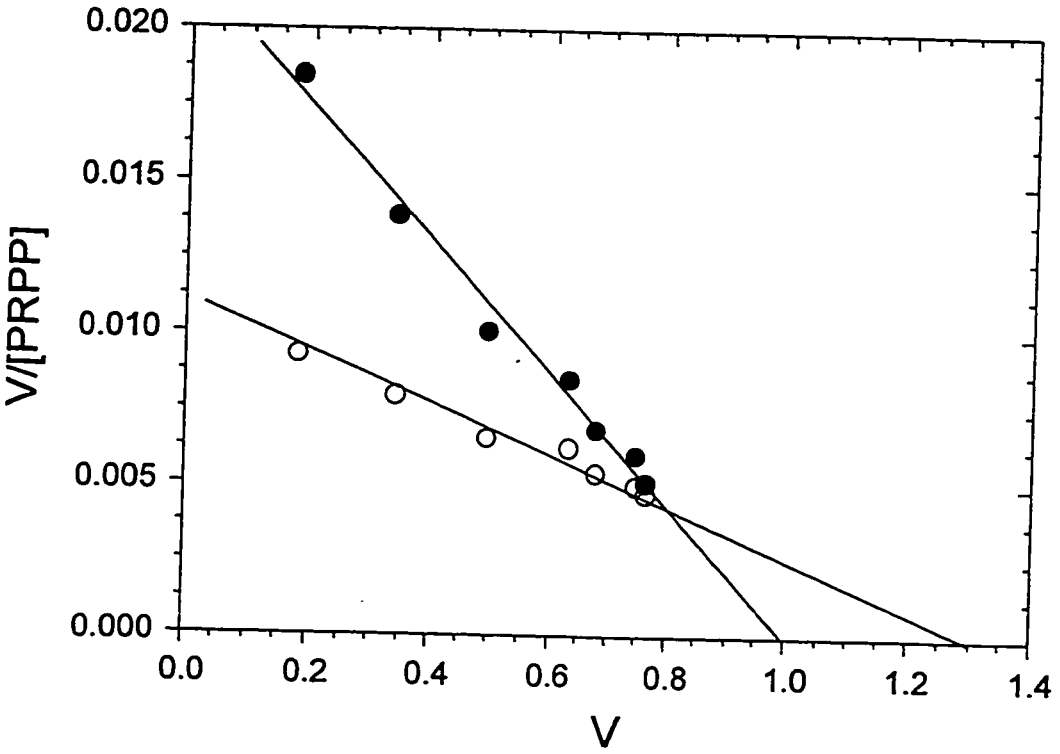
0.020
0.015
0.010
0.005
0.000
V/[PRPP]
0.0
0.2
0.4
0.6
0.8
1.0
1.2
1.4
V

Table 3.3 PRPP Binding to Chimera

Parameter	Ligand	Chimera
K_d (μM)	none	46.0 ± 1.9
n [a]	none	1.0 ± 0.04
K_d (μM)	UTP	133.5 ± 15.8
n [a]	UTP	1.52 ± 0.25

[a] number of binding sites per polypeptide chain

plot gave an intercept corresponding to an n value of 1 ± 0.04, indicating that there is one binding site for PRPP per molecule of the chimera. This fits the previous determination of one PRPP site per molecule of CAD.

Effect of UTP on PRPP Binding to the CPS- A12^{e}B3^{m}

A similar binding experiment could not be used to determine the dissociation constant for UTP as the K_d for UTP of CAD is as high as 1 mM and therefore would require an extremely high concentration of protein. However, the displacement of the bound PRPP by the addition of UTP indicates that the nucleotide effector also binds to the chimeric protein. In the presence of saturating UTP (5 mM), the K_d for PRPP increases 3-fold. Using the same equation as above, a Scatchard plot was calculated (Figure 3.8). The plot shows that although the total number of sites was not changed significantly, the dissociation constant increased to 133.5 μM (Table 3.3). Thus the presence of UTP reduces the affinity of the chimera for PRPP suggesting that UTP is also binding to the chimera. Similar results were obtained for CAD.

3.7 Basis for Construction of a deletion mutant CPS-A12^{e}B3$^{m}\Delta$

Rubio and his associates' (57) identified a region within the regulatory domain, which they proposed to be crucial for allosteric regulation in *E.coli*. A photoaffinity labeling experiment identified lysine 992 in the interaction with the *E. coli* inhibitor UMP. On the basis of the identification of lysine 992 and the analysis of sequences surrounding the residue, the UMP binding fold was proposed. The fold comprises two contiguous regions. The first region surrounding lysine 992, extending downstream to the cluster of conserved residues containing an invariant asparagine 1014 (by alignment Asn 1394 in CAD). This region presumably interacts with the pyrimidine ring of the inhibitor. The second region extends from the invariant asparagine 1014 to an invariant arginine 1029 (by alignment arg 1416 in CAD) and possibly interacts with the phosphate moiety of the nucleotide, at least in the enzymes that are inhibited by UTP. This was

Figure 3.9 Schematic representation and construction of the deletion mutant CPS-A12^{e}B3$^{m}\Delta$

The chimera CPS-A12^{e}B3^{m} was restricted by *Sal* I (site in CAD, 4205) and *EcoR* I (site in vector pUC 119 multiple cloning region). The ends were made flush with the Klenow fragment, prior to religation of the 4.2 kb plasmid. The 4.2 kb plasmid pNS-A12^{e}B3$^{m}\Delta$ encodes the *E. coli* CPS A1A2 subdomains and a truncated mammalian regulatory domain. The chimeric deletion mutant lacks 59 of 163 residues from the carboxyl end of the wild type chimera CPS-A12^{e}B3^{m}.

Chimera ($A1^eA2^eB3^m$)

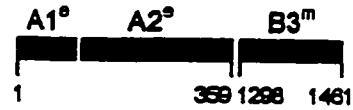

Hybrid deletion mutant
($A1^eA2^eB3^m\Delta$)

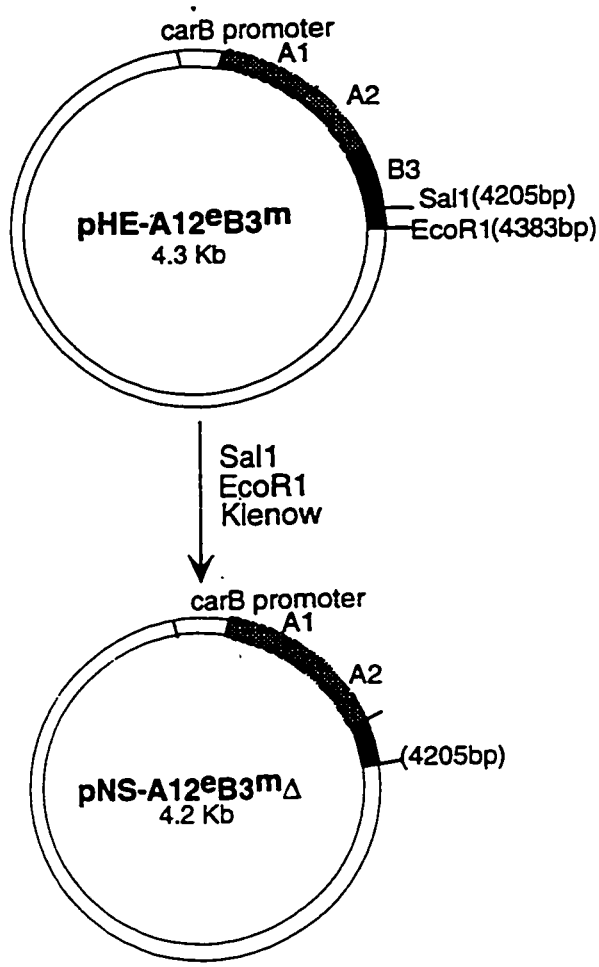

further supported by previous mutagenesis studies (77) involving a deletion of 91 and 119 residues representing about two thirds of the *E. coli* regulatory domain, which abolished UMP inhibition although the enzyme was still sensitive to ornithine.

On the basis of sequence alignment, in CAD, the two regions correspond to tyrosine 1364 to asparagine 1394 and asparagine 1394 to arginine 1416. To examine the effect of a deletion that would disrupt the sequence proposed to be crucial by Cervera et al, a deletion mutant was constructed. The truncation was at Glycine 1402 within the B3 subdomain of CAD. The mutant lacked 59 of the 163 residues from the carboxyl end of the B3 subdomain of the chimera (Figure 3.9), and by alignment to the *E. coli* sequence, lacked 14 amino acid residues from proposed UTP fold.

Construction of the plasmid pNS-A12^{e}B3$^{m}\Delta$

The plasmid pHE-A12^{e}B3^{m} was reacted with *Sal* I (site in CAD, 4205) and *Eco* RI (site in vector). The ends were made flush using the Klenow fragment of DNA polymerase. The 4.2-kb fragment was gel purified and religated using *T4* DNA ligase. The 4.2 kb plasmid pNS-A12^{e}B3$^{m}\Delta$ encodes the *E. coli* CPS A1 and A2 subdomains (residues 1-364) and a truncated mammalian CAD regulatory subdomain (residues1297–1402). The segment-encoding residue 1402 to 1461 was excised from the plasmid pHE-A12^{e}B3^{m} (Figure 3.9).

Expression and Purification of the Deletion mutant CPS-A12^{e}B3$^{m}\Delta$

The plasmid was transformed into the *E. coli* strain RC50 that lacked the *carA* and *carB* genes encoding the small and large subunits of *E. coli* carbamoyl phosphate synthetase. The deletion mutant was constitutively expressed under the control of the *car* AB promoter. A 20-µl overnight culture was typically innoculated into a 200 ml 2XYT media supplemented with 0.1% glucose and 125 µg/ml ampicillin at 37°C. Cells were grown 18-20 hours, and harvested at stationary phase by centrifugation at 4000 rpm, 4°C, 30 minutes. SDS gel electrophoresis revealed a new 51-kDa species not present in

extracts of untransformed cells. The truncated protein was partially purified by a fast flow Q-Sepharose column, using the same approach as for the wild type chimera. However in this case, there were several contaminants in the preparation. The concentration of the recombinant truncated protein was estimated by scanning densitometry of a Coomassie stained SDS gel as described previously.

3.8 Kinetics of the Deletion Mutant CPS-A12^{e}B3$^{m}\Delta$

The ammonia-dependent carbamoyl phosphate synthetase activity of the partially purified deletion mutant CPS-A12^{e}B3$^{m}\Delta$ was measured as a function of ATP concentration. The rate of the carbamoyl phosphate synthetase reaction was measured by initiating the reaction with [^{14}C] $NaHCO_3$ and trapping the radiolabeled carbamoyl phosphate as carbamoyl aspartate. The deletion mutant was slightly more active than the full-length chimeric protein (Table 3.4) when the protein amount was taken into consideration, and the mutant had reduced sensitivity to allosteric effectors. The ATP saturation curves (Figure 3.10) obtained in the absence and presence of allosteric effectors were almost indistinguishable. At low concentrations of ATP, 3 mM UTP had no significant effect on the activity, although slight inhibition was observed at ATP concentrations above 1 mM.

3.9 Effector binding to the Deletion Mutant

PRPP binding to the deletion mutant was carried out by the previously described microcolumn method. The data obtained by plotting PRPP bound per mole of protein as a function of the PRPP concentration was fitted to a Michaelis Menten equation. PRPP binds to the deletion mutant with a dissociation constant of 79 μM, which is almost 2-fold higher than the value obtained for the parent chimera. In the presence of 5 mM UTP, the K_d increased to 152.6 μM, suggesting that UTP still binds but with a much lower affinity relative to the parent chimera as the effect on the PRPP binding is at least 1 fold lower than in the wild type chimera (Table 3.4). A Scatchard was plotted in order to

Figure 3.10 ATP Saturation Curves of the Deletion Mutant

The ammonia-dependent CPSase activity of 3.8 μg of the deletion mutant was assayed as a function of ATP concentration in the presence of 200 μM PRPP (-●-) and 3 mM UTP (-■-). The effect of the same concentrations of PRPP (-○-) and UTP (-□-) on 3 μg of the phosphorylated protein was also determined.

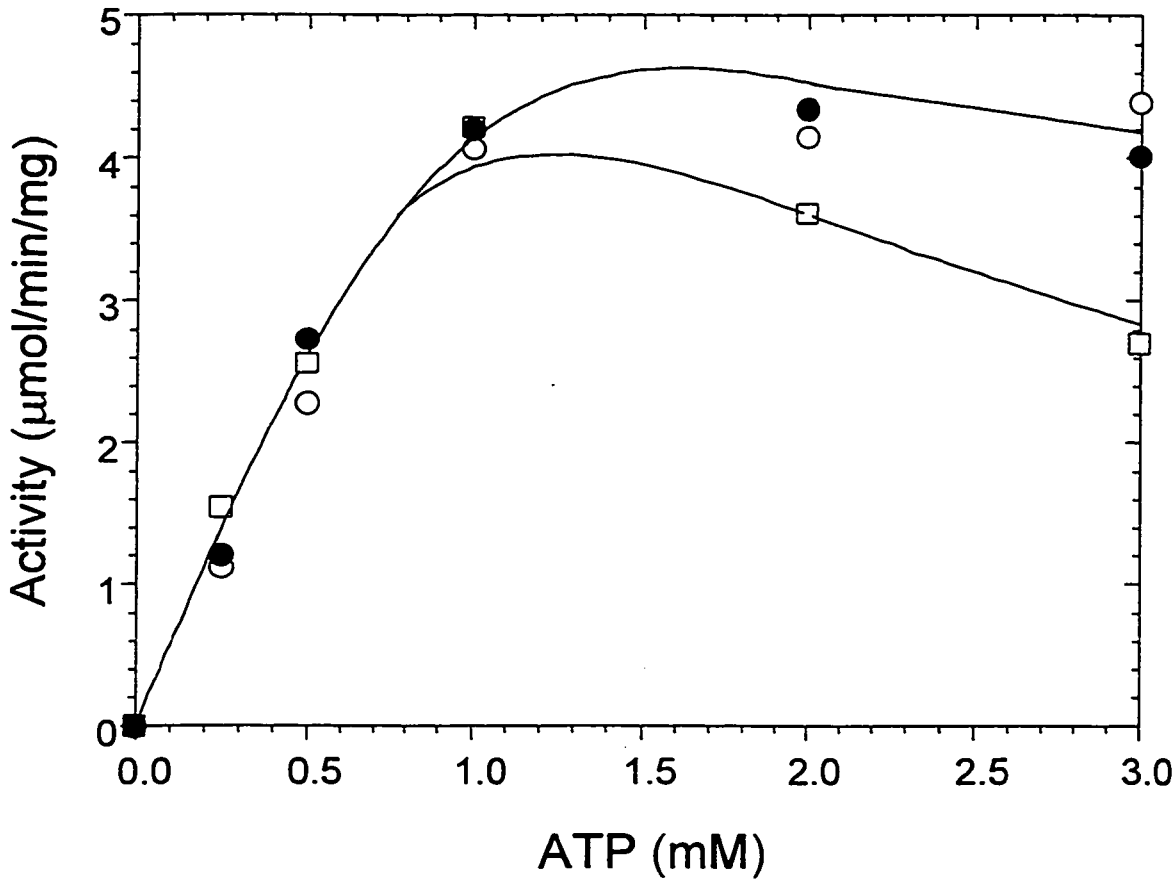
Activity (µmol/min/mg)
0
1
2
3
4
5
0.0
0.5
1.0
1.5
2.0
2.5
3.0
ATP (mM)

Table 3.4 Summary of Kinetic Parameters of Chimeria Deletion Mutant CPS-A12^{e}B3$^{m}\Delta$

Protein	Ligand	Km	Vmax	Kcat	Kcat/Km
		mM	μmol/min/mg	s^{-1}	$M^{-1}s^{-1}$
E.coli CPSase[a]	none	0.43 ± 0.02	3.0 ± 0.10	8.0 ± 0.3	18,600
CAD CPSase[b]	none	2.14±0.16	0.194±0.006	0.78 ± 0.02	363
Chimeric CPSase	none	0.46 ± 0.14	3.46 ± 0.22	3.35 ± 0.21	7270
	200μM PRPP	0.43 ± 0.12	5.18 ± 0.30	5.01 ± 0.29	11,600
	3 mM UTP	0.45 ± 0.11	1.64 ± 0.08	1.59 ± 0.08	3520
Deletion Mutant	none	0.53 ± 0.10	6.08 ± 0.30	5.30 ± 0.26	9940
	200μM PRPP	0.64 ± 0.11	6.36 ± 0.29	5.51 ± 0.25	8610
	3 mM UTP	0.51 ± 0.23	5.80 ± 0.85	5.03 ± 0.73	9860

[a]Data from ref 66
[b]Data from ref 65

Figure 3.11 Binding of PRPP to the deletion mutant

The binding of labeled PRPP to 9.8 μg of the deletion mutant CPS-A12^{e}B3$^{m}\Delta$ was measured by the microcolumn method in the absence (-●-) and the presence (-○-) of 5 mM UTP. In the Scatchard plot, V represents the ratio of PRPP-protein complex/protein and PRPP represents free PRPP. The kinetic parameters obtained by a least squares fit of the Scatchard plot are given in Table 3.5

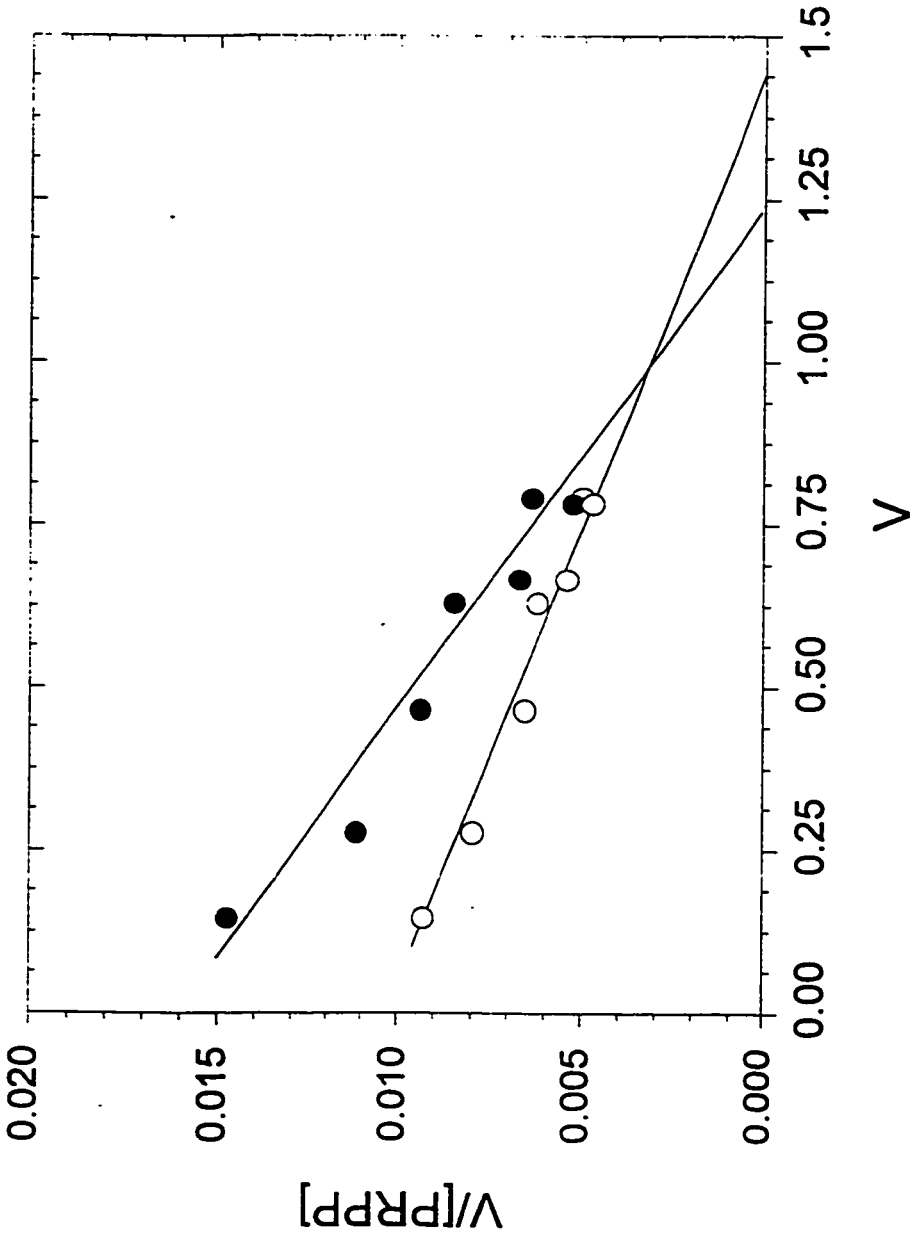
V/[PRPP]
0.020
0.015
0.010
0.005
0.000
0.00
0.25
0.50
0.75
1.00
1.25
1.5
V

Table 3.5 Comparison of PRPP Binding parameters for Chimera wild type and Deletion Mutant

Parameter		Ligand	Chimera	Deletion Mutant
K_d	(μM)	none	46.0 ± 1.9	78.6 ± 6.6
n [a]		none	1.0 ± 0.04	1.23 ± 0.10
K_d	(μM)	UTP	133.5 ± 15.8	152.6 ± 24.7
n [a]		UTP	1.52 ± 0.25	1.52 ± 0.25

[a] number of binding sites per polypeptide chain

determine the number of binding sites in the deletion mutant (Figure 3.11).

Thus, the carboxyl end residues that were truncated in the deletion mutant seem to be essential for signal transmission, but are not crucial for ligand binding.

3.10 Discussion

Previous studies by Liu, Guy and Evans have demonstrated that the catalytic activity of *E. coli* CPSase can be placed under the control of the mammalian allosteric effectors by swapping the putative *E. coli* regulatory domain for the corresponding region of CAD. In the original construct, the borders of the regulatory domain of CAD were defined (15,17) by sequence homology and controlled proteolysis experiments. In the new construct pHE-A12^{e}B3^{m}, additional 25 residues were deleted from the amino end of the mammalian regulatory domain so that it corresponded more closely to the size of the regulatory domain described in the X-ray structure of the *E. coli* CPSase (48). The A2 and A3 junction was identified as the CPS.A and CPS.B sequence was sufficiently similar to allow an unambiguous alignment.

The chimera consists of two *E. coli* subdomains A1 and A2. The 31-kDa A2 subdomain (97) is the catalytic domain that alone can catalyze ammonia-dependent carbamoyl phosphate synthetase activity, at a rate that is ten times faster than either the CPS.A or the intact CPSase. The 9-kDa A1 subdomain is an attenuation domain as it modulates the hyperactivity of the A2 subdomain. The CPS.A and CPS.B halves can carry out the overall synthesis of carbamoyl phosphate only in the form of a homodimer. In case of the chimeric CPS-A12^{e}B3^{m}, the dimeric structure was confirmed by chemical cross-linking. The functional studies of the isolated components (97) suggest that the A3 domain is not required for catalytic activity. This may explain why the K_m and K_{cat} for the chimeric protein lacking the A3, is so similar to the values obtained for the *E. coli* CPSase.

The response of the chimera to allosteric ligands shows that CPS.A, like CPS.B,

can be allosterically regulated. The binding of ligands to the regulatory domain triggers an allosteric signal that is transmitted as efficiently to the CPS.A catalytic site, as to the CPS.B. Changes in the catalytic activity may result from a global change in the tertiary structure of the regulatory domain resulting in an alteration in the way it interacts with the catalytic subdomain. For instance, all activators are likely to induce the same conformational change in the regulatory domain, which modifies its interaction with the catalytic domain in the same way and promotes catalysis. Again the conformation produced by all inhibitors would be expected to be similar.

Since *the E. coli* catalytic subdomains in the chimera $A12^{e}B3^{m}$ as well as in the pHL2 $A123B12^{e}B3^{m}$ can be regulated by mammalian effectors, it is indicative of the fact that the signaling mechanism is virtually identical in *E. coli* and mammals. Although the sequence of the regulatory domain in *E. coli* and mammalian CPSase is quite dissimilar (21% sequence identity), the domains in each case must have a similar tertiary fold and a similar interaction with the catalytic domains.

E. coli CPSase is not phosphorylated by cAMP-dependent protein kinase. In CAD CPSase, the phosphorylation site has been identified within the regulatory domain (71). In the chimera where the regulatory domain B3 replaces the A3, phosphorylation has the same effect on the *E. coli* catalytic domain as in case of CAD CPSase. The effect is consistent with the previous observation that the conformational changes induced by both allosteric effectors and phosphorylation occur entirely within the regulatory domain, and its response is mediated by a change in its juxtaposition relative to the catalytic sites.

Rubio and his associates (57) clearly established the location of the UMP site in E. coli CPSase using photoaffinity labeling. This specifically modified a Lysine 992. Analysis of the sequence of several CPSases around this residue supported the existence of a nucleotide-binding fold located entirely within the carboxyl terminal

domain. Previous mutagenesis studies (74,75,77) showed that a deletion of 91 or 119 residues from the carboxyl end of the regulatory domain abolished allosteric regulation by UMP but not ornithine. In order to study the function of the carboxyl end of the regulatory domain, a deletion mutant was constructed which lacked 59 of the 163 residues from the carboxyl end of the regulatory domain in the chimera $A12^{e}B3^{m}$. This site was selected because it disrupted the sequence proposed by Cervera et al to be essential for UMP. The mutant CPS-$A12^{e}B3^{m}\Delta$ was truncated four residues on the amino aide of Ser1406 in CAD, the residue phosphorylated in CAD CPSase. Thus, the deletion mutant lacked the phosphorylation site. The results obtained demonstrated that, as predicted, the CPSase activity of the mutant was almost insensitive to the effectors PRPP and UTP. Although, interestingly, a binding study indicated that both the effectors were still bound to the mutant but with a significantly higher dissociation constant as compared with the wild type chimera. Thus, we propose that the residues deleted from the carboxyl end must be involved in the transmission of the signal to the catalytic subdomain or that because of a change in the conformation of the deletion protein, the transmission of the allosteric signal to the catalytic subdomain is being disrupted.

The UMP binding site has not yet been identified in the crystal structure of the *E.coli* CPSase structure it has been tentatively identified by mutagenesis and photoaffinity labeling. In the crystal structure, inorganic phosphate has been shown to bind through interactions with Lys954, Thr974, Thr977 and Lys992. Site-directed mutagenesis at Thr977 abolishes UMP inhibition while Lys992 has been shown to be photolabeled by UMP. In CAD, the residues corresponding to *E. coli* Lys954 and Thr977 are conserved, while Thr974 is replaced by a serine, and Lys992 by a tryptophan. The fact that UTP still binds to the deletion mutant that is truncated downstream from Gly1402 (in CAD), suggests that in addition to the above corresponding residues, most

of the other ligand interaction residues must be located upstream of Gly1402. In case of PRPP, the deletion mutant binds with a K_d that is two-fold higher than in case of the wild type chimera. Although the affinity for PRPP is lower, the activator binding site must be located in the amino half of the regulatory domain. This is consistent with the CAD gene deletion studies of Davidson et al that suggested that PRPP binds closer to the amino end of the regulatory domain than does UTP.

The results with the chimera and the deletion mutant demonstrate that the regulatory domain behaves as an exchangeable module, which has differentiated in different species to bind a diverse array of allosteric effectors. The allosteric ligands and phosphorylation induce conformational changes exclusively within the regulatory domain, thereby altering its interaction with the catalytic subdomains resulting in activation or inhibition. The response of the chimera to effectors has shown that although typically, the CPS.B domain is the regulatory locus, CPS.A can be placed under allosteric control. Deletion studies demonstrate that the PRPP and UTP binding sites are in the amino half of the regulatory domain. A deletion of the carboxyl residues disrupted signal transmission suggesting that the carboxyl end, which interfaces between the catalytic and regulatory domains is essential for mediating interdomain interactions.

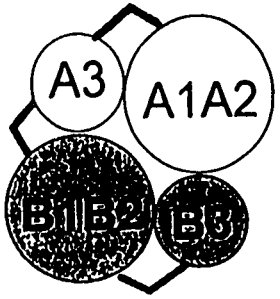

CPS Domain
A1A2A3-B1B2B3

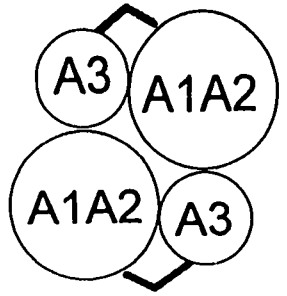

CPS.A Dimer
$(A1A2A3)_2$

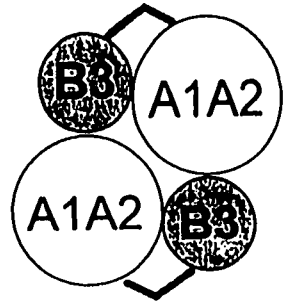

Chimeric Dimer
$(A1A2B3)_2$

CHAPTER 4 Cloning, Expression and Characterization of the Regulatory Domain of CAD

4.1 The Regulatory Subdomain Hypothesis

Carbamoyl phosphate synthetases from different organisms have similar catalytic mechanisms and amino acid sequences, but their structural organization, subunit structure, and mode of regulation can be very different (Table 4.1). The CPSase domain of CAD is the locus of allosteric control in the *de novo* pyrimidine pathway. It undergoes feedback inhibition by UTP and activation by PRPP and cAMP-dependent protein kinase. A second distinctly different carbamoyl phosphate synthetase CPSase I found in the liver and small intestine of ureotelic animals, is localized in the mitochondrial matrix, where it catalyzes the first step in urea synthesis. Arginine specific CPSase I is regulated by N-acetyl glutamate (AGA), which acts as an allosteric activator (101). Mg^{2+} in excess of that required for the formation of MgATP (102), and K^+ (103) are also essential activators. The *E. coli* CPSase provides carbamoyl phosphate for both pyrimidine and arginine biosynthesis and is therefore regulated by metabolites from each pathway. It is activated by L-ornithine, NH_3 and IMP and inhibited by UMP. Binding studies have demonstrated the presence of one site for each of the ligands UMP and IMP (104). Recently, with the elucidation of the crystal structure of *E.coli* by Rayment and Thoden (48) two ornithine sites have been located. In yeast, the arginine specific CPSase, the product of the *CPA2* gene does not appear to be regulated (63) whereas the pyrimidine specific CPSase, a part of the yeast *URA2* protein is inhibited by UTP.

Although the overall sequence identity of these CPSases is 37-67%, the extreme carboxyl end of the protein, i.e. the B3 region, is poorly conserved (Figure 4.1). The significantly lower homology of only 24-58 percent in the B3 region of all CPSases may

Table 4.1 Comparison of the Allosteric Effect and Amino Acid Sequence Homology of Different CPSases

Protein	Activator	Inhibitor	Homology to CAD	
			overall	*In B3 Region*
CAD CPS domain	PRPP	UTP	—	—
CPSase I	N-Acetyl glutamate	none	53%	36%
Yeast Arg CPSase	none	none	53%	28%
Yeast Ura2 CPS domain	none	UTP	59%	48%
E. coli CPSase	IMP, ornithine, NH_4^+	UMP	40%	24%

Figure 4.1 Comparison of the Amino Acid Sequence at the COOH terminal end of different CPSases

Identical residues in CAD (HAM), rat mitochondrial (CPSI), Drosophila (DROS), yeast URA2, yeast arginine specific CPSase (CPA2), and *E. coli* CPSase (*carB*) are boxed. The two vertical arrows indicate the end of the 140-kDa fragment and the 150-kDa fragment of CAD, respectively. The horizontal arrow indicates the beginning of the CAD DHOase domain.

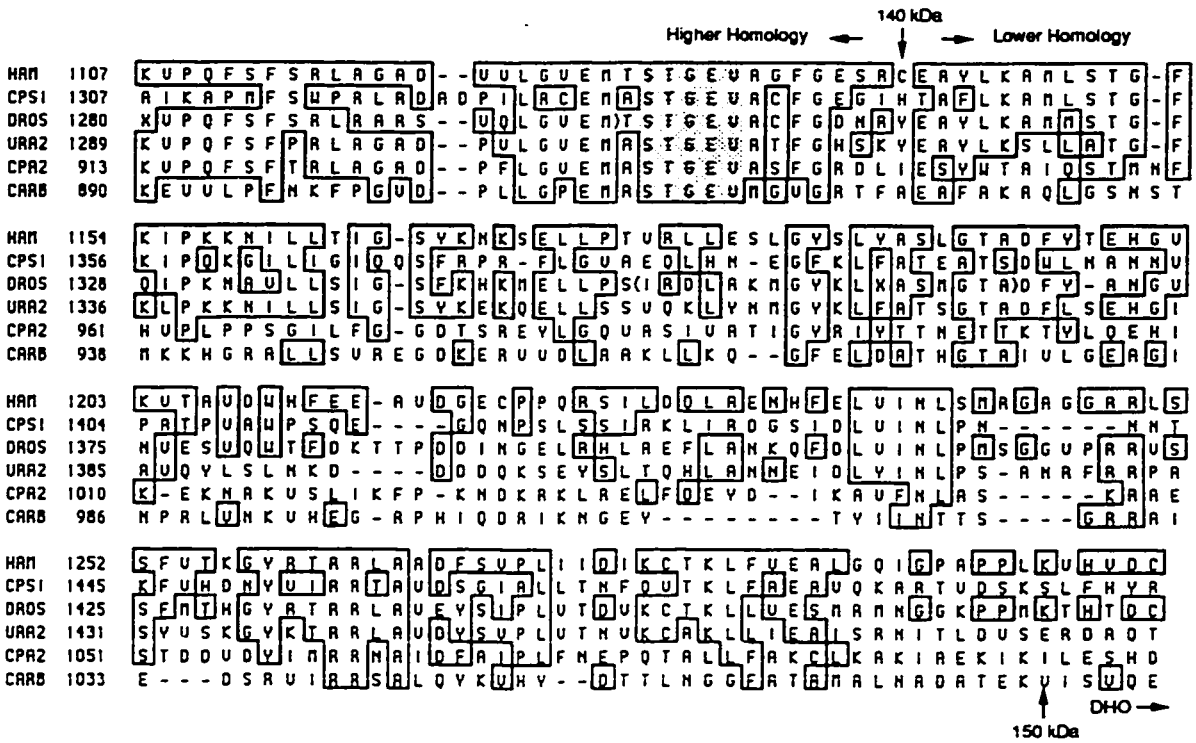
140 kDa
Higher Homology
Lower Homology
HAM 1107
CPS1 1307
DROS 1280
URA2 1289
CPA2 913
CARB 890
HAM 1154
CPS1 1356
DROS 1328
URA2 1336
CPA2 961
CARB 938
HAM 1203
CPS1 1404
DROS 1375
URA2 1385
CPA2 1010
CARB 986
HAM 1252
CPS1 1445
DROS 1425
URA2 1431
CPA2 1051
CARB 1033
DHO
150 kDa

be a reflection of differences in the types of allosteric ligands that regulate these enzymes. A comparison of the amino acid sequence homology among different CPSases and their allosteric effectors (Table 4.1) indicates that a higher homology exists in the B3 region of CPSases regulated by the same allosteric effector. For example, the CPSase of the *URA2* protein in yeast, can be allosterically regulated by UTP, which, is also an allosteric inhibitor of CAD CPSase. Accordingly, the B3 region of both the *ura2* CPSase and CAD CPSase, shows a homology of 48 percent. On the contrary, the mammalian mitochondrial CPSase (CPSase I), which is activated by N-acetyl glutamate, shows only a 36 percent homology with CAD in the B3 region despite a 53 percent overall homology between the two CPSases. The lower homology is also evident in case of the CAD CPSase in comparison to the yeast arginine specific CPSase and *E. coli* CPSase.

Controlled proteolysis studies of CAD have demonstrated that the 150 kDa fragment corresponding to the whole GLN-CPS domain immediately cleaved at the carboxyl end, releasing a 140 kDa and a 14 kDa species, suggesting that the 14 kDa carboxyl end represented a separately folded subdomain.

Chemical modification and photoaffinity labeling studies by Rubio and associates (76) demonstrated that the carboxyl end of mitochondrial CPSase I contained the binding site for the activator N-acetyl glutamate. UMP was used to photoaffinity label the allosteric inhibitor site in *E.coli* CPSase. UMP was observed to incorporate into the COOH terminal of the large subunit of the enzyme (74). More recently, Rubio et al have specifically identified lysine 992 as a residue in the carboxyl end of *E. coli* CPSase that covalently attached to UMP (57). The identification of lysine 992 as the site of photochemical addition of UMP, and the analysis of sequences surrounding this lysine provided strong evidence for the location of the binding fold for the nucleotide inhibitor at the carboxyl end of the *E. coli* CPSase.

CAD is activated by phosphorylation. The phosphorylation site believed to regulate CAD CPSase activity (71) is located within the B3 region of the mammalian multifunctional protein.

Since all the evidence for the location of the allosteric binding sites were converging to the carboxyl end of the CPSase domain, an *E. coli*-mammalian chimera was constructed by replacing the regulatory region of the *carB* gene of *E. coli* with the corresponding cDNA of CAD (56). The resulting recombinant protein was a chimera consisting of *E. coli* CPSase catalytic domains and the mammalian CPSase regulatory domain. The protein was fully active, and no longer sensitive to the *E. coli* CPSase specific inhibitor UMP. Instead, the recombinant protein responded to the mammalian effectors PRPP and UTP. ATP saturation kinetics in the presence of UTP increased the K_m for ATP to 2.5 mM from a value of 1.66 mM while the activator PRPP decreased this value to 0.5 mM. This domain swapping experiment clearly established the carboxyl end of the CPSase as a regulatory domain.

The regulatory subdomain B3, in the *E. coli*-mammalian hybrid described above, has been shown to contain the allosteric binding sites. The results obtained and described in Chapter 3 demonstrate that the subdomain B3 behaves as an exchangeable module by replacing the A3 subdomain of CPS.A, and efficiently transmitting regulatory signals to the *E. coli* CPS.A active site thereby placing CPS.A under allosteric control.

Considering the evidence described above, an interesting question was "could the regulatory subdomain exist as an independent autonomously folded functional subdomain that binds allosteric ligands in the absence of the CPSase catalytic sites?" To answer this question, the cDNA encoding the mammalian regulatory subdomain was cloned into an overexpression vector to obtain a recombinant protein for allosteric binding studies.

4.2 Cloning and Overexpression of the Regulatory Domain

Construction of pJB-B3

The 190-residue mammalian regulatory subdomain was defined according to Liu et al [Liu 1994] and by a significantly lower sequence homology at the carboxyl terminal end of the CAD CPSase compared to other CPSases. The 570-bp cDNA encoding CAD residues 1265 to 1455 was amplified by PCR using the plasmid pCKCAD10 (20) as a template. The 5' primer incorporated an *Nde*1 site and the 3' primer an *Eco*R1 site with a stop codon. The amplified PCR fragment contained at its 5' and 3' ends restriction sites *Nde*1 and *Eco*R1, respectively. The 570-bp fragment was cleaved with *Nde*1 and *Eco*R1, gel purified, and cloned into the *Nde*1 and *Eco*R1 sites of a vector derived from pEK81 (91). which consists of a pUC 119 with a 2.8 kb insert encoding the entire *pyr* BI operon including the upstream regulatory region. The *pyr* B and *pyr* I genes code for the *E. coli* ATCase catalytic and regulatory subunits, respectively.

Expression of pJB-B3

The recombinant pJB-B3 was transformed into L673 and grown on minimal media containing limiting amounts of uracil (Materials and Methods) in order to induce expression of the regulatory protein. A single colony of pJB-B3/L673 was inoculated into 10 ml LB media containing 100 μg/ml ampicillin and grown overnight at 37°. The overnight culture was then used to inoculate a 100-ml media that contained 100 μg/ml ampicillin and 12 μg/ml of uracil in a one-liter flask. The cells were grown at 37°C for 18-20 hours at which time, the protein was induced. When uracil is exhausted after 16-18 hours, the protein is induced following derepression of the *pyr* BI promoter.

The cells were harvested by centrifugation at 4000 rpm, 4°C for 30 minutes. The cell pellet was resuspended in 2 ml of 50 mM Tris/HCl, pH 8, 1 mM DTT, 1mM EDTA and 5% glycerol and 1 mM PMSF was added immediately prior to lysis. The cells were lysed by sonicating on ice, 5X for 10 seconds each. SDS-Page

Figure 4.2: Construction of the Regulatory subdomain

The 570 bp cDNA insert encoding the mammalian regulatory domain was excised from the pJB-B3 recombinant by cleaving the plasmid with *Nde*I, the 5' overhang made flush using the Klenow fragment of DNA Polymerase, followed by an *Eco*RI digestion. The pRSETA vector was prepared for cloning of the insert by treatment with *Bam*HI, its 5' ends made flush with Klenow, and finally cleaved with *Eco*RI. Following gel purification, the insert and vector were ligated.

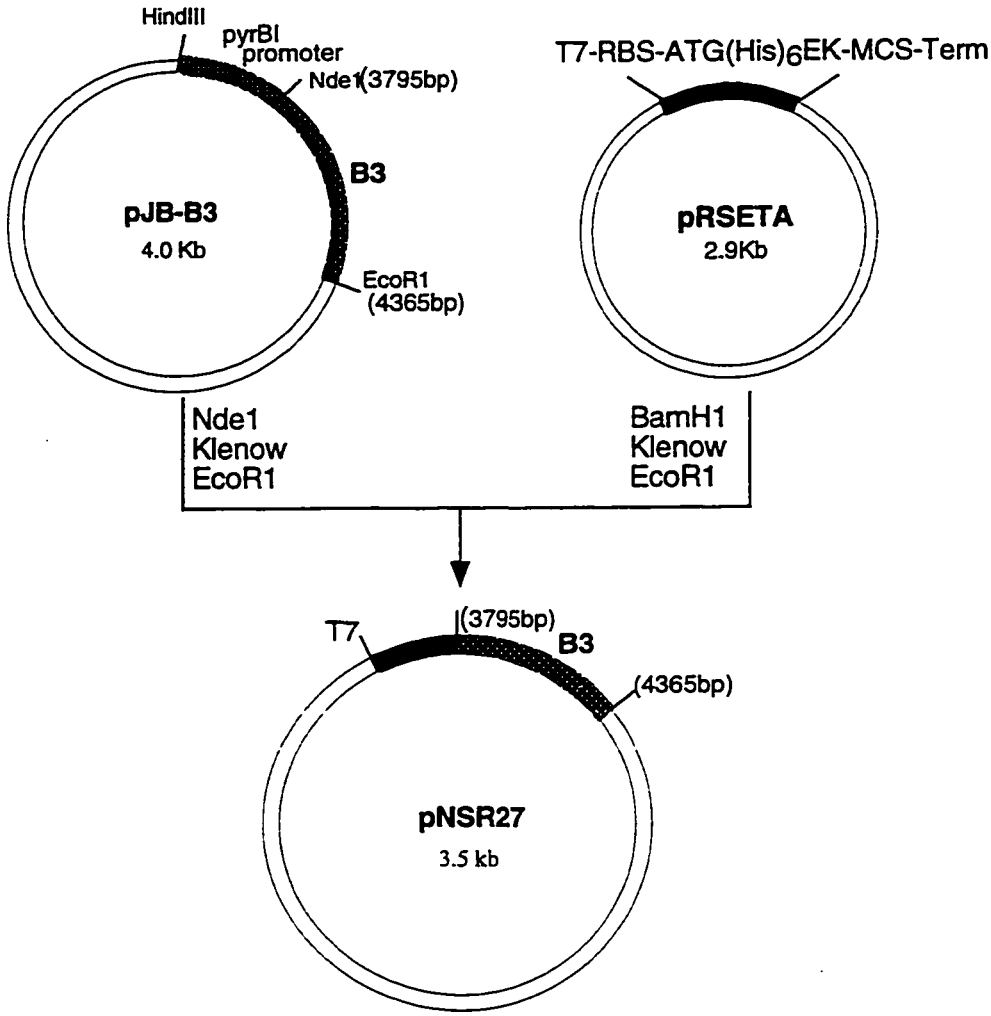
HindIII
pyrBI promoter
Nde1(3795bp)
B3
pJB-B3
4.0 Kb
EcoR1
(4365bp)
T7-RBS-ATG(His)6EK-MCS-Term
pRSETA
2.9Kb
Nde1
Klenow
EcoR1
BamH1
Klenow
EcoR1
T7
(3795bp)
B3
(4365bp)
pNSR27
3.5 kb

electrophoresis revealed the presence of a new species with a molecular weight of 20 kDa. This species was confirmed to be of mammalian origin by immunoblotting using anti-CAD antibodies. However, expression of the regulatory protein was very low and insufficient for further binding and kinetic studies. In order to improve the yield of the regulatory recombinant, another overexpression vector was used as described below.

Cloning of the Regulatory Domain coding sequences into the pRSET expression vector

The 570 bp cDNA insert in the recombinant pJB-B3 was excised by treatment with *Nde*1, the 5' overhang was made flush using the Klenow fragment, followed by an *Eco*R1 digestion. The pRSET vector is a 2.9 kb pUC based vector. Sequences inserted into the multiple cloning sites are expressed as a fusion protein containing an N-terminal poly-histidine tag. The pRSETA vector was prepared for cloning of the insert by treatment with *Bam*H1, its 5' ends made blunt with Klenow, and finally restricted with *Eco*R1. Both the insert and the vector DNA were gel purified and ligated using T4 DNA ligase. The resulting recombinant pNSR27, was confirmed by restriction analysis to contain the CAD regulatory coding sequences.

Overexpression and Purification of the pNSR27 recombinant

The recombinant pNSR27 was transformed into BL21 (DE3) host cells. The BL21 (DE3) strain is a λDE3 lysogen carrying the T7 RNA polymerase gene under *lac*UV control and is therefore a suitable host for expression from T7 promoters. A one-liter culture was typically grown from a 10 ml overnight culture grown in Luria Broth containing a 100 μg/ml ampicillin at 37°C. The culture was grown for about 3 hours till the O.D. at 600nm was 0.6-0.8. Isopropyl-1-thio-β-D-galactopyranoside (IPTG) was added to a concentration of 0.4 mM and the induction continued for an additional two hours. The culture was then placed on ice and the cells were harvested at 4000 xg for 20 min at 4°C. At this point the cell pellets could be frozen at -20°C and stored until

further use.

Prior to purification, the cell pellets were thawed and resuspended in ice-cold 5 ml of 50 mM Tris, pH 8.0, 150 mM NaCl, 10 mM β-mercaptoethanol and 5% glycerol. 1 mM PMSF was added just before lysis. The cells were lysed by sonication 5 times on ice, 15 sec each. The sonicate was centrifuged at 14,000 X g, 30 min at 4°C. The supernatant and the pellet fractions were analyzed on a 10% SDS-PAGE gel.

Analysis of the cell lysates showed that the BL21 (DE3) cells transformed with the recombinant pNSR27, contained a new species with a molecular mass of 26.7 kDa, which was absent in untransformed cells. Although the majority of the recombinant protein was found in the pellet, a significant amount remained soluble. Solubility was enhanced to an optimum level by inducing with 0.1 mM IPTG and shifting the cells from 37°C to 30°C for two hours following induction by IPTG.

Purification of the recombinant regulatory domain was carried out using a batch procedure. The batch procedure entails binding of the protein to the Nickel resin forcing the equilibrium towards binding of the tagged protein and the exclusion of other naturally occurring His-proteins which bound much weaker. Again, the purification process was optimized by closely matching the amount of tagged protein to the capacity of the resin used. Since the 6X His-tagged regulatory recombinant would presumably have a higher affinity for the nickel resin, if it filled all the available binding sites on the resin, fewer background proteins would be retained on the resin.

Purification was performed at 4°C. The supernatant was added to 3 ml of Nickel resin (Invitrogen) previously equilibrated in 50 mM Tris/HCl, 10 mM mercaptoethanol, 10% glycerol, pH 8.0. The protein-resin was stirred gently on ice for 1 hour following which it was loaded on to a 10 ml BIORAD column and the flow-through collected. The 3-ml bed volume resin was washed with 5 X bed volume of the above Tris buffer, pH 8.0,

Figure 4.3 Expression and Purification of the Regulatory Domain of CAD

The cell pellet from 1 liter culture was resuspended in 10 ml of 50 mM Tris/HCl, pH 8.0, 150 mM NaCl, 10 mM -mercaptoethanol and 5% glycerol. 1 mM PMSF, freshly prepared was added prior to lysis. Cells were lysed by sonication 5 x 10 seconds each. The cell extract was centrifuged at 14,000 X g, 30 min at 4°C. Purification was carried out by a batch procedure. The supernatant was incubated with the Nickel resin (Invitrogen) for one hour. The protein-resin complex was loaded on to a column to form a 2-ml bed. The column was washed with the above buffer, followed by a wash with the Tris/HCl buffer containing 30 mM imidazole until the absorbance at 280 nm was negligible. The his-tagged protein was eluted with 50 mM Tris/HCl pH 8.0, 150 mM NaCl, 10 mM mercaptoethanol, 5% glycerol containing 200 mM Imidazole.

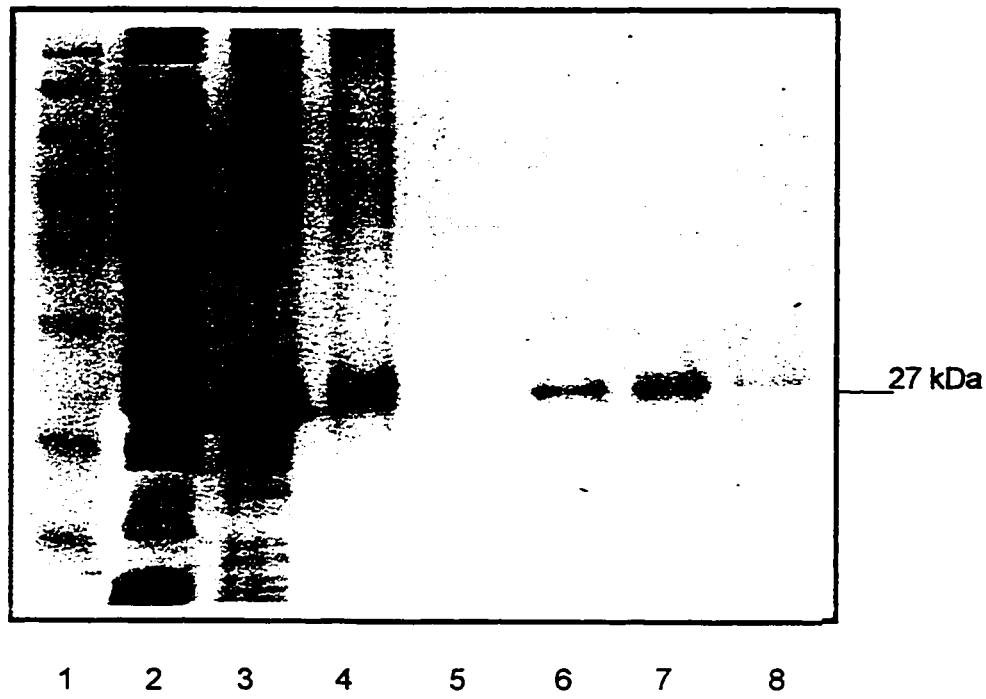
27 kDa
1
2
3
4
5
6
7
8

until the absorbance at 280 nm was less than 0.05. The resin was then washed with five times the bed volume of the above Tris/HCl buffer containing 30 mM imidazole until the A_{280} was less than 0.05. Finally, the histidine tagged protein was eluted with 0.250 M imidazole. Fractions were collected and analyzed on SDS-PAGE. The elution fractions containing the purified 26.7 kDa protein were pooled and stored at -70°C. The identity of the 26.7 kDa his- tagged regulatory domain was confirmed by western-blotting using anti-His antibodies (Invitrogen). The protein was passed through a NICK-spin column (Pharmacia) equilibrated with 50 mM Tris, pH 8.0, 1 mM DTT and 5% glycerol in order to remove the NaCl and imidazole.

Protein concentration was determined using the Micro BCA detection system by PIERCE., and by scanning Coomassie-blue stained polyacrylamide gels. The gels were scanned and the concentration of the purified protein determined by measuring the ratio of the peak density to the total density in a given lane and the total amount of protein applied. The background density was subtracted and all measurements were made within the linear range of the densitometer. A one-liter culture gave approximately 500 μgs of purified protein, sufficient for binding studies.

4.3 Binding of Allosteric ligands to the Regulatory Domain

^{32}PRPP was synthesized and assayed, as described in Chapter 3. The binding of PRPP to the isolated regulatory domain was determined using the spin column procedure, which separates free ligand from protein-bound ligand. The regulatory domain (12.5 μg) was incubated 15 min, at 37°C with increasing concentrations of ^{32}PRPP in a 150 μl reaction. The reaction was then transferred very carefully to the top center of a G-50 Sephadex bed of a NICK spin column (Pharmacia). The column was then centrifuged at 1000 X g for 4 min at 4°C. The effluent containing the protein-bound PRPP was transferred to a scintillation vial and counted in a Tri-Carb Scintillation counter. The data obtained by plotting PRPP bound per mole of protein as a function of

Figure 4.4 PRPP Binding to the Regulatory Domain

The binding of [^{32}P] phosphoribosyl-5'-pyrophosphate to 12.5 μg of the regulatory recombinant (-●-) was measured by the microcolumn method as described in Chapter 3. Data obtained for PRPP bound per mole of the protein as a function of the PRPP concentration was fitted to a binding isotherm. In the Scatchard plot, V represents the ratio of PRPP-protein complex/protein, and PRPP represents free PRPP. The kinetic parameters obtained by a least squares fit of this Scatchard is shown in Table 4.2.

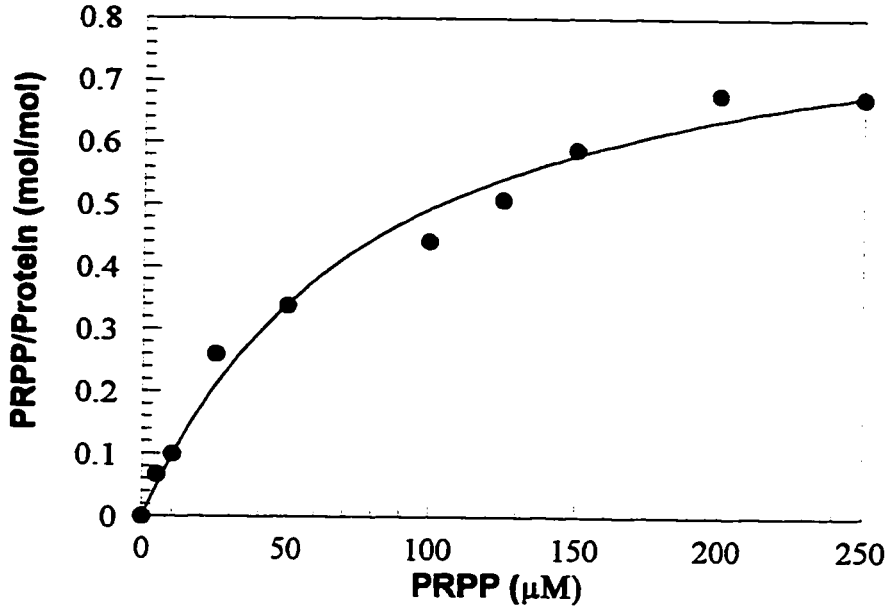
0.8
0.7
0.6
0.5
0.4
0.3
0.2
0.1
0
PRPP/Protein (mol/mol)
0
50
100
150
200
250
PRPP (μM)

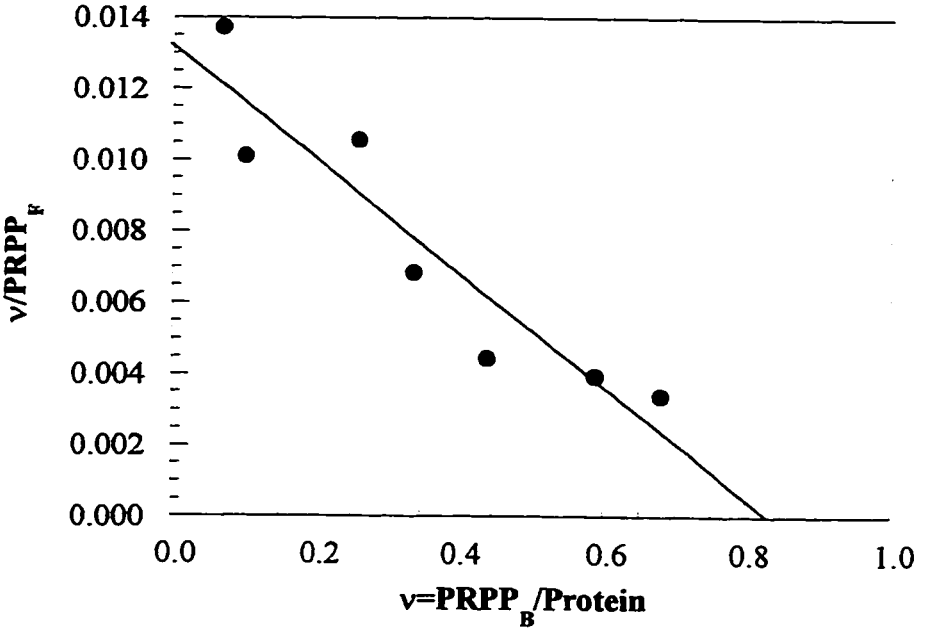
0.014
0.012
0.010
0.008
0.006
0.004
0.002
0.000
v/PRPP_F
0.0
0.2
0.4
0.6
0.8
1.0
v=PRPP_B/Protein

the PRPP concentration was fitted to a binding isotherm. PRPP binds to the regulatory domain with a dissociation constant (K_d) of 83.5 μM, as compared to 10 μM for CAD and 46 μM for CPS-A12^{e}B3^{m} chimera. A scatchard plot was generated (Figure 4.4) using the equation $\upsilon / [L] = n / K - \upsilon / K$, where υ is the mole of ligand bound per mole of protein, [L] is the concentration of free ligand (μM), n is the total number of binding sites, K is the dissociation constant (μM). The Scatchard plot of the binding data was linear and gave a dissociation constant (Table 4.2) that was 8-fold higher than the value obtained for CAD. The Scatchard plot gave an intercept corresponding to an n value of 0.89 indicating that there is one site for PRPP per molecule of the regulatory domain. This fits the previous determination of one PRPP site per molecule of CAD as well as in the chimera CPS-A12^{e}B3^{m}.

Effect of UTP on PRPP Binding to the Regulatory Domain

The value for the dissociation constant for UTP cannot be determined by a direct binding experiment as the K_d for UTP is as high as 1 mM and would require a relatively high concentration of protein. An effect of the nucleotide on PRPP binding to the regulatory domain indicated that UTP does bind to the domain. In the presence of a saturating concentration of 5 mM UTP, the affinity for PRPP decreased more than two fold. The data was used to produce a Scatchard plot. A plot with and without UTP showed that although the total number of sites did not change significantly, the dissociation constant increased significantly thereby reducing the affinity of the regulatory domain for PRPP (Figure 4.5).

4.4 Cloning of the CAD whole CPSase and CPS.A domains

The recombinant clone, pHL1, encoding for the CAD GLN CPSase domains (70) was used to construct a recombinant containing only the CPSase domains. The 3.2 kb fragment encoding the CAD CPSase domain (1095-4362 bps) was excised using *Sma*1 and *EcoR* 1. Following treatment with calf intestinal alkaline

Figure 4.5 Effect of UTP on PRPP binding to the Regulatory Domain

The binding of UTP was measured by determining the effect of the nucleotide on PRPP binding to the regulatory domain. A Scatchard plot of PRPP binding to the regulatory protein in the presence of (-●-) 5 mM UTP showed that although the number of PRPP binding sites remained unchanged, the affinity of PRPP decreased significantly.

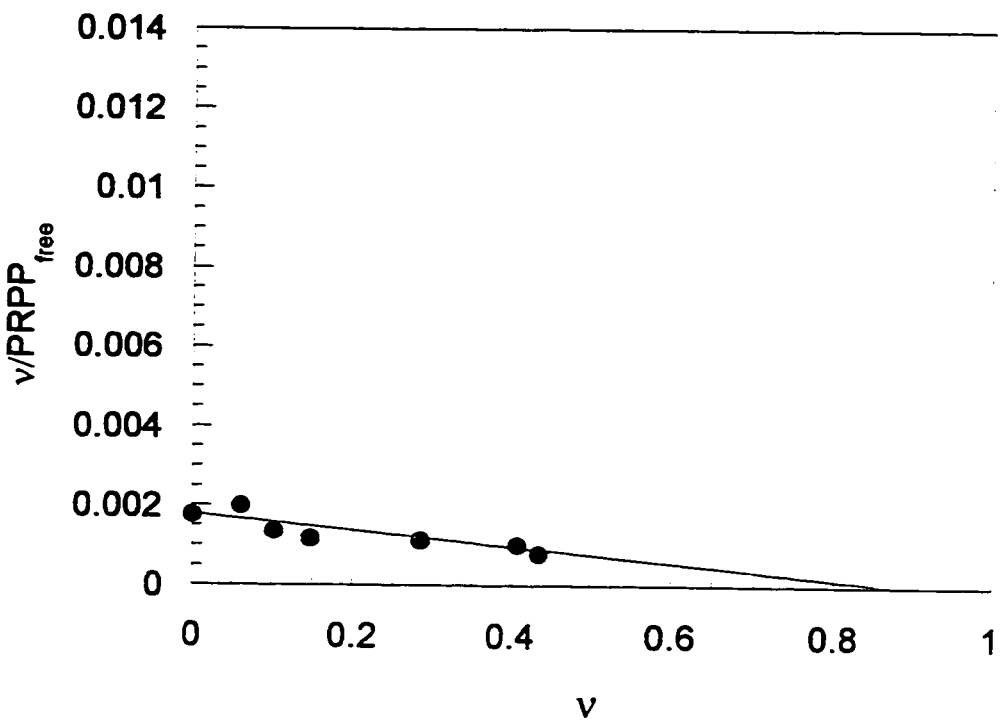
0.014
0.012
0.01
0.008
0.006
0.004
0.002
0
v/PRPP free
0
0.2
0.4
0.6
0.8
1
v

Table 4.2 Comparison of binding parameters for Regulatory Domain, CAD and Chimera

Parameter		Ligand PRPP± UTP	Regulatory Domain (B3)	CAD (native)	Chimera CPS-A12^{e}B3^{m}
K_d	(μM)	none	82.3 ± 15.6	10.1	46.0 ± 1.9
n [a]		none	0.9 ± 0.06	1.0	1.0 ± 0.04
K_d	(μM)	UTP	208 ± 23.2	68.0	133.5 ± 15.8
n [a]		UTP	0.86 ± 0.1	1.0	1.52 ± 0.25

[a] number of binding sites per polypeptide chain

Figure 4.6 Construction of the whole CPSase and the CPS.A domain

The 3.2 kb fragment encoding the CAD CPSase domain (residue 365–1454) was excised using *Sma* I and *EcoR* I, then treated with calf intestinal alkaline phosphatase (CIAP). The vector pRSETC was prepared for the cloning of the 3.2 kb insert by treatment with *Pvu* II and *EcoR* I and calf intestinal phosphatase (CIAP). The insert and the vector were ligated to form the 6.1 kb recombinant pHN-mAB. pHN-mAB was then cleaved with *BspE* I and *EcoR* I, the 5' end made flush using the Klenow fragment, and the 4.7 kb fragment encoding the CAD CPS.A domain extending from residue 365 to 961 was religated to produce pNS-A72.

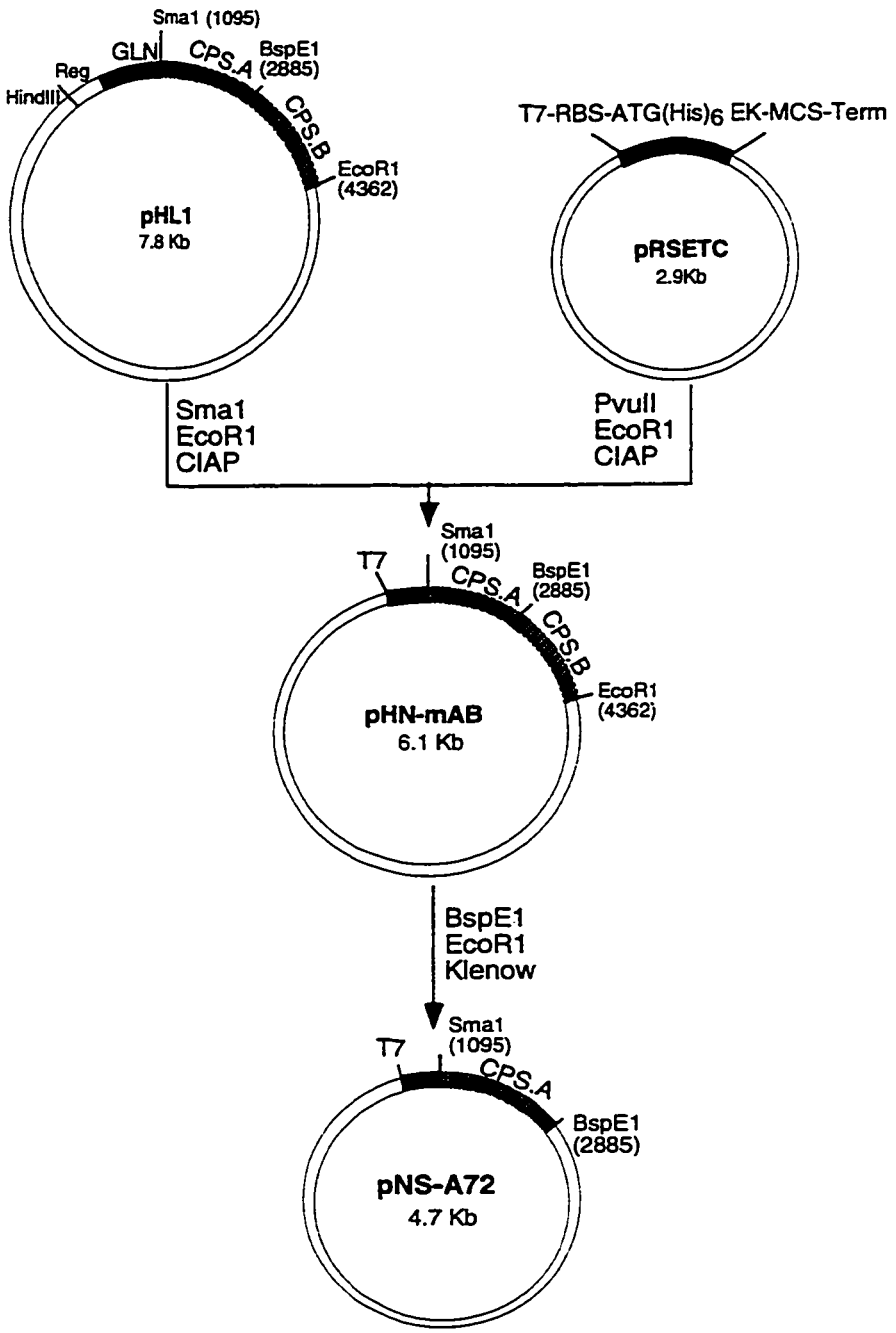
Sma1 (1095)
GLN
CPS.A
BspE1 (2885)
Reg
HindIII
CPS.B
EcoR1 (4362)
pHL1
7.8 Kb
T7-RBS-ATG(His)6 EK-MCS-Term
pRSETC
2.9Kb
Sma1
EcoR1
CIAP
PvuII
EcoR1
CIAP
Sma1 (1095)
T7
CPS.A
BspE1 (2885)
CPS.B
EcoR1 (4362)
pHN-mAB
6.1 Kb
BspE1
EcoR1
Klenow
Sma1 (1095)
T7
CPS.A
BspE1 (2885)
pNS-A72
4.7 Kb

phosphatase (CIAP), the fragment was gel purified using the QIAGEN gel extraction kit. The pRSET C vector was prepared for cloning the 3.2 kb insert by treating with *Pvu* II and *EcoR* 1, followed by treatment with calf intestinal phosphatase (CIAP). The insert and the vector were ligated using T4 DNA Ligase resulting in the 6.1 kb recombinant pHN-mAB.

To obtain the CAD CPS.A domain extending from residue 365 to 961, pHN-mAB was cleaved with *BspE* 1 and *EcoR* 1. This resulted in the removal of the CPS.B coding sequences. The 5' end of the remaining 4.7 kb fragment was made flush using the Klenow fragment, and the ends religated resulting in the 4.7 kb recombinant, pNS-A72 (Figure 4.6).

Expression and Purification of CPS.A

The 4.7 kb pNS-A72 was transformed into BL21 (DE3) cells. A one-liter culture was grown from a 1:1000 dilution of an overnight culture grown in Luria Broth containing 100 μg ampicillin, at 37°C. Cell growth was monitored spectrophotometrically. When the cells reached an OD_{600} of 0.60-0.8, isopropyl-1-thio-β-D-galactopyranoside (IPTG) was added to a final concentration of 0.4 mM. At this time, the cells were shifted to a lower temperature of 30°C, and the induction continued for two hours. Cells were harvested by centrifugation at 4000 X g, 30 min at 4°C. The cell pellets were stored at -20°C until further use.

The cell pellets were thawed and resuspended in 10 ml of 50 mM Tris,/HCl pH 8.0, 150 mM NaCl, 10 mM β-mercaptoethanol and 5% glycerol. PMSF was added to a final concentration of 2 mM. Cells were disrupted by sonication on ice, 5 X, 10 sec each. The cell sonicate was then centrifuged at 14000 X g, 30 min at 4°C. The supernatant and pellet fractions were analyzed on a 10% SDS-PAGE gel. Cells transformed with the pNS-A72 recombinant contained a new species with amolecular mass of 72.8 kDa, which was not present in untransformed cells. Although the majority of the protein was

Figure 4.7 Expression and Purification of the CPS.A domain of CAD

The cell pellet from 1 liter culture was resuspended in 10 ml of 50 mM Tris/HCl, pH 8.0, 150 mM NaCl, 10 mM β-mercaptoethanol and 5% glycerol. 2 mM PMSF, freshly prepared, was added prior to lysis. Cells were lysed by sonication 5 x 10 seconds each and centrifuged at 14,000 X g, 30 min at 4°C. Purification was carried out by a batch procedure. The supernatant was incubated with the Nickel resin (Invitrogen) for an hour, following which the protein-resin complex was loaded on to a column. The column bed was washed with the above buffer, followed by a wash with buffer containing 30 mM imidazole until the absorbance at 280 nm was negligible. The his-tagged protein was eluted with 50 mM Tris/HCl pH 8.0, 150 mM NaCl, 10 mM mercaptoethanol, 5% glycerol and 200 mM Imidazole.

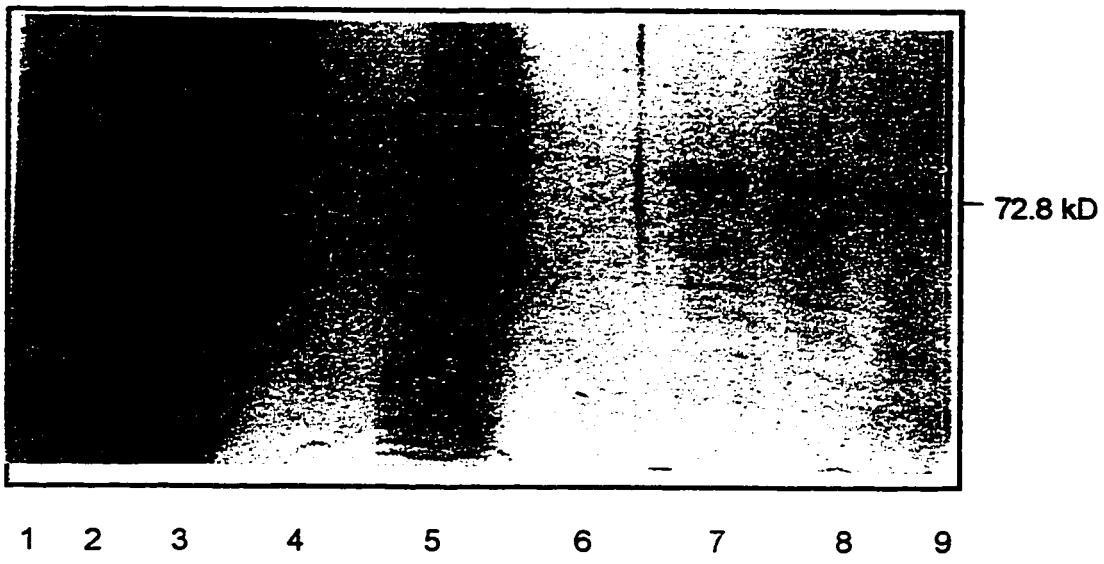
72.8 kD
1
2
3
4
5
6
7
8
9

present in the pellet, a small, but significant amount remained soluble. Due to the presence of the His-tag, the protein could be easily purified over a nickel column.

The CPS.A recombinant protein was purified using the batch purification method as described earlier for the regulatory domain. The 10 ml cell free lysate was incubated with 3 ml of Nickel resin previously equilibrated in 50 mM Tris, pH 8.0, 150 mM NaCl, 10 mM β-mercaptoethanol and 5% glycerol. The protein-resin was then loaded into a 10 ml BIORAD column and the protein purified as explained in Section 4.2. After washing off the contaminants with buffer containing 30 mM imidazole, the CPS.A recombinant was eluted using 50 mM Tris/HCl, pH 8.0, 150 mM NaCl, 10 mM β-mercaptoethanol, 5% glycerol, 200 mM imidazole.

Fractions (1 ml) were collected and analyzed by SDS-PAGE (Figure 4.7). Fractions containing the purified CPS.A were pooled. NaCl and imidazole, were removed by passing the purified protein through a NICK spin column from Pharmacia equilibrated in 50 mM Tris/HCl pH 8.0, 1 mM DTT, 5% glycerol and the protein stored at –70°C.

4.5 Steady State Kinetics of the CPS.A recombinant

The overall ammonia-dependent carbamoyl phosphate synthetase activity of the CPS.A recombinant was assayed by initiating the reaction with [^{14}C] $NaHCO_3$ and trapping the radiolabeled carbamoyl phosphate as carbamoyl aspartate as described in Materials and Methods. CPS.A exhibited typical hyperbolic ATP saturation kinetics for the ammonia-dependent carbamoyl phosphate synthetase activity (Figure 4.8). The K_m of 1 ± 0.15 mM for ATP is lower than the value of 2.1 mM obtained (11) for intact CAD, but higher than 0.482 ± 0.084 mM obtained for GLN CPS.A (70). The V_{max} for CPS.A is 0.216 ± 0.007 μmol/min/mg as compared to 0.102 ± 0.003 μmol/min/mg for GLN-CPS.A and 0.194 μmol/min/mg for native CAD. As expected, the ATP saturation curves of CPS.A in the presence of 2 mM UTP or 200 μM PRPP, were indistinguishable from the

Figure 4.8 Titration of the CPS.A with the Regulatory Domain in the presence of constant concentrations of the activator PRPP and the inhibitor UTP

A fixed amount (4 μg) of CPS.A was titrated with increasing amount (0.36-7.2 μg) of the regulatory domain in the presence of saturating concentration of the activator PRPP or inhibitor UTP. The effect of PRPP and UTP on the CPSase activity was determined as the concentration of the regulatory domain was increased. CPS.A showed no activation or inhibition in the absence of the regulatory domain. However, with a gradual increase in the amount of the regulatory protein, an activation or inhibition effect was seen in the presence of 200 μM PRPP (-●-) or 4 mM UTP (-○-) respectively. The allosteric effect reached saturation when the molar ratio of CPS.A to the regulatory domain was 1:1, the molar ratio calculated using a molecular mass of 26.7 kDa for the regulatory domain and 72.8 kDa for CPS.A.

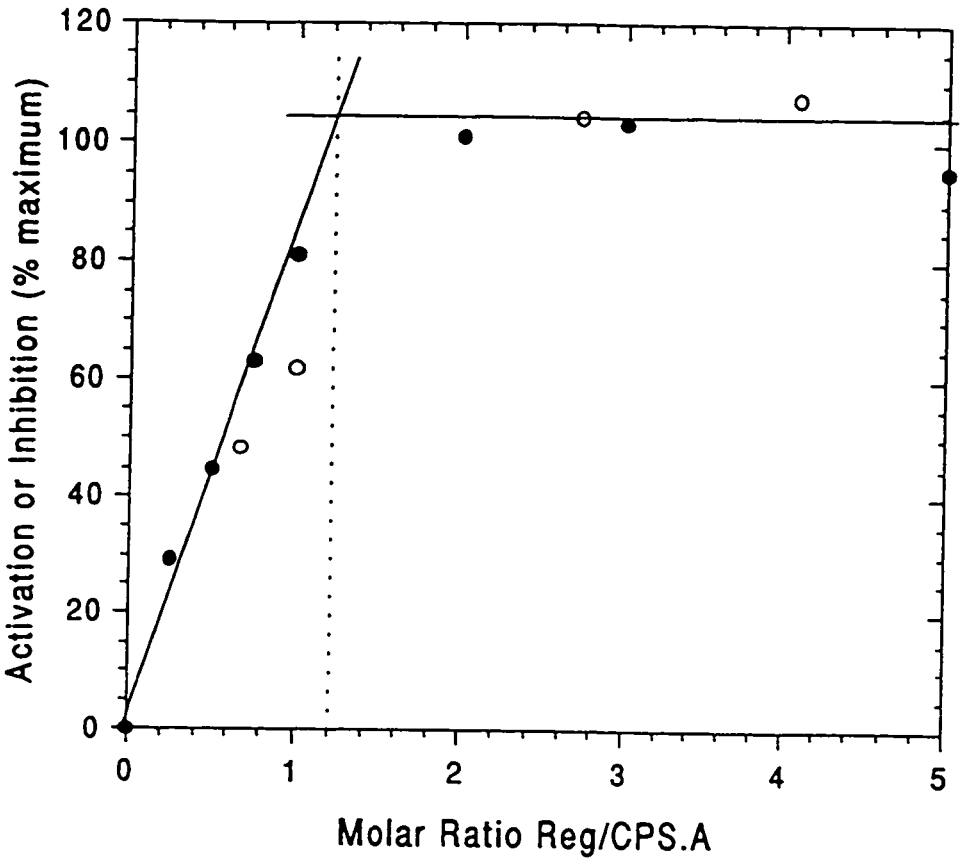
120
100
80
60
40
20
0
Activation or Inhibition (% maximum)
0
1
2
3
4
5
Molar Ratio Reg/CPS.A

curve obtained in the absence of both allosteric effectors, as CPSB and not CPS.A is the locus of allosteric control.

4.6 Titration of the CPS.A domain with the Regulatory Domain B3 of CAD

In native CAD and other CPSases, the CPS.B is the normal locus of allosteric control, while the CPS.A remains unaffected by UTP and PRPP. As discussed previously in this chapter, the isolated regulatory domain was fully functional and bound the allosteric effectors PRPP and UTP. In order to examine whether the regulatory domain B3 can interact with the amino terminus half of the CPSase (CPS.A)$_{,,}$ a titration experiment was designed. Titration was done by incubating a fixed concentration of the CPS.A with increasing concentrations of the purified regulatory subdomain in the presence of saturating concentrations of the activator PRPP or the inhibitor UTP and the effect of activation or inhibition on the ammonia-dependent carbamoyl phosphate synthetase activity measured. Addition of the regulatory domain to the CPS.A did not significantly affect the activity of CPS.A. As expected, the CPS.A activity showed no activation or inhibition in the absence of the regulatory domain. However, with a gradual increase in the amount of the regulatory domain (0.36-7.2 μg), an activation and an inhibition effect was observed in the presence of constant saturating concentration of PRPP (200 μM) and UTP (4 mM), respectively. The allosteric effect reached saturation when the molar ratio of CPS.A/Regulatory domain was 1:1 (Figure 4.8). This demonstrated that the mammalian CPS.A and the regulatory domain formed a functional one to one stable stoichiometric hybrid complex (CPS.A-REG).

4.7 Steady State Kinetics of the CPS.A-REG Hybrid

The effect of allosteric ligands on the ammonia-dependent CPSase activity of the CPS.A-REG hybrid, prepared by mixing equimolar ratios of the purified CPS.A and the regulatory domain, was measured as a function of ATP concentration (Figure 4.9). Allosteric effectors had little effect on the K_m for ATP. K_m decreased from a value of

Figure 4.9 ATP Saturation curves of the CPS.A-REG Hybrid

The ammonia-dependent carbamoyl phosphate synthetase activity of the CPS.A-REG hybrid was measured as a function of the ATP concentration in the absence of ligands (-●-), in the presence of 200 μM PRPP (-❑-) and 4 mM UTP (-○-).

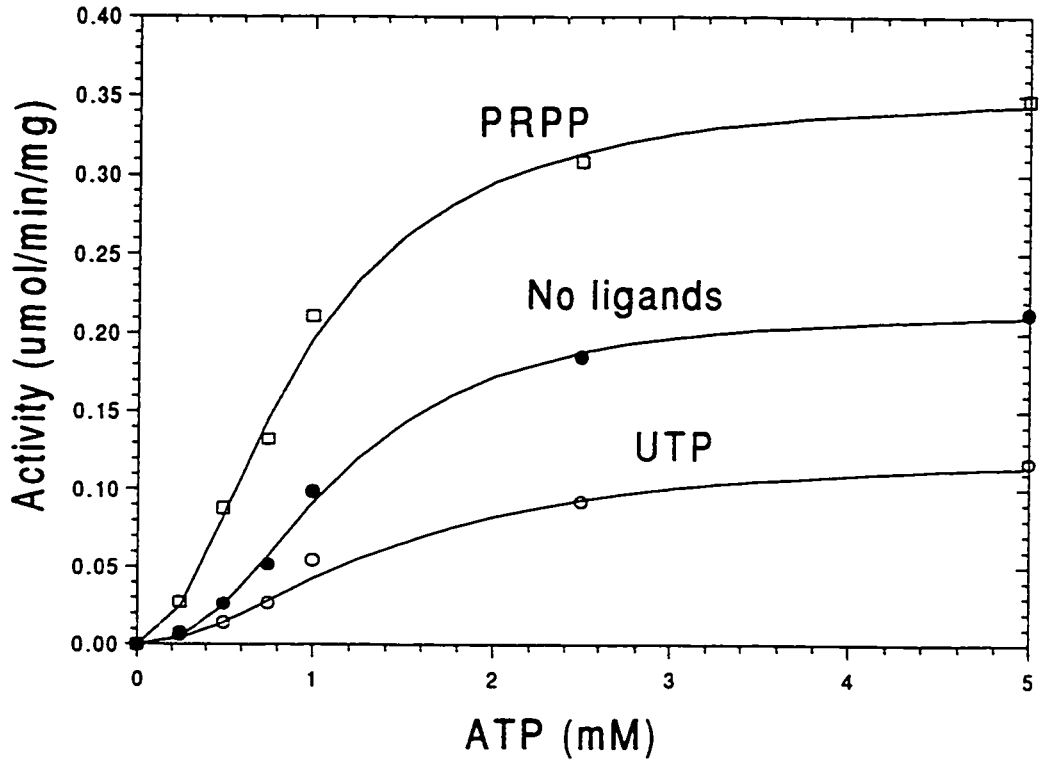
Activity (umol/min/mg)
0.40
0.35
0.30
0.25
0.20
0.15
0.10
0.05
0.00
0
1
2
3
4
5
ATP (mM)
PRPP
No ligands
UTP

Table 4.3 Kinetic Parameters for CPS.A, CPS.A-REG hybrid, CAD CPSase[a] and GLN-CPS.A[b]

Protein	Ligand	Km	Vmax
		mM	μmol/min/mg
CAD CPSase[a]	none	2.14 ± 0.16	0.194±0.006
GLN-CPS.A[b]	none	0.482 ± 0.08	0.102 ± 0.01
	50 μM PRPP	0.482 ± 0.08	0.102 ± 0.01
	2 mM UTP	0.482 ± 0.08	0.102 ± 0.01
CPS.A	none	1.0 ± 0.10	0.216 ± 0.007
	200μM PRPP	1.0 ± 0.15	0.216 ± 0.007
	4 mM UTP	1.0 ± 0.15	0.216 ± 0.007
CPS.A-REG (Hybrid)	none	1.0 ± 0.15	0.216 ± 0.007
	200μM PRPP	0.89 ± 0.11	0.355 ± 0.013
	4 mM UTP	1.19 ± 0.35	0.124 ± 0.010

[a] Data from reference 11
[b] Data from reference 70

Figure 4.10 Effector response curves of the CPS.A-REG hybrid

The ammonia-dependent CPSase activity of the CPS.A-REG hybrid was assayed in the presence of increasing PRPP (-○-) and increasing UTP (-●-). ATP concentration was maintained at 0.75 mM and all other substrates were at saturating concentrations.

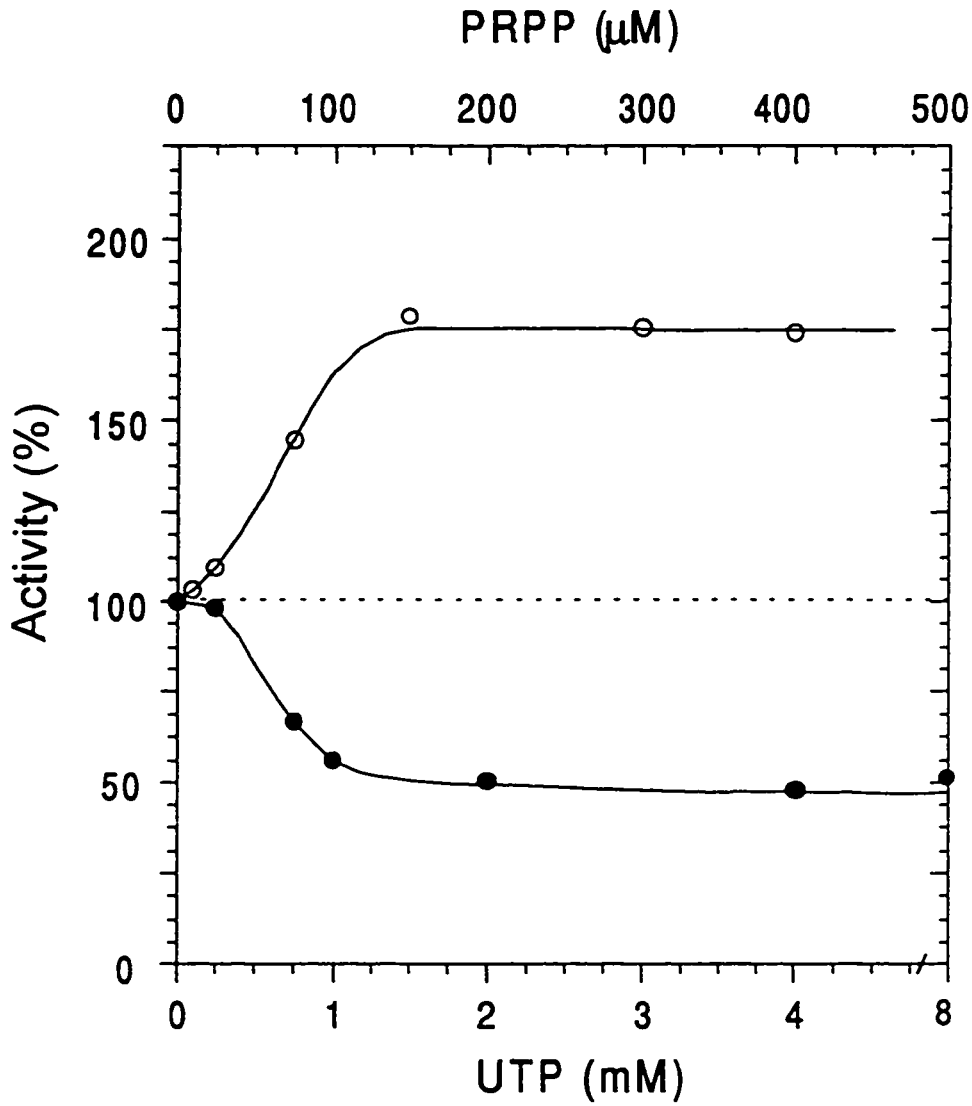
PRPP (μM)
0
100
200
300
400
500
200
150
100
50
0
Activity (%)
0
1
2
3
4
8
UTP (mM)

Table 4.4 Allosteric Regulation of CAD and the CPS.A-REG Hybrid protein

	CPS.A-REG Hybrid		CAD [a]	
	UTP inhibition	PRPP activation	UTP inhibition	PRPP activation
K_d [b] (μM)	595	75.85	640 ± 80	13.5 ± 0.9
Maximum effect (%)	51.0	175	91.0 ± 0.9	238 ± 1.20

[a] data from reference 56

[b] the apparent dissociation constants were calculated from the equation $[X]_{½} = \alpha K_d([S]+K_s)/(K_d+[S])$, where $[X]_{½}$ is the concentration of the allosteric effector which produced half maximum activation or inhibition, [S] is the substrate concentration, K_d and K_s is the apparent dissociation constant of the allosteric ligand and the substrate respectively and α is the ratio of K_m (no ligand)/K_m (saturating ligand)

1 ± 0.15 mM in the absence of effectors to 0.89 ± 0.11 mM in the presence of 200 μM PRPP. In the presence of 4 mM saturating UTP, Km increased to 1.19 ± 0.3 mM. The predominant effect was on the K_{cat} and not on the K_m.. The V_{max} increased from 0.216 ± 0.007 to 0.355 ± 0.013 μmol/min/mg in the presence of 200 μM PRPP, and decreased to 0.124 ± 0.01 with UTP (Table 4.3).

The extent of activation and inhibition of the ammonia-dependent carbamoyl phosphate synthetase activity of the CPS.A-REG hybrid (Figure 4.10) was tested. The hybrid complex was activated 175 percent as compared to 238% for the native CAD. The apparent dissociation constant K_a for PRPP was 85.7 μM for the CPS.A-REG hybrid, the affinity of the activator being 7-fold lower than the value (13.5 μM) obtained for CAD. Saturating UTP inhibited the hybrid 51% as compared to 91% in CAD. The apparent dissociation constant Ki for UTP was found to be 0.5 mM compared to a value of 0.64 mM obtained for CAD.

The steady state kinetic parameters suggest that the CPS.A and the regulatory domain form a stable functional 1:1 stoichiometric complex. The physical interaction of the regulatory domain with the CPS.A confers allosteric properties to the CPS.A domain by allowing transmission of regulatory signals to the catalytic subdomain A2 of CPS.A.

4.8 Discussion

Carbamoyl phosphate synthetases involved in pyrimidine or arginine biosynthesis, have very similar amino acid sequences, but the sequence differs significantly at the carboxyl terminal of the CPS.A and CPS.B domains. Mammalian and *E. coli* CPSase share an overall 40% sequence identity, but only a 22% identity in the B3 region. Similarly, mammalian CPSases I and II involved in urea and pyrimidine biosynthesis, respectively, have an overall identity of 53%, but only 36% in the B3 region. The sequence homology in the B3 region is higher in CPSases that have common allosteric effectors. The divergence in sequence at the carboxyl terminal end of

all CPSases may be a reflection of the differences in allosteric effectors that regulate these molecules.

Multifunctional proteins like CAD are proposed to originate by fusion of exon-encoded contiguous domains which can fold and function independently. Controlled proteolysis studies of CAD (17), showed that proteases generally cleave at interdomain junctions and provided the initial support for the existence of a discrete regulatory domain. The CPSase domain of CAD undergoes a series of proteolytic cleavages indicative of a complex domain structure (10,11,13,17). Following cleavage at the junction between the CPSase and the DHOase domain, a 20-kDa fragment corresponding to the B3 region is excised. Similar cleavage patterns were observed for *E. coli* CPSase and mitochondrial CPSase.

Several concrete evidences support the proposal that the B3 region of all CPSases is the regulatory domain. Rubio et al (74) demonstrated that photoaffinity labeling of *E. coli* CPSase resulted in the incorporation of the labeled UMP in the 20 kDa carboxyl terminal end of the CPSase molecule. Recent studies have identified lysine 992 residue as a critical residue within the UMP binding site (57). IMP, UMP and ornithine induced reversible transitions in the *E. coli* CPSase endotherm obtained by differential scanning calorimetry (55). The transition did not occur in a mutant lacking 171 residues of the carboxy terminal domain, suggesting that the effectors bind to this carboxyl region. The obligatory activator N-acetyl-L-glutamate also binds to the corresponding carboxyl terminal end of the mammalian CPSase (76). In CAD, the cAMP-dependent phosphorylation site I (71) is located in the B3 region. Since phosphorylation severely abolishes UTP inhibition, the phosphorylation site and the UTP site must be close to one another (105). B3 was positively identified as the regulatory domain in CAD by the domain swapping experiments of Liu, Guy and Evans (56). This experiment involved the construction of a chimeric molecule consisting of 83% of the *E.*

coli CPSase, including both the ATP binding catalytic domains, fused to a 190-residue segment corresponding to the B3 domain in CAD. The sensitivity of the chimera to UTP and PRPP clearly indicated that the effectors bound to the B3 region of the mammalian protein.

Although all the evidence demonstrates that the B3 subdomain can bind allosteric effectors and has the phosphorylation site, it was yet to be shown that B3 could exist as an independent functional domain. In order to address this question, residues 1265-1455 encoding the B3 domain was cloned into a His-tag over-expression vector and the domain expressed as a 26.7 kDa his-tag recombinant. Although the majority of the protein was insoluble, a significant amount remained in solution. The protein was purified in a single step over a nickel affinity column. Binding studies with the purified recombinant protein have shown that PRPP does bind to the isolated domain. However, the affinity of the activator to the isolated regulatory domain is about 8-fold lower as compared with CAD and less than two-fold as compared to the CPS-A12^{e}B3^{m} chimera, the K_d values being 83.5 μM, 10μM and 46μM respectively. The binding of the inhibitor UTP was studied indirectly by its effect on PRPP binding. UTP changed the K_d for PRPP by almost two-fold. Scatchard plots demonstrated the existence of one binding site for PRPP, which was in agreement with results obtained for native CAD (Liu, Sahay, Herve and Evans, unpublished results). Thus, binding studies with both allosteric effectors demonstrate that the regulatory domain is an autonomously functional domain. The decreased affinity of the effectors may be attributed to differences in the conformation of the regulatory domain when existing independent of the rest of the CPSase molecule.

Deletion studies of the CPS-A12^{e}B3^{m} chimera discussed in Chapter 3, suggests that the 59 residues at the carboxyl end of the regulatory domain may be involved in transmission of the allosteric signal to the CPSase active sites A2 and B2. An interesting question then emerges: "Can the independently folded regulatory B3 domain

interact with the CPS.A domain (A1-A2-A3) and allow the transmission of the allosteric signal to the A2 catalytic site?" To test this idea, the CPS.A domain was cloned and expressed as a His-tag recombinant. The expression of a functional mammalian CPS.A that catalyzed the overall carbamoyl phosphate synthetase reaction was in agreement with the recently discovered novel finding that both the halves of the CPSase molecule are functionally equivalent (70). Measurements of the steady state kinetic parameters of CPS.A showed that it catalyzed the overall reaction nearly as well as the native enzyme. The K_m for ATP was found to be 1 ± 0.15 mM compared to 2.1 mM obtained for intact CAD and 0.482 ± 0.084 mM for the GLN-CPS.A recombinant. ATP saturation curves of CPS.A in the presence of UTP or PRPP were indistinguishable from the curve in the absence of the allosteric effectors.

With the expression of a functional mammalian CPS.A recombinant, the following questions were addressed: "Can the CPS.A domain physically interact with the isolated regulatory domain forming a CPS.A-REG hybrid?" And if so, "can the allosteric signals generated by the binding of the effectors to the B3, be transmitted to the CPS.A active site?" Titration of CPS.A with increasing concentrations of the regulatory domain B3 resulted in a 1:1 stoichiometric complex. Steady state kinetics of the CPS.A-REG hybrid shows that PRPP and UTP alter the catalytic activity of the hybrid to approximately the same extent as the parent mammalian protein. However, the effect is mainly on the V_{max} and not on the K_m. The apparent dissociation constant and the maximum UTP inhibition seen in the CPS.A-REG hybrid is comparable to that in CAD. This suggests that the UTP site is contained entirely within the B3 region, and that the signal is almost as efficiently transmitted to the CPS.A active site in the hybrid as it is in the parent CAD molecule. Although PRPP activates to nearly the same extent for the CPS.A-REG hybrid (175%) and CAD (238%), the apparent affinity for the activator is almost 7-fold lower.

In an attempt to explain the transmission of regulatory signals to the catalytic subdomain A2 of CPS.A generated by the binding of allosteric effectors to the regulatory domain in the CPS.A-REG hybrid complex, a displacement model is proposed. According to this model, the presence of the isolated B3 subdomain causes the A3 subdomain of CPS.A to be displaced by B3, thereby allowing B3 to complex with A1 and A2. The effect of allosteric ligands that bind to the B3 subdomain are then transmitted to the A2 subdomain causing an activation or inhibition effect on the CPSase activity of the molecule.

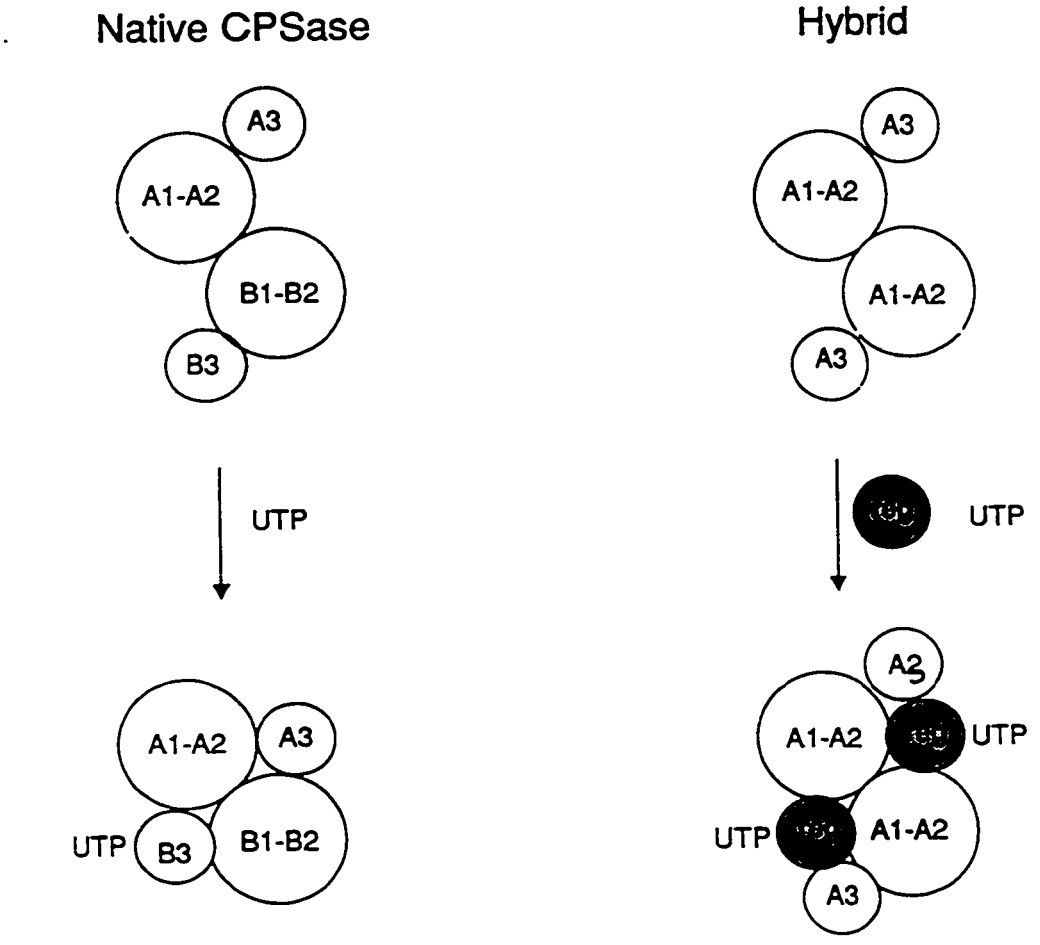
Native CPSase
A3
A1-A2
B1-B2
B3
UTP
A1-A2
A3
UTP
B3
B1-B2
Hybrid
A3
A1-A2
A1-A2
A3
UTP
A2
A1-A2
UTP
UTP
A1-A2
A3

CHAPTER 5 5 Phosphoribosyl 1-pyrophosphate Binding to Aspartate Transcarbamoylase of *Pseudomonas aeruginosa*

5.1 Overview of Purine and Pyrimidine Nucleotide Metabolism

Purine and pyrimidine nucleotides are critically important metabolites that participate in many cellular functions. These functions range from serving as monomeric precursors of nucleic acids, to serving as energy stores, effectors, group transfer agents, and mediators of hormone action. The nucleotides are formed in the cell, *de novo,* from amino acids, ribose, formate and CO_2. The *de novo* pathways for the synthesis of nucleotides require a relatively high input of energy. To compensate for this, most cells have very efficient "salvage" pathways by which the preformed purine or pyrimidine bases can be reutilized.

Because of the manner in which nucleotides are synthesized and salvaged, the purines and pyrimidines occur primarily as nucleotides in the cell. The concentrations of free bases or free nucleosides under normal conditions are exceedingly small. The levels of nucleotides in the cell are very finely regulated by a series of allosterically controlled enzymes in the pathway. Nucleotides are the regulators of these reactions. Quantitatively, the major purine derivatives found in the cell are those of adenine and guanine. Other purine bases encountered are hypoxanthine and xanthine. The pyrimidine nucleotides found in highest concentrations in the cell are those containing uracil, cytosine, and thymine. Uracil and cytosine nucleotides are the major pyrimidine components of RNA, whereas cytosine and thymine are the major pyrimidine components of DNA.

5.2 Role of 5-Phosphoribosyl 1-Pyrophosphate in the cell: Synthesis and Utilization

The intracellular concentration of 5-phosphoribosyl 1-pyrophosphate (PRPP)

plays an important role in regulating several important pathways. The synthesis and utilization of PRPP by the cell determines the steady state concentration of PRPP and hence affect the metabolic pathways that compete for PRPP.

PRPP is synthesized in the cell in a reaction catalyzed by PRPP synthetase which utilizes ribose 5-phosphate and ATP, in the presence of Mg^{+2} ions. The ribose 5-phosphate is generated from glucose 6-phosphate metabolism via the hexose monophosphate shunt or from ribose 1-phophate via a phosphoribomutase reaction. As expected for such a critical reaction, the PRPP synthetase is tightly regulated. The enzyme has an absolute requirement for Pi ions. At the concentration of Pi normally found in the cell, the activity of PRPP synthetase is markedly depressed.

The levels of PRPP synthetase are elevated in cells undergoing rapid cell division and decrease to basal levels in cells that have reached confluence. Factors that lead to increased flux of glucose 6-phosphate through the hexose monophosphate shunt pathway can result in increased intracellular levels of PRPP. Pyrroline 5-carboxylate (an intermediate in the interconversions of amino acids, ornithine, glutamate and proline) stimulates the hexose monophosphate shunt via the generation of $NADP^+$ in the pyrroline 5-carboxylate reductase catalyzed reaction. This can lead to elevated intracellular concentrations of PRPP.

PRPP formed in the cells is a required substrate for many key metabolic reactions depending on the cell type. The reactions and pathways in which PRPP is utilized are as follows:

1. *De novo* purine nucleotide synthesis

   PRPP + glutamine → 5-phosphoribosylamine + glutamate + PPi

2. Salvage of purine bases

   PRPP + hypoxanthine (guanine) → IMP (GMP) + PPi

   PRPP + adenine → AMP + PPi

3. *De novo* pyrimidine nucleotide synthesis

   PRPP + orotate → OMP + PPi

4. Salvage of pyrimidine bases

   PRPP + uracil →UMP + PPi

5. NAD^+ synthesis

   PRPP + nicotinate → nicotinate mononucleotide + PPi

   PRPP + nicotinamide → nicotinamide mononucleotide + PPi

   PRPP + quinolinate → nicotinate mononucleotide + PPi

The direction in which PRPP would be consumed would depend on several factors, including the relative K_m values of the competing enzymes for PRPP, the availability of the second substrate and the concentration of the effector for the particular reaction. In addition to PRPP acting as a substrate in the above reactions, PRPP is an allosteric activator of carbamoyl phosphate synthetase, the locus of regulation in the mammalian *de novo* pyrimidine biosynthetic pathway.

5.3 Aspartate Transcarbamoylase holoenzyme of *P. aeruginosa*

Although the pyrimidine metabolic pathway remains conserved in *Pseudomonas*, it differs significantly from that found in other well-characterized species. The aspartate transcarbamoylase of *Pseuodomonas* is unique. The ATCase gene is arranged in an operon with two open reading frames: a 5' ORF corresponding to the *pyr*B gene, with a 40 percent homology to the ATCase gene from *E. coli*, and a downstream ORF with a low homology to the *pyr*C gene of DHOase. The coding region of the downstream ORF overlaps the 3' end of the *pyr*B gene by 4 base pairs such that a translational coupling occurs. In *P. aeuginosa*, the *pyr*B encodes a 34 kDa polypeptide while the downstream *pyr*C' encodes a 44.1 kDa protein that bears 30 percent homology to the *E. coli* DHOase.

Although the downstream ORF has significant homology with the *pyr*C gene

encoding for the active dihydroorotase, the product of the downstream *pyr*C' is devoid of DHOase activity. Purified ATCase holoenzymes from several *Pseudomonas* species including *aeruginosa* and *putida*, show no DHOase activity. Instead the DHOase activity maps to a *pyr*C locus neighboring yet distinct from the *pyr*C' gene.

Cloning, Expression, and Purification of the ATCase holoenzyme

The *P. aeruginosa* ATCase *pyr*BC' gene was sequenced by Vickrey and Donovan (Accession # L19649, L19648). The 3.2 kb gene locus was cloned into the pRSET vector, overexpressed to 40 percent of the total cell protein, and purified to homogeneity (Vickrey, Herve, Evans, manuscript in preparation). The holoenzyme had a molecular mass of 474 kDa and consisted of a 34 kDa catalytic chain and a 45 kDa DHOase-like chain.

Catalytic Activity of the purified ATCase holoenzyme

Steady state kinetics showed that the enzyme had a K_m of 1.3 mM for aspartate at saturating carbamoyl phosphate concentration of 5 mM, 0.4 mM for carbamoyl phosphate at saturating (20 mM) aspartate, and a V_{max} of 20,000 μmol/hr/mg. The enzyme is strongly inhibited by very low concentrations of nucleotide triphosphates ATP, UTP, GTP and CTP. The extent of inhibition measured as a function of the effector concentration gave apparent dissociation constant (K_i) values of as low as 1 μm for ATP, UTP and GTP while CTP had a K_i of 1 mM. (Vickrey, Herve and Evans, unpublished)

Within the cell, the concentrations of nucleotide triphosphates are significantly higher than the K_i values observed for the ATCase holoenzyme. An interesting question then arises: "If the enzyme is inhibited by such low concentrations of nucleotide triphosphates, how can it function within the cell?" This prompted the search for metabolites that may reverse the nucleotide inhibition.

5.4 Binding of PRPP to the ATCase holoenzyme

Radiolabeled PRPP was synthesized enzymatically and assayed as described

previously. A fixed concentration of the purified ATCase holoenzyme (50 μg) in 50 mM Tris/HCl, pH 8.5, 10% glycerol, was incubated with increasing (0-150 μM) concentrations of [^{32}P] PRPP for 15 minutes at 37°C. The reactions were then carefully transferred to the top of a NICK spin column (Pharmacia) equilibrated with the same buffer. The column was centrifuged at 1000 x g for 4 min. The eluent containing protein bound PRPP was counted in a scintillation counter.

PRPP bound per mole of protein was plotted as a function of the PRPP concentration and the plot fitted to a Michaelis Menten equation. PRPP binds to the ATCase holoenzyme with a dissociation constant of 34 μM (Figure 5.1). A scatchard plot was generated using the equation $v / [L] = n / K - v / k$, where v is the mole of ligand bound per mole of the protein, [L] is the concentration of free ligand (μM), n is the number of binding sites and K is the dissociation constant. The scatchard plot of the binding data was linear and gave an intercept corresponding to an n value of 6, (Figure 5.1) indicating that there were six sites per molecule of the enzyme. Based on the mass of the constituent subunits of the holoenzyme and the stoichiometry of the complex, the holoenzyme is dodecameric, consisting of six copies of the 34 kDa catalytic chain and six copies of the 45 kDa polypeptide chain. An n number of six signifying six binding sites for PRPP may then suggest that either the sites are located exclusively on the catalytic chain, or on the DHO-like chain or the site may be shared between the two polypeptides.

Specificity of PRPP as a radioactive ligand

As the binding of PRPP to the ATCase holoenzyme was quite a novel result, an experiment was carried out to eliminate any error in concluding that PRPP was a ligand and not a radioactive contaminant. The radiolabeled PRPP is converted to PPi by an orotidylate phosphoribosyl transferase (OPRTase)–orotidylate decarboxylase (ODCase) coupling reaction.

Figure 5.1 PRPP Binding to the ATCase Holoenzyme

The binding of [^{32}P] phophoribosyl-5'pyrophosphate (22,000 cpm/nmol) to 50 μg of the purified ATCase holoenzyme (-●-) was measured by the microcolumn method. In the Scatchard plot, ν represents the PRPP-protein complex/protein, and PRPP represents free PRPP.

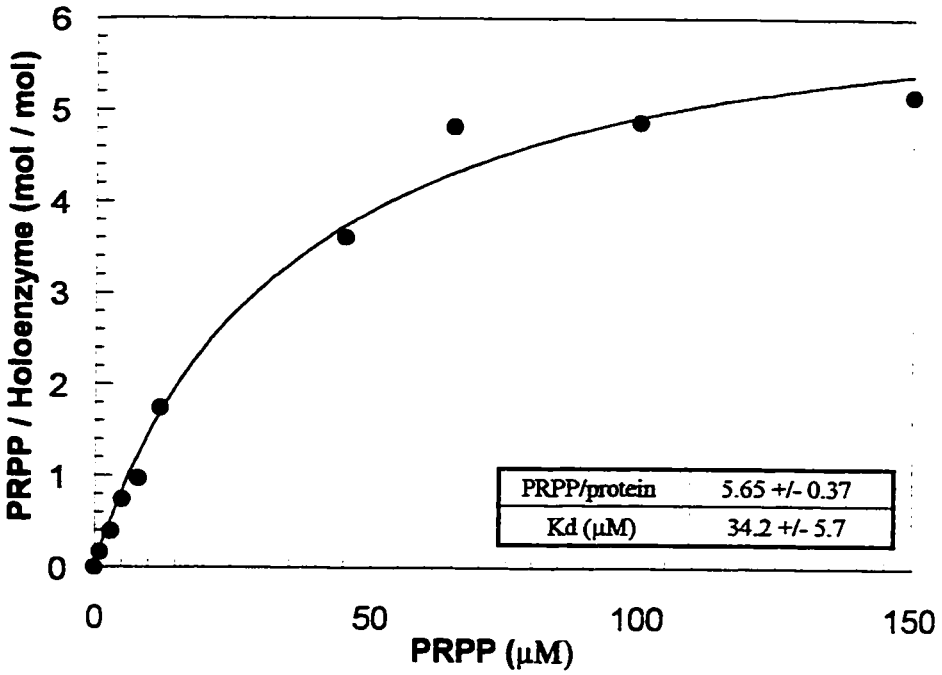
PRPP / Holoenzyme (mol / mol)
PRPP (μM)
PRPP/protein 5.65 +/- 0.37
Kd (μM) 34.2 +/- 5.7

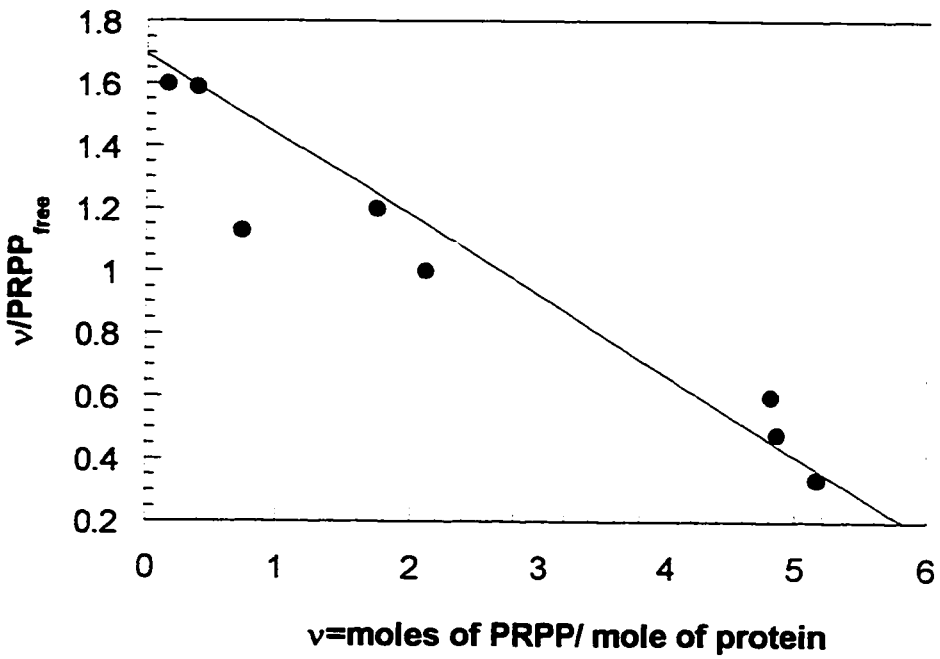
ν/PRPP free
ν=moles of PRPP/ mole of protein

$$\text{Orotic Acid} + {}^{32}\text{PRPP} \rightarrow \text{OMP} + \text{PPi}$$

$$\text{OMP} \rightarrow CO_2 + \text{UMP}$$

The reaction was carried out as described in Chapter 3, but the reaction volume was reduced from 1 ml to 25 μl. A set of reactions was incubated for 1 hr in the presence of increasing concentrations of the OPRTase-ODCase mixed enzyme to allow the enzymatic conversion of PRPP to PPi. The reactions were then incubated with 50 μg of the ATCase holoenzyme in a reaction volume of a 100-μl and binding carried out by the microcolumn method. A 25 μl control reaction was set up without any OPRtase-ODCase mixed enzyme. As before, it was incubated with 50 μg of ATCase holoenzyme and the 100 μl reaction centrifuged through the NICK spin column. In case of the control experiment, the eluent containing the intact ^{32}PRPP bound to the protein gave significantly high counts. For the set of the reactions in which PRPP was converted to PPi prior to incubation with the holoenzyme, the eluents did not show counts significantly above background (Figure 5.2). This confirmed that the counts obtained in the eluent when intact ^{32}PRPP bound to the protein were due to the ^{32}P label in PRPP.

Effect of UTP and ATP on the PRPP binding to the ATCase holoenzyme

As micromolar concentrations of ATP and UTP inhibited the ATCase holoenzyme activty, it was interesting to determine what effect if any, the nucleotides had on PRPP binding. The effect of 100 μM ATP and 100 μM UTP were determined on the affinity of the holoenzyme for PRPP. In the presence of 100 μM UTP, the K_d for PRPP increased from 34 μM to 65 μM although the V_{max} remained unaffected. This suggests that UTP lowers the affinity of the holoenzyme for PRPP, but does not affect the moles of PRPP bound per mole of protein. In the presence of 100 μM ATP, K_d remains unaffected but the mole of PRPP bound per mole of protein is reduced 4-fold (Figure 5).

5.5 Effect of PRPP on the catalytic activity of the ATCase holoenzyme

The effect of increasing PRPP on the ATCase holoenzyme activity was

Figure 5.2 Specificity of ^{32}PRPP as a Ligand

^{32}PRPP was first converted to PPi in a set of reactions (25 μl each) containing increasing concentration of the OPRTase-ODCase mixed enzyme, and constant orotate. Following a one hour incubation, the binding reaction was initiated by the addition of 50 μgs of the ATCase holoenzyme in a 100 μl reaction. Binding was carried out using the microcolumn procedure. A control experiment was set up without any mixed enzyme. 50 μg of the holoenzyme was added and the effluents in each case counted in a scintillation counter.

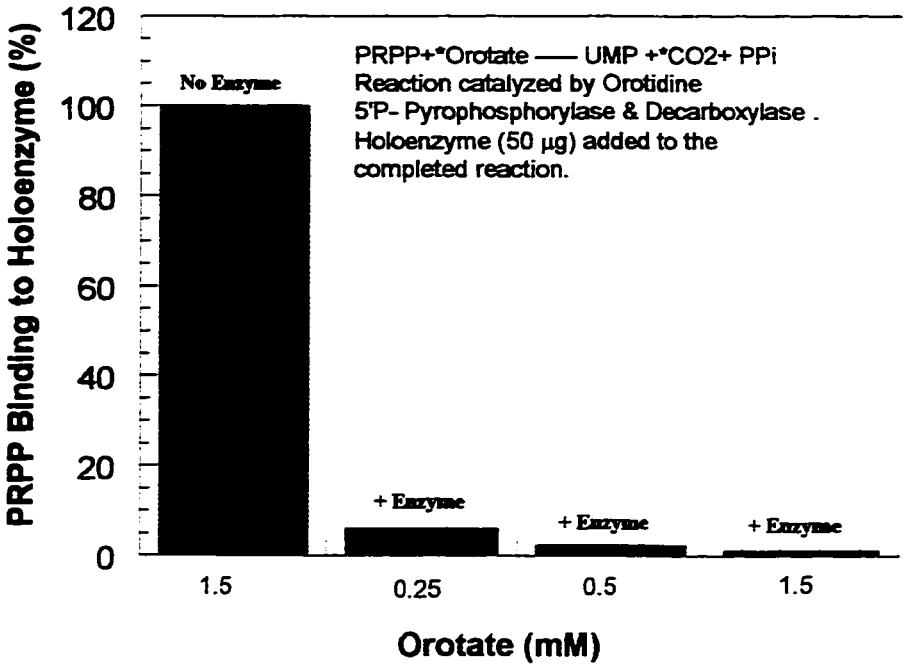
PRPP Binding to Holoenzyme (%)
120
100
80
60
40
20
0
No Enzyme
+ Enzyme
+ Enzyme
+ Enzyme
PRPP+*Orotate —— UMP +*CO2+ PPi
Reaction catalyzed by Orotidine
5'P- Pyrophosphorylase & Decarboxylase .
Holoenzyme (50 µg) added to the
completed reaction.
1.5
0.25
0.5
1.5
Orotate (mM)

Figure 5.3 Effect of ATP and UTP on PRPP binding to the ATCase Holoenzyme

PRPP binding to 50 μg of the holoenzyme was assayed in the absence (-●-), and presence of 100 μM ATP (-○-) and 100 μM UTP (-□-). Typically, 100 μM concentrations of ATP and UTP inhibit the enzyme over 80 percent. The binding curves are plotted as moles of PRPP bound per mole of protein versus PRPP concentration. A scatchard plot shows the effect of UTP and ATP on the K_d of PRPP.

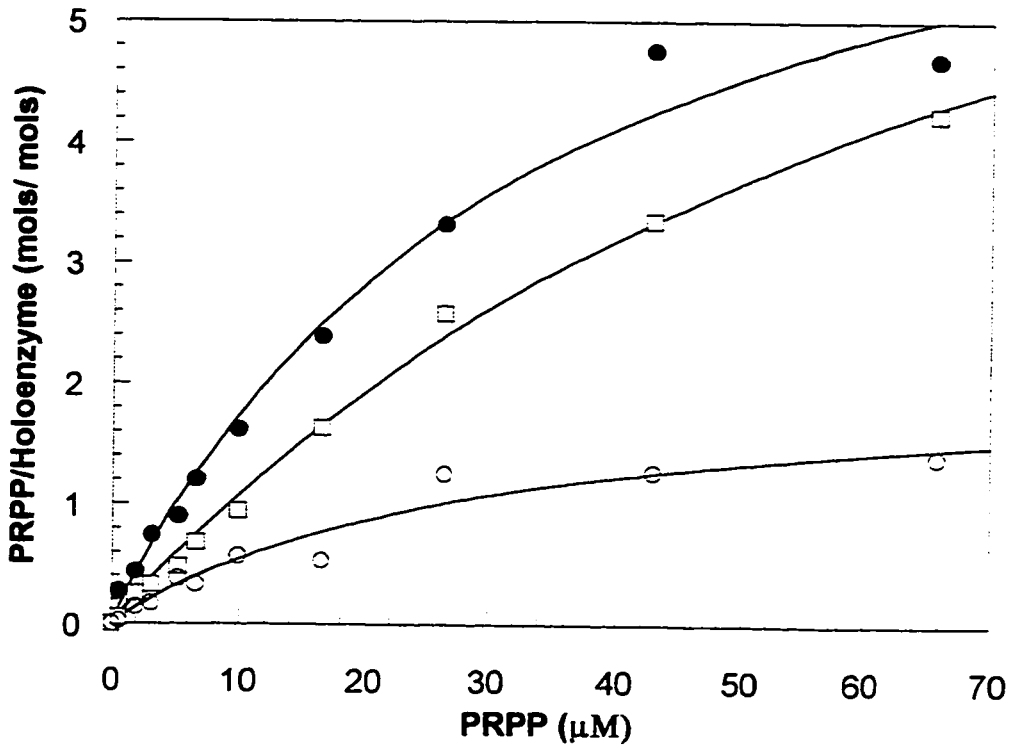

Ligand	K_d (μM)	PRPP/protein
PRPP	33.1+/- 3.1	7.52 +/- 0.66
PRPP,UTP	74.9+/-9.68	9.16+/-0.75
PRPP,ATP	28.7 +/- 8.8	2.10+/- 0.31

determined as a function of PRPP concentration. At a fixed concentration of 5 mM aspartate and 2 mM carbamoyl phosphate, the effect of increasing PRPP displays an erratic effect on the ATCase activity without a marked activation or inhibition. At 0.5 mM aspartate and 1 mM carbamoyl phosphate, there was a two fold activation effect with increasing PRPP (0.025–5 μM).

5.6 Cloning, expression, and purification of the DHO-like chain

The 1.2 kb *pyr*C' gene encoding the DHO-like chain was cloned by PCR into the his-tag expression vector, pRSETC. The 5' primer incorporated a *Xho* I site while the 3' primer incorporated an *Eco*R I site. The 3' primer was designed such that the first two bases of *Eco*R I were part of an engineered stop codon TGA. The 1.2 kb PCR product was purified using PCR QIAquick (Qiagen), double digested with *Xho* I and *Eco*R I. The 1.2 kb insert was gel purified and ligated into the *Xho* I and *Eco*R I sites of the pRSETC vector to obtain pNS-D47 (Figure 5.4).

The clone was transformed into BL21 (DE3) cells. A single colony was used to inoculate a 3 ml LB overnight culture containing 100 μg/ml of ampicillin. The overnight culture (0.5 ml) was used to inoculate a 100 ml culture, and the cells grown at 37 °C. When the cells reached an absorbance of 0.6-0.8 at 600 nm, expression was induced with 0.4 mM IPTG. Induction was continued for 2 hours at 37°C. Cells were harvested at 4000 x g, 20 min at 4°C.

The pellet was resuspended in 2 ml of 50 mM Tris/HCl, pH 8.4, 150 mM NaCl, 10 % glycerol, 1 mM PMSF. The cells were lysed by sonication 5 X, 10 seconds each. The cell extract was centrifuged at 14,000 x g for 20 minutes. SDS-gel electrophoresis revealed a new 47 kDa species not present in extracts of untransformed cells. The 47.7 kDa his-tagged DHOlike recombinant overexpressed to 35% of the total soluble protein and could be purified in a single step using the Nickel column (Invitrogen).

The supernatant was added to a 2 ml nickel bed equilibrated with

50 mM Tris/HCl, pH 8.4, 10 mM β-mercaptoethanol, 150 mM NaCl and 10% glycerol. The column bed was washed with buffer containing 50 mM imidazole until the absorbance at 280 nm was negligible. The His-tag recombinant was finally eluted with buffer containing 200 mM imidazole. The one-ml fractions collected were analyzed on a 10% SDS-gel (Figure 5.5). Fractions containing the purified protein were pooled and dialyzed three times, one hour each, against 50 mM Tris/HCl, pH 8.4, 1 mM DTT and 10% glycerol in order to remove NaCl and imidazole. Protein concentration was determined using the Micro BCA kit from Pierce. A 100 ml culture gave almost 20 mg purified protein. The purified protein was used for PRPP binding studies and for crystallization setups.

5.7 PRPP Binding to the purified pseudo DHOase chain

PRPP binding to the DHO-like chain was studied using the microcolumn procedure as described previously. When a fixed concentration of ^{32}PRPP was incubated with increasing concentrations of the pseudo DHOase protein, there was a linear increase in the moles of PRPP bound per mole of protein. This suggested that PRPP did bind to the pseudo-DHOase. In a second set of experiments, 250 μg of the protein was incubated with increasing concentrations of ^{32}PRPP for 15 min at 37°C. A plot of the mole of PRPP bound per mole of the protein as a function of the PRPP concentration showed sigmoidal kinetics with a K_d of 112.4 ± 8.6 μM (Figure 5.6). As the PRPP bound was quite low relative to the ATCase holonzyme, one possibility may be that the PRPP site is not contained entirely within the Pseudo-DHOase chain or that the site may be shared between the catalytic and the pseudo DHOase chains. Another possibility is that the protein is aggregated and the PRPP site is not easily accessible. In order to determine the oligomeric structure of the pseudo-DHOase, the protein was applied to a 1 X 35-cm Superose 12, HR10/35 (Pharmacia FPLC system) gel filtration column calibrated with protein standards (29 kDa carbonic anhydrase, 66 kDa bovine

Figure 5.4 Cloning of the *pyr*C' gene into the overexpression vector pRSETC

The ORF of 1269 base pairs was cloned into the overexpression vector pRSETC by PCR. The primers were designed such that a *Xho* I site was engineered into the 5' primer, and an *Eco*R I site overlapping a stop codon in the 3' primer. The PCR product was double digested with *Xho* I and *Eco*R I, gel purified and ligated into the *Xho* I and *Eco*R I sites of the pRSETC vector.

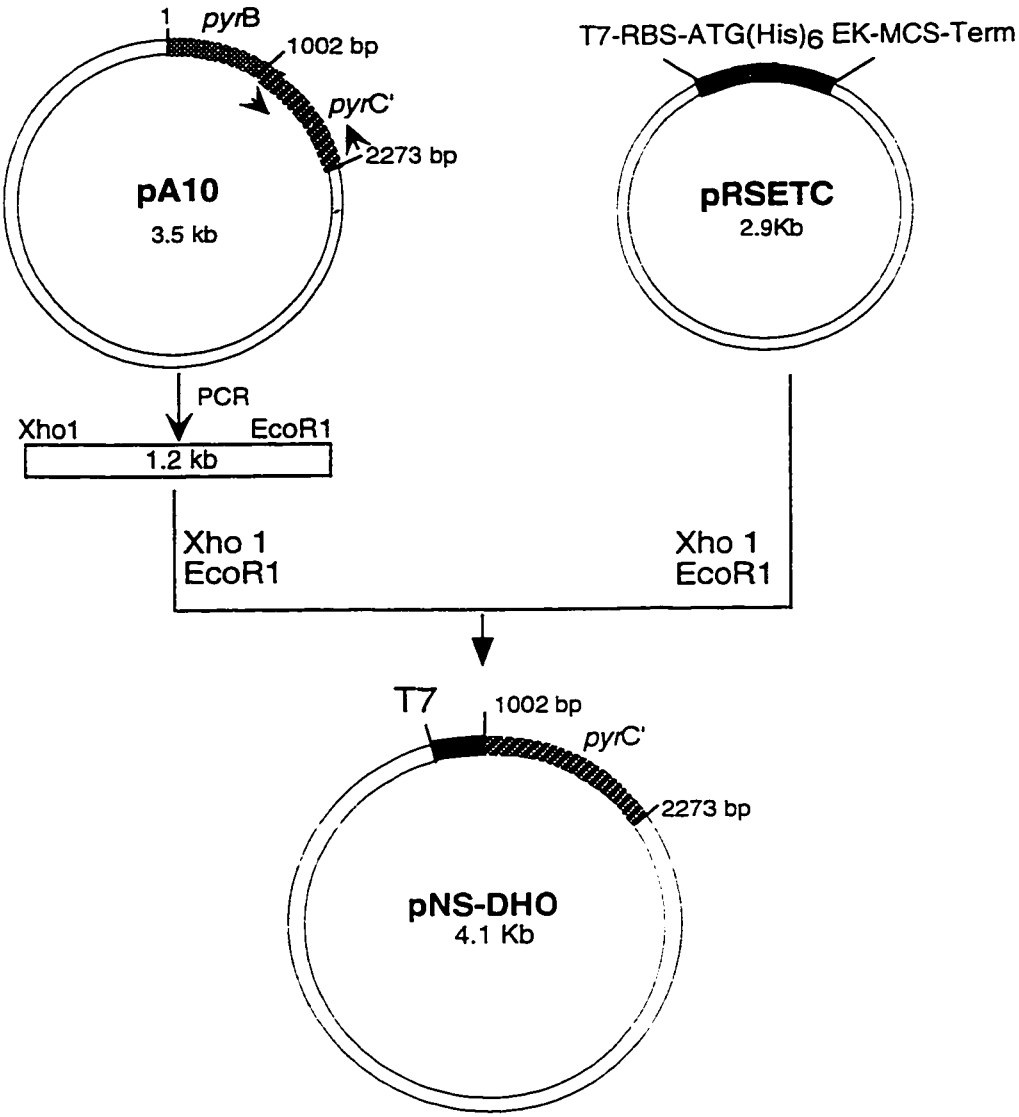
1
pyrB
1002 bp
pyrC'
2273 bp
pA10
3.5 kb
T7-RBS-ATG(His)6 EK-MCS-Term
pRSETC
2.9Kb
PCR
Xho1
EcoR1
1.2 kb
Xho 1
EcoR1
Xho 1
EcoR1
T7
1002 bp
pyrC'
2273 bp
pNS-DHO
4.1 Kb

Figure 5.5 Expression and Purification of the Pseudo DHOase

The pellet from a 100 ml induced culture was resuspended in 2 ml of 50 mM Tris/HCl, pH 8.4, 10 mM β-mercaptoethanol, 150 mM NaCl, and 10% glycerol. PMSF (1mM) was added prior to lysis and the cells lysed by sonication 5 X 10 seconds each, on ice. Cells were harvested by centrifuging at 4000 x g, 20 min, 4°C. The supernatant fraction was added on to a 2 ml nickel-resin bed. The contaminants were washed off using the above buffer containing 50 mM imidazole until the absorbance at 280 nm was negligible. The histidine tagged pseudo-DHOase recombinant was eluted from the nickel beads by competition with buffer containing 150 mM imidazole. The SDS-gel (10%) shows lanes with the supernatant (1), molecular marker (2), pellet (3), 50 mM wash fraction (4), followed by 150 mM imidazole elution fractions (5-13) containing the 47.7 kDa his-tagged recombinant. The top gel shows elution fractions of the ATCase holoenzyme consisting of the 34 kDa catalytic chain and the 45 kDa pseudo-DHO chain (expression and purification by Dr. J. F. Vickrey)

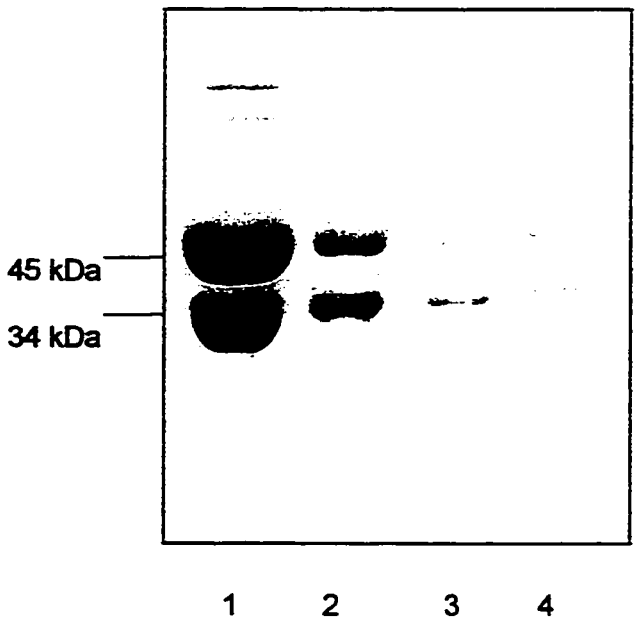
45 kDa
34 kDa
1
2
3
4

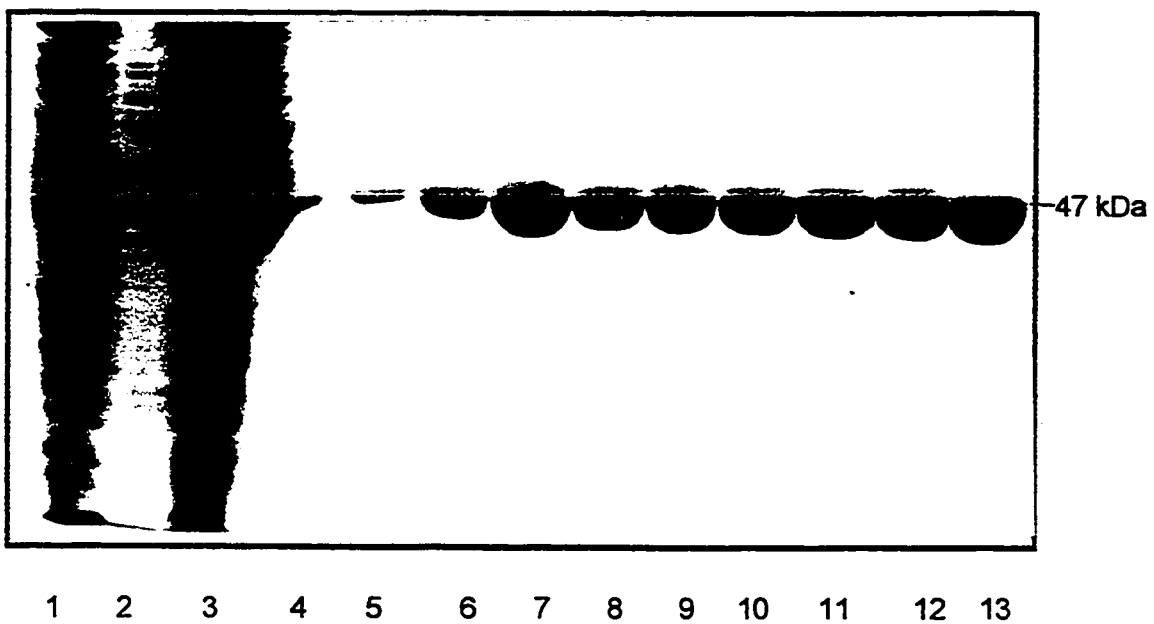
47 kDa
1
2
3
4
5
6
7
8
9
10
11
12
13

Figure 5.6 PRPP Binding to the recombinant pseudo-DHOase protein

PRPP binding to 250 μg of the pseudo DHOase protein was carried out by the spin column method. The number of moles of PRPP, bound per mole of protein, was plotted as a function of the PRPP concentration.

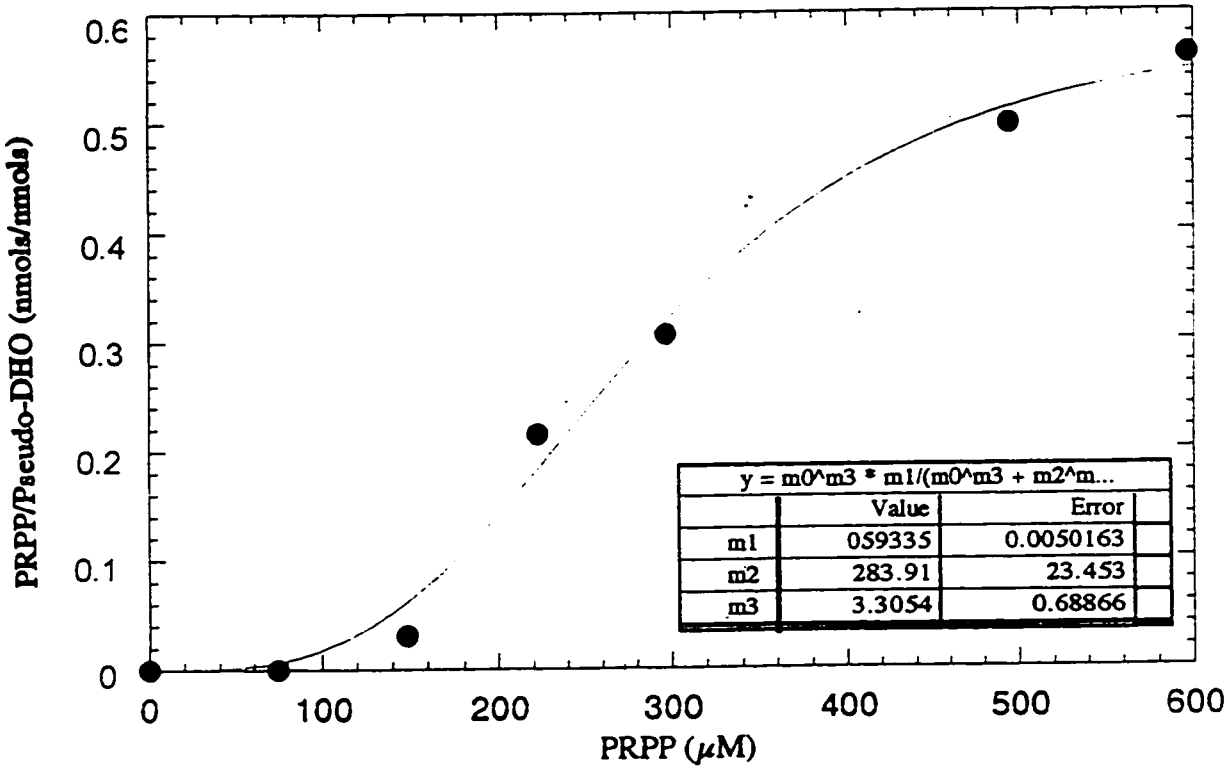
0.6
0.5
0.4
0.3
0.2
0.1
0
PRPP/Pseudo-DHO (nmols/nmols)
0
100
200
300
400
500
600
PRPP (μM)
y = m0^m3 * m1/(m0^m3 + m2^m...
Value
Error
m1
059335
0.0050163
m2
283.91
23.453
m3
3.3054
0.68866

serum albumin, 150 kDa alcohol dehydrogenase and 600 kDa blue dextran). The column elution pattern showed that the pseudo DHOase existed as an aggregrate of 12 polypeptide chains with an overall molecular mass close to 600 kDa. Since the pseudo-DHOase protein is aggregated, the PRPP binding site may not be as accessible as it is in the holoenzyme, where the oligomeric structure consists of six polypeptide chains of the catalytic subunit surrounded by six pseudo DHOase chains. This finding may explain the weaker binding of PRPP to the isolated pseudo-DHOase. In order to determine whether PRPP can bind to the ATCase catalytic chain, the *pyr*B gene was subcloned into the overexpression vector pRSET.

5.8 Cloning, Expression and purification of the ATCase catalytic chain

The 1 kb *pyr*B gene encoding the catalytic chain of the ATCase holoenzyme was cloned into the pRSETA vector by PCR. Restriction sites were engineered within the 5' and 3' primers for ease of cloning. The 5' primer incorporated a *Xho* I site while the 3' primer contained an *Eco*R I site overlapping a stop codon. The 1008 base pair PCR fragment was purified, double digested with *Xho* I and *Eco*R I, gel purified, and ligated to the 2.9 kb *Xho* I and *Eco*R I fragment of the pRSETA vector to obtain pNS-ATC (Figure 5.7).

The clone pNS-ATC was transformed into BL21 (DE3) cells. The overnight culture (0.5 ml) was used to inoculate 100 ml LB containing 100 μg/ml ampicillin and the cells grown at 37°C. Cell growth was monitored spectrophotometrically. When the cells reached an absorbance of 0.6-0.8 at 600 nm, expression was induced with 0.4 mM IPTG and induction was continued for 2 hours at 37°C. Cells were harvested at 4000 x g, 20 min at 4°C and the pellets frozen at -70°C.

The cells were thawed and the pellet resuspended in 2 ml of 50 mM Tris pH 8.4, 150 mM NaCl, 10 mM β-mercaptoethanol, 10 % glycerol, and 1mM PMSF. The cells were lysed by sonication 5 X 10 seconds each. The cell extract was centrifuged at

14,000 x g for 20 minutes. SDS-gel electrophoresis revealed a new 40.4 kDa species not present in extracts of untransformed cells. The 40.4 kDa histidine tagged ATCase catalytic recombinant was confirmed by immunoblotting with anti-Xpress antibodies (Invitrogen). Although the protein expressed in the soluble fraction, the level of expression was very low and insufficient for binding studies.

Immunoprecipitation was used to purify the histidine tagged ATCase recombinant from the supernatant fraction. The procedure involved an incubation of the 2 ml of the supernatant containing the histidine tagged recombinant with the Anti-Xpress antibody (Invitrogen) for 2-3 hours at 4°C. Protein G Sepharose (Santa Cruz Biotechnology, cat# sc-2002) was added to the reaction and incubation continued for 3 hours at 4°C. The reaction was then gently centrifuged to pellet the enzyme-antibody-bead complex. Following two washes with the ATCase assay buffer, the beads were resuspended in 50 µl of the assay buffer.

Although a PRPP binding experiment could not be performed, an interesting paradox regarding the catalytic activity of the ATCase catalytic chain without the 45 kDa pseudo-DHOase chain could be tested. Currently, it is thought that the 34 kDa catalytic chain of the ATCase holoenzyme, requires the association of the 45 kDa pseudo DHOase chain for catalytic activity, and hence the translational overlap of the two. In case of the *E. coli* ATCase, however, it has been demonstrated that the 34 kDa catalytic chain is active without the 17 kDa regulatory dimers. Based on this fact, it may be envisioned that the P. *aeruginosa* ATCase 34 kDa catalytic chain may also be active without the 45 kDa pseudo DHOase chain. An ATCase activity assay, as described in Materials and Methods, was performed using the enzyme-antibody-bead complex. Activity was plotted as a function of the aspartate concentration. As the BL21 (DE3) cells contain background ATCase activity, the untransformed cells were used as blank. The recombinant histidine tagged ATCase demonstrated activity above

Figure 5.7 Cloning of the catalytic chain *pyrB* in to pRSETA

The ORF of 1008 base pairs was cloned into the overexpression vector pRSETA by PCR. The primers were designed such that a *Xho* I site was engineered into the 5' primer, and an *EcoR* I site overlapping a stop codon in the 3' primer. The 1 kb PCR product was double digested with *Xho* I and *Eco*R I , gel purified, and ligated into the *Xho* I and *Eco*R *I* sites of the pRSETA vector.

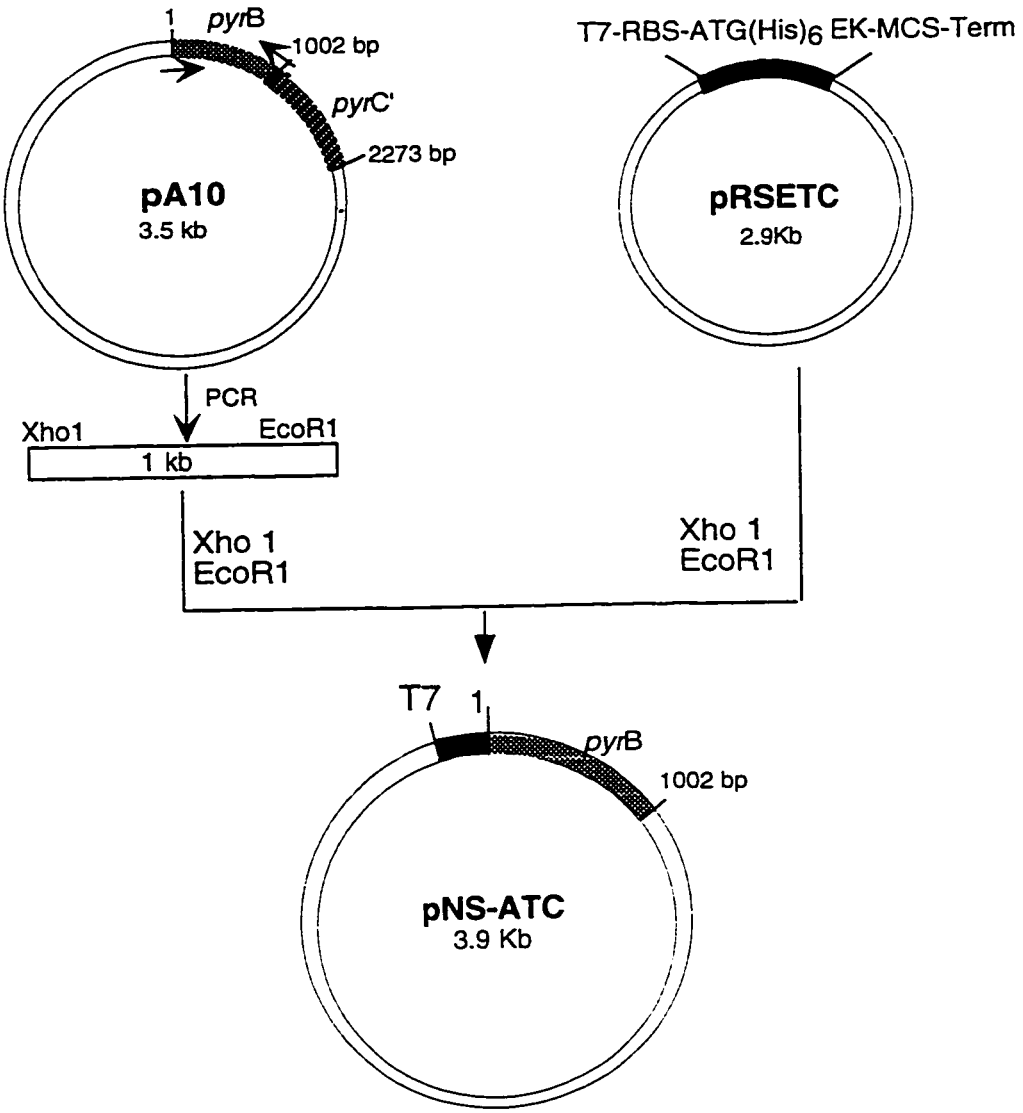
1
pyrB
1002 bp
pyrC'
2273 bp
pA10
3.5 kb
T7-RBS-ATG(His)6 EK-MCS-Term
pRSETC
2.9Kb
PCR
Xho1
EcoR1
1 kb
Xho 1
EcoR1
Xho 1
EcoR1
T7
1
pyrB
1002 bp
pNS-ATC
3.9 Kb

background. However, the results need to be verified further in order to state that the ATCase catalytic chain *of P. aeruginosa* is catalytically active in the absence of the pseudo DHOase.

5.9 Discussion

The PRPP binding results show that PRPP binds to the ATCase holoenzyme with a K_d of 34 μM. This result is quite novel as none of the other well studied ATCases, bind, or are in any way affected by PRPP. The Scatchard plot confirms the presence of six binding sites to the overall enzyme. The overall enzyme is a dodecamer consisting of six polypeptide chains of the 34 kDa catalytic subunit and six polypeptides of the 45 kDa pseudo DHOse chain. The existence of six PRPP binding sites per molecule of the ATCase holoenzyme may be interpreted as being located either exclusively on the ATCase catalytic subunit or on the pseudo-DHOase subunit, or the sites may be shared between the two subunits.

In the holoenzyme, a fixed concentration of ^{32}PRPP and increasing protein showed a linear increase in PRP- bound per mole of protein. However, binding to the isolated pseudo-DHOase is not very significant as compared with the holoenzyme. This may be due to the aggregated condition of the protein as determined by gel filtration studies. The pseudo DHOase exists as an aggregated molecular mass of about 600 kDa, which corresponds to 12 polypeptide chains. Typically, in the ATCase holoenzyme, the pseudo-DHOase exists as six chains presumably surrounding the two catalytic trimers. Perhaps the pseudo-DHOase when expressed separately, preferentially adopts a native conformation where it exists as a dimer of six chains surrounding one another. In such an aggregated situation, it may be that the PRPP sites are inaccessible. On the other hand, the PRPP site may not be exclusively located within the 45 kDa subunit and may be a shared one. Binding studies to the catalytic chain was not possible, as the yield of the catalytic recombinant was very low.

The effect of PRPP on the activity of the ATCase holoenzyme was determined at different concentrations of aspartate. However, it is unclear whether PRPP acts as an effector. The fact that the overall holoenzyme binds PRPP and that PRPP maybe a substrate rather than an allosteric effector, suggests that there may be yet another function to this holoenzyme or that the 45 kDa pseudo DHOase may play an unknown role within the cell. Thus, whether the pseudo DHOase exists for the catalytic chain to be active or if it has another unknown function is still a mystery. An important clue is that the other unknown function possibly involves PRPP.

During the analysis of the different reactions in which PRPP is involved, the reaction catalyzed by pyrimidine phosphoribosyltransferase in the pyrimidine salvage pathway may be relevent. Pyrimidine phosphoribosyltransferases salvage pyrimidines to the nucleotide level in the presence of PRPP, using orotate, uracil and thymine as substrates. The reaction with orotate and PRPP can be ruled out as when the holoenzyme replaced the OPRTase-ODCase mixed enzyme in the OPRTase-ODCase coupled assay, no labeled CO_2 was generated according to the reaction Orotic Acid + **PRPP** $\rightarrow$ OMP + **PPi** / OMP $\rightarrow$ $^{14}CO_2$ + UMP. The reactions with uracil and thymine are to be investigated. A BLAST search using the GCG program showed that the pseudo DHOase has slight homology to Dihydopyrimidinase, an enzyme that catalyzes degradation of uracil or thymine to β-alanine and β-aminoisobutyrate, respectively. Perhaps the homology between the pseudo DHOase and dihyropyrimidinase may be due to uracil/thymine being a common substrate. In addition to the pyrimidine salvage reactions, several other PRPP utilizing reactions will be tested. The purine and pyrimidine bases and their nucleoside and nucleotide derivatives can be separated by a variety of techniques, one of which involves the use of high-performance liquid chromatography (HPLC).

CHAPTER 6 SUMMARY

Pyrimidine nucleotides play a central role in cellular regulation. Most cells have two pathways to fulfill their pyrimidine nucleotide pools, the *de novo* and the salvage pathway. The *de novo* pathway begins with ATP, bicarbonate and glutamine, and through six enzymatic steps yields uridine monophosphate (UMP). In mammals, the first three enzyme activities i.e. the glutamine-dependent carbamoyl phosphate synthetase (CPSase), aspartate transcarbamoylase (ATCase), and the dihydroorotase (DHOase), are carried on a single 240 kDa polypeptide chain called CAD. Sequencing studies and controlled proteolysis of the CAD cDNA, revealed the multidomain nature of CAD. In recent studies, all of the functional domains of CAD have been individually expressed in *E.coli.*

Carbamoyl phosphate synthetase (CPSase) is the first enzyme in the *de novo* pyrimidine pathway. It catalyzes the synthesis of carbamoyl phosphate from bicarbonate, two moles of ATP, and ammonia derived from the hydrolysis of glutamine. The CPSase domain consists of two 60 kDa homologous halves, CPS.A and CPS.B, each of which has recently been shown to be functionally equivalent, and each, as a homodimer, can catalyze the overall CPSase reaction (70). Sequence homology, proteolysis studies and the recently solved crystal structure of the *E. coli* CPSase have shown that the two halves are further subdivided into subdomains A1, A2, A3 and B1, B2 and B3. The catalytic sites are located entirely in the 27-kDa central A2 and B2 subdomains (97). The 11-kDa A1 and B1 subdomains act as attenuation subdomains by suppressing the intrinsically high catalytic activity of the A2 and B2 subdomains. The 20-kDa A3 and B3 subdomains are not required for catalytic activity. A3 has been termed the 'oligomerization domain' although its function is quite undefined at this time. B3 is known to bind allosteric effectors, and modulates the activity of the catalytic

subdomains (56).

The CPSase domain is the locus of allosteric control in the mammalian *de novo* pyrimidine pathway. It undergoes feedback inhibition by UTP, and activation by PRPP, a purine precursor that coordinates purine and pyrimidine biosynthesis. It is also activated by cAMP-dependent protein kinase A phosphorylation.

Several lines of evidence have shown that the carboxyl end, B3, of the CPSase molecule is involved in allosteric regulation. The domain swapping experiments by Liu et al involved the construction of an *E.coli*-mammalian chimera, in which the B3 region of the *E. coli* CPSase protein was replaced by the putative regulatory region of CAD. The resulting chimera failed to respond to *E. coli* effectors, but instead, responded to mammalian effectors PRPP and UTP.

My dissertation project was outlined based on the above findings and involved the characterization of the B3 region, focussing on the following three questions:

- Can B3 act as an exchangeable ligand-binding module by replacing A3 in the CPS.A half, thereby placing the CPS.A under allosteric control?
- Can B3 function independently as an autonomously folded, stable subdomain that binds the allosteric ligands?
- Can the regulatory domain form a stoichiometric complex with the isolated CPS.A domain and transmit the allosteric signals to the catalytic subdomain A2?

A chimera consisting of the *E. coli* subdomains A1 and A2 fused to mammalian B3 was constructed. The catalytic parameters of this 58 kDa chimeric protein were similar to those of the *E. coli* enzyme, but the activity was regulated by the mammalian effectors PRPP and UTP, and by protein kinase A phosphorylation. Binding kinetics demonstrated the presence of one PRPP binding site, which binds the activator with a dissociation constant of 46 μM. UTP binding to the chimeric protein was inferred from its effect on PRPP binding. The presence of the B3 subdomain thus placed the CPS.A

domain under allosteric control, demonstrating that B3 behaves as an exchangeable ligand-binding module.

Analysis of the carboxyl end of the regulatory domain of several CPSases supported the existence of a nucleotide-binding fold located entirely within the carboxy terminal domain. Photoaffinity labeling studies by Cervera et al identified a Lys 992 residue involved in UTP binding in *E. coli.* In order to study the function of the carboxyl end of B3 in CAD, a deletion mutant was constructed which lacked 59 residues, from the carboxyl end of the chimera CPS-A12^{e}B3^{m}, out of the total 163 residues of the B3 subdomain. This site was specifically chosen as it disrupted the UTP sequence proposed by Cervera et al. The CPSase activity of the deletion mutant was almost insensitive to PRPP and UTP. However, binding studies indicated that both effectors still bound to the deletion mutant, though with a significantly higher dissociation constant. The results thus showed that the deletion of the 59 residues significantly affected the transmission of the allosteric signal to the active site, even though the effectors still bound weakly. In the case of PRPP, the deletion mutant has a two fold higher K_d as compared with the wild type chimera. Although the affinity for PRPP is lower, the activator must bind to the amino half of B3. This is consistent with the theory that PRPP binds upstream of UTP. The UMP site in *E. coli* has been proposed to consist of two contiguous regions: the first surrounding lys 992 (residue tryptophan 1364 in CAD, by alignment) and extending to an invariant asparagine 1014 (asparagine 1394 in CAD), while the second extends from 1014 (asparagine 1394 in CAD) to an invariant arg 1029 (Arg 1416 in CAD). The deletion mutant was truncated at glycine 1402 (in CAD), and thus, by sequence alignment of the proposed UMP binding fold in *E. coli*, lacked only 14 residues of the nucleotide fold. The binding of UTP to the deletion mutant truncated downstream from glycine 1402 (in CAD), suggests that most of the ligand interaction residues must be located upstream of this glycine 1402. The 59 residues deleted from

the carboxyl end of B3 disrupted the signal transmission, suggesting that the carboxyl end, which seems to interface between the catalytic and regulatory subdomain, is essential for mediating interdomain interactions.

Although several lines of evidence demonstrate that the B3 subdomain can bind the alloseric ligands, and has the phosphorylation site, it was yet to be shown that B3 can exist as an independent functional domain. The regulatory domain was subsequently cloned into an expression vector, and expressed as a 26.7 kDa histidine-tagged recombinant. Binding studies performed with enzymatically synthesized radiolabeled PRPP demonstrated that PRPP binds to the regulatory recombinant with a Kd of 83.5 μM, although the affinity of the activator is about 8-fold lower as compared with CAD, and less than two-fold as compared with the CPS-A12^{e}B3^{m} chimera. UTP binding was studied by its effect on PRPP binding. UTP changed the K_d by almost two-fold. A Scatchard plot showed the presence of one binding site for PRPP, which was in agreement with the results obtained for native CAD. Thus, binding studies with both allosteric effectors suggests that the regulatory domain is an autonomously functional subdomain. The decreased affinity of the effectors may be attributed to the conformation of the regulatory subdomain when it exists independently of the rest of the CPSase molecule.

Deletion studies with the chimera suggests that the 59 residues at the carboxyl end of B3 may be involved in the transmission of allosteric signal to the CPSase active site A2 and B2. In such a case, there may be an interaction between the regulatory subdomain B3 and the CPS.A domain. The CPS.A domain was cloned and expressed as a 72.8 kDa recombinant. Measurements of the steady state kinetic parameters of CPS.A showed that it catalyzed the overall reaction nearly as well as the native enzyme. ATP saturation curves in the presence of UTP and PRPP were indistinguishable from the curve in the absence of effectors, which was as expected, as CPS.B and not CPS.A,

is the locus of allosteric control. Titration of CPS.A with increasing concentrations of the regulatory domain, B3, resulted in the formation of a 1:1 stoichiometric complex CPS.A-REG. The steady state kinetic parameters of CPS.A-REG showed that the allosteric effectors PRPP and UTP affect the V_{max} rather than the K_m, unlike in the native CAD. Effector response curves show that the catalytic activity is altered approximately the same extent as the parent mammalian protein. The apparent dissociation constant of PRPP is almost 7-fold lower but that of UTP is comparable to CAD. The results suggest that the PRPP and UTP sites are contained entirely within the B3 region, and that the signal is almost as efficiently transferred to the CPS.A active site in the CPS.A-REG hybrid, as it is in the parent CAD molecule.

In addition to the regulatory domain of CAD, another project involved studying the binding of PRPP to the aspartate transcarbamoylase holoenzyme of *P. aeruginosa*. The overall enzyme is a dodecamer consisting of six polypeptide chains of the 34 kDa catalytic subunit and six polypeptides of the 45 kDa pseudo-DHOase chain. The pseudo-DHOase chain, although homologous to the DHOase, does not show DHOase activity. Currently, it is proposed that the 45 kDa chain is required for the 34 kDa catalytic chain to be active. PRPP binding results show that PRPP binds to the ATCase holoenzyme with a K_d of 34 μM and that there exists six sites per molecule of the enzyme. This result is quite novel as the none of other well studied ATCases bind, or are in any way affected by PRPP. The effect of PRPP on the catalytic activity of the ATCase enzyme was unclear. The fact that PRPP binds tightly to the holoenzyme and may even be a substrate suggests that there may be yet another function to this enzyme or that the pseudo-DHOase may play an unknown role within the cell.

REFERENCES

1. Jones, M. (1972) *Curr. Topics Cell Reg.* **6,** 227-265

2. Hoogenraad, N., Levine, R., and Kretchmer, N. (1971) *Biochem. Biophys. Res. Commun.* **44,** 981-988

3. Shoaf, W., and Jones, M. (1971) *Biochem. Biophys. Res. Commun.* **45,** 796-802

4. Coleman, P., Suttle, D., and Stark, G. (1977) *J. Biol. Chem.* **252,** 6379-6385

5. Padgett, R. A., Wahl, G. M., and Stark, G. R. (1982) *Mol Cell Biol* **2**(3), 293-301

6. Lee, L., Kelly, R. E., Pastra-Landis, S. C., and Evans, D. R. (1985) *Proc Natl Acad Sci U S A* **82**(20), 6802-6

7. Wahl, G. M., Padgett, R. A., and Stark, G. R. (1979) *J Biol Chem* **254**(17), 8679-89

8. Shigesada, K., Stark, G. R., Maley, J. A., Niswander, L. A., and Davidson, J. N. (1985) *Mol Cell Biol* **5**(7), 1735-42

9. Mally, M. I., Grayson, D. R., and Evans, D. R. (1980) *J Biol Chem* **255**(23), 11372-80

10. Davidson, J. N., Rumsby, P. C., and Tamaren, J. (1981) *J Biol Chem* **256**(10), 5220-5

11. Mally, M. I., Grayson, D. R., and Evans, D. R. (1981) *Proc Natl Acad Sci U S A* **78**(11), 6647-51

12. Grayson, D. R., and Evans, D. R. (1983) *J Biol Chem* **258**(7), 4123-9

13. Grayson, D. R., Lee, L., and Evans, D. R. (1985) *J Biol Chem* **260**(29), 15840-9

14. Kelly, R. E., Mally, M. I., and Evans, D. R. (1986) *J Biol Chem* **261**(13), 6073-83

15. Simmer, J. P., Kelly, R. E., Rinker, A. G., Jr., Zimmermann, B. H., Scully, J. L., Kim, H., and Evans, D. R. (1990) *Proc Natl Acad Sci U S A* **87**(1), 174-8

16. Simmer, J. P., Kelly, R. E., Rinker, A. G., Jr., Scully, J. L., and Evans, D. R. (1990) *J Biol Chem* **265**(18), 10395-402

17. Kim, H., Kelly, R. E., and Evans, D. R. (1992) *J Biol Chem* **267**(10), 7177-84

18. Farnham, P. J., and Kollmar, R. (1990) *Cell Growth Differ* **1**(4), 179-89

19. Bein, K., Simmer, J., and Evans, D. (1991) *J Biol Chem* **266,** 3791-9

20. Guy, H. I., and Evans, D. R. (1994) *J Biol Chem* **269**(38), 23808-23816

21. Anderson, P. M., and Meister, A. (1965) *Biochemistry* **4**(12), 2803-9

22. Wimmer, M. J., Rose, I. A., Powers, S. G., and Meister, A. (1979) *J Biol Chem* **254**(6), 1854-9

23. Anderson, P. M., and Meister, A. (1966) *Biochemistry* **5**(10), 3157-63

24. Powers, S. G., and Meister, A. (1976) *Proc Natl Acad Sci U S A* **73**(9), 3020-4

25. Powers, S. G., and Meister, A. (1978) *J Biol Chem* **253**(4), 1258-65

26. Powers, S. G., and Meister, A. (1978) *J Biol Chem* **253**(3), 800-3

27. Raushel, F. M., and Villafranca, J. J. (1979) *Biochemistry* **18**(15), 3424-9

28. Raushel, F. M., and Villafranca, J. J. (1980) *Biochemistry* **19**(14), 3170-4

29. Trotta, P. P., Pinkus, L. M., and Meister, A. (1974) *J Biol Chem* **249**(6), 1915-21

30. Anderson, P. M., and Marvin, S. V. (1968) *Biochem Biophys Res Commun* **32**(6), 928-34

31. Lusty, C. J. (1978) *J Biol Chem* **253**(12), 4270-8

32. Lusty, C. J., and Lu, J. (1982) *Proc Natl Acad Sci U S A* **79**(7), 2240-4

33. Nyunoya, H., Broglie, K. E., Widgren, E. E., and Lusty, C. J. (1985) *J Biol Chem* **260**(16), 9346-56

34. Powers-Lee, S. G., and Corina, K. (1986) *J Biol Chem* **261**(33), 15349-52

35. Britton, H. G., and Rubio, V. (1988) *Eur J Biochem* **171**(3), 615-22

36. Britton, H. G., Garcia-Espana, A., Goya, P., Rozas, I., and Rubio, V. (1990) *Eur J Biochem* **188**(1), 47-53

37. Anderson, P. M. (1980) *Science* **208**(4441), 291-3

38. Anderson, P. M. (1981) *J Biol Chem* **256**(23), 12228-38

39. Casey, C. A., and Anderson, P. M. (1983) *J Biol Chem* **258**(14), 8723-32

40. Hong, J., Salo, W. L., Lusty, C. J., and Anderson, P. M. (1994) *J Mol Biol* **243**(1), 131-140

41. Kaseman, D. S., and Meister, A. (1985) *Methods Enzymol* **113**, 305-26

42. Meister, A. (1989) *Adv Enzymol Relat Areas Mol Biol* **62**, 315-74

43. Trotta, P. P., Burt, M. E., Haschemeyer, R. H., and Meister, A. (1971) *Proc Natl Acad Sci U S A* **68**(10), 2599-603

44. Trotta, P. P., Pinkus, L. M., Haschemeyer, R. H., and Meister, A. (1974) *J Biol Chem* **249**(2), 492-496

45. Nyunoya, H., and Lusty, C. J. (1983) *Proc Natl Acad Sci U S A* **80**(15), 4629-3

46. Piette, J., Nyunoya, H., Lusty, C. J., Cunin, R., Weyens, G., Crabeel, M., Charlier, D., Glansdorff, N., and Pierard, A. (1984) *Proc Natl Acad Sci U S A* **81**(13), 4134-8

47. Rubino, S. D., Nyunoya, H., and Lusty, C. J. (1986) *J Biol Chem* **261**(24), 11320-7

48. Thoden, J. B., Holden, H. M., Wesenberg, G., Raushel, F. M., and Rayment, I. (1997) *Biochem.* **36**, 6305-6316

49. Guy, H. I., and Evans, D. R. (1995) *J Biol Chem* **270**(5), 2190-2197

50. Rubino, S. D., Nyunoya, H., and Lusty, C. J. (1987) *J Biol Chem* **262**(9), 4382-6

51. Mullins, L. S., Lusty, C. J., and Raushel, F. M. (1991) *J Biol Chem* **266**(13), 8236-40

52. Miran, S. G., Chang, S. H., and Raushel, F. M. (1991) *Biochemistry* **30**(32), 7901-7

53. Rubio, V. (1993) *Biochem Soc Trans* **21**(1), 198-202

54. Purcarea, C., Simon, V., Prieur, D., and Herve, G. (1996) *Eur J Biochem* **236**, 189-199

55. Cervera, J., Conejero-Lara, F., Ruiz-Sanz, J., Galisteo, M. L., Mateo, P. L., Lusty, C. J., and Rubio, V. (1993) *J Biol Chem* **268**(17), 12504-11

56. Liu, X., Guy, H. I., and Evans, D. R. (1994) *J Biol Chem* **269**(44), 27747-27755

57. Javier Cervera, E. B., Huubert G. Britton, Jorge Bueso, Zeina Nassif, Carol J. Lusty, and Vincente Rubio. (1996) *Biochemistry* **35**(22), 7247-7255

58. Raushel, F. M., Anderson, P. M., and Villafranca, J. J. (1978) *Biochemistry* **17**(26), 5587-91

59. Powers, S. G., Griffith, O. W., and Meister, A. (1977) *J Biol Chem* **252**(10), 3558-60

60. Powers-Lee, S. G., and Corina, K. (1987) *J Biol Chem* **262**(19), 9052-6

61. Potter, M. D., and Powers-Lee, S. G. (1992) *J Biol Chem* **267**(3), 2023-31

62. Potter, M. D., and Powers-Lee, S. G. (1993) *Arch Biochem Biophys* **306**(2), 377-82

63. Lusty, C. J., Widgren, E. E., Broglie, K. E., and Nyunoya, H. (1983) *J Biol Chem* **258**(23), 14466-7

64. Post, L. E., Post, D. J., and Raushel, F. M. (1990) *J Biol Chem* **265**(14), 7742-7

65. Guy, H. I., and Evans, D. R. (1994) *J Biol Chem* **269**(10), 7702-8

66. Guy H. I, Rotgeri. A., and Evans. D. R. (1997) *J. Biol. Chem.* **272**(32), 19913-19918

67. Boettcher, B. R., and Meister, A. (1980) *J Biol Chem* **255**(15), 7129-33

68. Kim, H. S., Lee, L., and Evans, D. R. (1991) *Biochemistry* **30**(42), 10322-9

69. Mareya, S. M., and Raushel, F. M. (1995) *Bioorg Med Chem* **3**(5), 525-532

70. Guy, H. I., and Evans, D. R. (1996) *J. Biol. Chem.* **272**

71. Carrey, E. A., Campbell, D. G., and Hardie, D. G. (1985) *Embo J* **4**(13B), 3735-42

72. Carrey, E. A., and Hardie, D. G. (1988) *Eur J Biochem* **171**(3), 583-8

73. Carrey, E. A. (1993) *Biochem Soc Trans* **21**(1), 191-5

74. Rubio, V., Cervera, J., Lusty, C. J., Bendala, E., and Britton, H. G. (1991) *Biochemistry* **30**(4), 1068-75

75. Bueso, J., Lusty, C. J., and Rubio, V. (1994) *Biochem. Biophys. Res. Commun.* **203**(2), 1083-9

76. Rodriguez-Aparicio, L. B., Guadalajara, A. M., and Rubio, V. (1989) *Biochemistry* **28**(7), 3070

77. Czerwinsky, R.M., Mareya, S.M., and Raushel, F. M. (1995) *Biochemistry* **34**:13920-27

78. Davidson, J. N., and Jamison, R. S. (1994) *Adv Exp Med Biol* **370**, 591-59

79. Bethel, M. R., and Jones, M. E. (1969) *Arch. Biochem. Biophys* **134**, 352-365

80. Adair, L. B., and Jones, M.E. (1972) *J. Biol. Chem* **247**, 2308—2315

81. Babson, J. S. a. S., R. L. (1975) *J. Biol.Chem* **250**, 8664-8669

82. Bergh, S. T., and Evans, D. R. (1993) *Proc Natl Acad Sci U S A* **90**(21), 9818-22

83. Schurr, M. J., Vickrey, J. F., Kumar, A. P., Campbell, A. L., Cunin, R., Benjamin, R. C., Shanley, M. S., and GA, O. D. (1995) *J Bacteriol* **177**(7), 1751-1759

84. Honzatko, R. B., Crawford, J. L., Monaco, H. L., Ladner, J. E., Ewards, B. F., Evans, D. R., Warren, S. G., Wiley, D. C., Ladner, R. C., and Lipscomb, W. N. (1982) *J Mol Biol* **160**(2), 219-63

85. Ke, H. M., Honzatko, R. B., and Lipscomb, W. N. (1984) *Proc Natl Acad Sci U S*

A **81**(13), 4037-40

86. Krause, K. L., Volz, K. W., and Lipscomb, W. N. (1987) *J Mol Biol* **193**(3), 527-5

87. Hoover, T. A., Roof,, W. D., Foltermann, K. F., O'Donovan, G. A., Bencini, D. A., and Wild, J. R. (1983) *Proc Natl.Acad Sci USA* **80**, 2462-2466

88. Robey, E. A and Schachman, H. K. (1985) *Proc Natl Acad Sci USA* **82**, 361-36

89. Schurr, M. J. (1993), Univ. of North Texas, Denton

90. Guillou, F., Rubino, S. D., Markovitz, R. S., Kinney, D. M., and Lusty, C. J. (1989) *Proc Natl Acad Sci U S A* **86**(21), 8304-8

91. Nowlan, S. F., and Kantrowitz, E. R. (1985) *J Biol Chem* **260**(27), 14

92. Maniatis, T., Fritsch, E. R., and Sambrook, I. (1982) *Molecular Cloning: A Laboratory Manual*, Cold Spring Harbor Laboratory, Cold Spring Harbor, N. Y.

93. Laemmli, U. (1970) *Nature* **227**, 680-685

94. Evans, D. R., and Balon, M. A. (1988) *Biochim Biophys Acta* **953**(2), 185-9

95. Alonso, E., Cervera, J., Garcia-Espana, A., Bendala, E., and Rubio, V. (1992) *J Biol Chem* **267**(7), 4524-32

96. Alonso, E., and Rubio, V. (1995) *Eur J Biochem* **229**(2), 377-384

97. Guy H. I., Bouvier., A., and Evans D. R. (1997) *J. Biol. Chem.* **272**, 29255-2926

98. Khorana, H. G., Femandes, J. F., and Komberg, A. (1958) *J. Biol. Chem* **230**, 941-948

99. Switzer, R. L., and Gibson, K. L. (1978) *Methods Enzyol* **51**, 3-11

100. Penefsky, H. S. (1979) *Methods Enzymol.* **56**, 527-530

101. Rubio, V., Britton, H. G., and Grisolia, S. (1983) *Eur J Biochem* **134**(2), 337-43

102. Kerson, L. A., and Appel, S. H. (1968) *J. Biol. Chem.* **243**, 4279-4285

103. Marshall, M., Metzenberg, R. L., and Cohen, P. P. (1958) *J. Biol. Chem.* **223**, 102-10

104. Anderson, P. M. (1977) *Biochemistry* **16**(4), 587-93

105. Carrey, E. A. (1986) *Biochem J* **236**(2), 327-35

106. Rubio, V., Britton, H.G.,and Grisolia, S. (1981) *Eur J Biochem* **93**(2), 245-56

107. Tatibana, M., and Shigesada, K. (1972) *Biochem. Biophys. Res.Comm* **46**:49

108. Lyons, S.D., and Christopherson, R.I. (1985) *Eur J Biochem* **147**(3), 587-9

109. Shaw, S.M. and Carrey, E.A. (1992) *Eur J Biochem* **207**(3) 951-65

110. Rumsby, P.C., Campbell, P. C. , Niswander, L. A. and Davidson, J. N. (1984) *Biochem J* **217**(2), 435-40

111. Powers Lee, S. G. and Corina, K. (1986) *J Biol Chem* **261**(33), 15349-52

112. Guadaljara, A., Grisolia, s. and Rubio, V. (1987) *Eur J Biochem* **165**(1) 163-9

ABSTRACT

CHARACTERIZATION OF THE REGULATORY DOMAIN OF THE MAMMALIAN MULTIFUNCTIONAL *DE NOVO* PYRIMIDINE BIOSYNTHETIC ENZYME CAD

by

NISHA SAHAY

MAY 1998

Advisor: Dr. David R. Evans

Major: Biochemistry and Molecular Biology

Degree: Doctor of Philosophy

Pyrimidine nucleotides play a central role in cellular regulation. Most cells have two pathways to fulfill their pyrimidine nucleotide pools: the *de novo* and the salvage pathway. The *de novo* pyrimidine pathway begins with glutamine, ATP and bicarbonate, and through six-enzymatic steps yields uridine monophosphate (UMP). In mammals, the first three activities i.e. the glutamine-dependent carbamoyl phosphate synthetase (CPSase), aspartate transcarbamoylase (ATCase), and dihydroorotase (DHOase) are carried on a single 240-kDa polypeptide chain called CAD.

Carbamoyl phosphate synthetase (CPSase), the first enzyme in the pathway catalyzes the synthesis of carbamoyl phosphate from two moles of ATP, bicarbonate, and ammonia derived from the hydrolysis of glutamine. The CPSase domain consists of two homologous halves, CPS.A and CPS.B, each of which is functionally equivalent, and as a homodimer can catalyze the overall CPSase reaction. Each of the two halves is further subdivided into subdomains A1, A2, A3, and B1, B2 and B3.

CPSase is the locus of allosteric control in the mammalian *de novo* pathway. It undergoes feedback inhibition by UTP and activation by PRPP, a purine precursor that coordinates purine and pyrimidine biosynthesis, and by cAMP-dependent protein kinase

phosphorylation. Several lines of evidence have demonstrated that the carboxyl end (B3) of the CPSase molecule is involved in allosteric regulation.

My dissertation project involved the characterization of the B3 region. A chimera consisting of *E. coli* subdomains A1 and A2 fused to the mammalian B3 was constructed. Presence of the regulatory domain, B3, placed the CPS.A domain under allosteric control, demonstrating that the B3 domain behaves as an exchangeable ligand-binding module. The B3 domain was subsequently subcloned and expressed as a 26.7 kDa histidine-tagged recombinant. Binding studies with enzymatically synthesized, radiolabeled PRPP, demonstrated that the regulatory domain functioned as an autonomously folded, stable subdomain that bound PRPP. UTP binding was measured indirectly as an effect on PRPP binding. The regulatory domain formed a stoichiometric complex with the independently expressed CPS.A. recombinant. The resulting hybrid was catalytically active and responded to allosteric effectors demonstrating that signals generated by the binding of effectors to B3 were transmitted to the CPS.A active site.

AUTOBIOGRAPHICAL STATEMENT

I obtained a Bachelor of Science in Physiology from Presidency College, University of Calcutta, India, in 1991. Based on my performance, I was honored with a National Certificate of Merit from the University Grants Commission, Government of India. Following graduation, I qualified, as an all-India runner-up, for the prestigious Rhodes Scholarship offered by Oxford University, UK. However, I elected to join a Ph.D. program in the United States. In the summer of 1992, I accepted a recruiting T.C. Rumble Fellowship offered to me by Wayne State University. I joined the Department of Biochemistry and Molecular Biology at the School of Medicine and began my doctoral dissertation under Dr. David R. Evans in the fall of 1993. I developed my leadership skills by serving as the student representative in 1995-1996. During my graduate program, I presented my research findings in several notable conferences, both national and international.

Publications and Presentations

Cloning, expression and characterization of the regulatory domain of the mammalian multifunctional *de novo* pyrimidine biosynthetic enzyme CAD. N.Sahay, H.I. Guy, D.R. Evans (1998) manuscript in preparation

Regulation of a chimeric *E.coli*-mammalian carbamoyl phosphate synthetase. N.Sahay, H. I. Guy and D. R. Evans (1998). Submitted to the Journal of Biological Chemistry

Phosphoribosyl-Pyrophosphate binding to Aspartate Transcarbamoylase of *Pseudomonas aeruginosa*. N.Sahay, J. F. Vickrey and D. R. Evans (1997) 17th Midwest Enzyme Chemistry Conference, Chicago, Illinois

Phosphoribosyl-Pyrophosphate binding to Aspartate Transcarbamoylase of *Pseudomonas aeruginosa*. N.Sahay, J. F. Vickrey and D. R. Evans (1997) Ist Wayne State University School of Medicine Graduate Student Research Conference

Phosphoribosyl-Pyrophosphate binding to Aspartate Transcarbamoylase of *Pseudomonas aeruginosa*. N.Sahay, J. F. Vickrey and D. R. Evans (1997) Talk at ATCase workshop, University Pierre et Marie Curie, Paris, France

Phosphoribosyl-Pyrophosphate binding to Aspartate Transcarbamoylase of *Pseudomonas aeruginosa*. N.Sahay, J. F. Vickrey and D. R. Evans (1997) 13th international Purine and Pyrimidine Congress, Gmunden, Austria

Expression and characterization of the regulatory domain of CAD. N. Sahay and D. R. Evans (1996) The FASEB journal 10: A2903, New Orleans

Cloning, expression and characterization of the regulatory domain of CAD. N. Sahay and D. R. Evans (1994) Oral presentation at the 12th International Symposium of Purine and Pyrimidine Metabolism in Man, Indiana